Part A: THEORETICAL STUDIES OF THE X-RAY ABSORPTION EDGE IN COPPER COMPLEXES

Part B: ELECTRON CORRELATION CONSISTENT CALCULATION OF BOND DISSOCIATION ENERGIES

Thesis by

Raymond Alan Bair

In Partial Fulfillment of the Requirements

for the Degree of

Doctor of Philosophy

California Institute of Technology

Pasadena, California

1982

(submitted June 5 , 1981)

ACKNOWLEDGMENTS

I would first like to thank Bill Goddard whose enthusiasm for chemistry has been contagious and whose wholehearted support of my research interests has made my studies a stimulating and worthwhile experience. There has always been a good deal of positive interaction among the members of the Goddard research group, in matters both theoretical and otherwise. For this I am grateful, and I would like to particularly acknowledge Tom Upton and Tony Rappé, my "classmates", whose support and skepticism have helped to keep me pointed in the right direction.

My thanks also go to Professor John Baldeschwieler and Dr. Stephen Crane for discussions of x-ray spectroscopy.

Last, but not least, I am indebted to Ilah, whose encouragement and understanding have been invaluable.

ABSTRACT

Part A: In order to elucidate the nature of the transitions involved in the x-ray absorption edge of molecular systems, we have used ab initio methods to examine the discrete transitions corresponding to the atomic 1s → 3d, 4s, 4p, 5s, and 5p transitions and the corresponding shakeup processes for Cu atom and for a Cu(II) model system, $CuCl_2$. The three common features of the K edge are described by the calculations. For $CuCl_2$, the lowest strong transitions have the character 1s → 4p (f = 0.00133). About 7.5 eV lower is a group of transitions involving 1s → 4p simultaneous with ligand-to-metal shakedown. About 18.7 eV below the main peak is a weak (65 times weaker) quadrupole-allowed transition corresponding to 1s → 3d (i.e., $1s^2 3d^9 \rightarrow 1s^1 3d^{10}$). In each case the spectral feature has been assigned to an allowed transition. Previously, the middle transition was assigned as 1s → 4s, whereas in this study the 1s → 4s transition was calculated to be too weak to be observed. We propose that the observed peak is due to the allowed transition involving 1s → 4p plus shakedown.

Part B: Ab initio generalized valence bond (GVB) and configuration interaction (CI) methods have been used to develop a generally applicable method for directly calculating bond energies. Particular effort has been put into obtaining a scheme in which all correlation terms that change upon dissociation of a particular bond are included consistently. The method uses in an essential way the localized orbitals from a GVB calculations, and is readily applicable to large systems [e.g., $(CH_3)_3C\text{-}C(CH_3)_3$]. To test our method, we selected two benchmark series of compounds, where the experimental bond energies are well known. Calculated bond energies are reported for the R-H bonds of CH_4, NH_3, H_2O, and HF, which are low by 3.5, 2.5, 3.0,

and 2.7 kcal/mol, respectively. We also report calculations of the R-R bond energies of C_2H_6, N_2H_4, H_2O_2, and F_2, which are low by 0.1, -3.2, -1.8, and 0.8 kcal/mol, respectively. In the application of our method, we have calculated all of the O-O, O-C, and O-H bond energies of HOOH, CH_3OOH, CH_3OOCH_3, CH_3OH, C_2H_5OH (O-H only), and CH_3O^-. Finally, we obtain the electron affinities of F, OH, and CH_3O with the same techniques.

TABLE OF CONTENTS

Part A:

THEORETICAL STUDIES OF THE X-RAY ABSORPTION EDGE IN COPPER COMPLEXES

PREFACE

In recent years, theoretical methods have become an important tool for understanding chemical phenomena. Quantum mechanical concepts of structure and bonding permit qualitative understanding of the spectra, reactivity, and other chemical properties of many organic and inorganic species. Also, modern theoretical methods permit accurate calculation of the electronic structure of molecules, both actual and hypothetical. These techniques have provided new insight and understanding of chemical processes and hold the promise of playing an even larger role in the design of industrially important chemical systems,in the development of analytical methods,and in the extension of chemical knowledge.

One of the important contributions of bound state theoretical methods has been the ability to accurately calculate the spectrum of electronic excited states of a chemically interesting molecule. Bonding and ligation often give rise to a complex set of energy levels within a molecule. This is further complicated by the electronic relaxation that occurs whenever an electron is excited within a molecule. This excitation changes the relative importance and number of electronic repulsion and stabilization terms. Consequently, the energy levels of the molecule are altered.

Most theoretical calculations of electronic transitions have concentrated on transitions in the visible and ultraviolet regions of the light spectrum. This is primarily because of the wealth of experimental information in this spectral domain. The electronic excitations in this region usually involve transitions of the valence electrons of a molecule. Consequently, the electronic relaxations that occur when an electron is excited have the most effect on the other valence electrons. However,

spectroscopic measurements in higher energy ranges, including soft and hard x-ray regions, are becoming more and more important as an analytical tool and a probe of molecular structure. These methods include x-ray absorption techniques (EXAFS, XAES), x-ray photoemission spectroscopy (XPS), and x-ray absorption/Auger emission spectroscopy, to name a few.

All of the x-ray spectroscopic methods cited produce excitation or ionization of the more tightly bound electrons of a molecule. These core electrons have excitation energies that are often quite characteristic of a particular element. Hence, x-ray techniques can provide probes of the chemical environment of a single element at a time. This specificity can be used to great advantage since it often allows one to concentrate on a single region of the molecular structure.

However, excitation of the core electrons to empty valence orbitals or to continuum states can have a major influence on all of the less tightly bound electrons of an atom and its immediate neighbors. This excitation will contract all of the orbitals of the center ionized, lowering all of the energy levels, both occupied and vacant. The premise of the research in Part A of this thesis is that the relative ordering of the valence electronic states can change upon core excitation; and that these changes need to be considered when analyzing experimental data.

As a test of this general idea, a model system was selected for detailed electronic structure calculations. The linear, triatomic, $CuCl_2$, was chosen for these studies since there are several good examples of the K edge x-ray absorption spectra of Cu(II) complexes. $CuCl_2$ is a d^9 complex (ground state $^2\Sigma_g^+$) with the vacancy in the $3d_{z^2}$ orbital directed toward the chlorine ligands. Here we calculated the 1s → 3d, 4s, 4p, 5s, and 5p transitions along with the satellites that were close in energy to these

transitions. Separate calculations were performed for the ground and excited states in order to properly describe the electronic relaxation effects. To gauge the intensity of these transitions, oscillator strengths were calculated for the 1s excitation to each excited state. The results of the $CuCl_2$ study are presented in Part A of this thesis. * They confirm our idea that there are observable changes, upon core excitation, in the relative ordering of the bound states of $CuCl_2$. Applications of these concepts to the x-ray absorption spectra of other transition metals is also discussed.

---

* Previously published in Phys. Rev. B, 22, 2767 (1980).

Chapter 1:

Calculation of the K Edge Features of Atomic Cu^{+2} and $CuCl_2$

I. Introduction

With the availability of synchrotron radiation sources, the analysis of extended x-ray absorption fine structure (EXAFS) has developed into a powerful tool for the study of the local environment of transition metals in enzyme systems,[1-5] on surfaces,[6] in solution,[7] and in crystalline complexes.[8] EXAFS spectroscopy allows the study of the coordination of a specific element. The modulation of the characteristic absorption provides specific information about the chemical environment, including the species, number, and distances of neighboring atoms. However, current methods of analysis of the fine structure do not provide information about bond angles.

Recently, EXAFS techniques have been used in studies of copper coordination spheres in several biologically important metalloproteins (cytochrome-c oxidase,[3] azurin,[4] superoxide dismutase,[5] and others) not generally amenable to x-ray crystallographic techniques. In addition, the analysis of the structure in the x-ray absorption edge (x-ray absorption edge spectroscopy, XAES) provides information about the oxidation state of the metal and about the electronic structure of the ligands bound to the metal.[2, 9, 10] A more detailed theoretical understanding of these absorption edge phenomena would provide the experimentalist with another useful tool in the analysis of molecular structure. The absorption edge often shows shoulders (Figure 1) which correspond to (1s) – valence and (1s)–empty bound state transitions on the metal. Previously, the analysis of these particular features has been based on state splittings of atomic spectroscopy,[9] although significant changes are expected in these states upon molecule formation.

In this paper we have carried out ab initio calculations on a model copper complex in order to elucidate the nature of the transitions involved in the

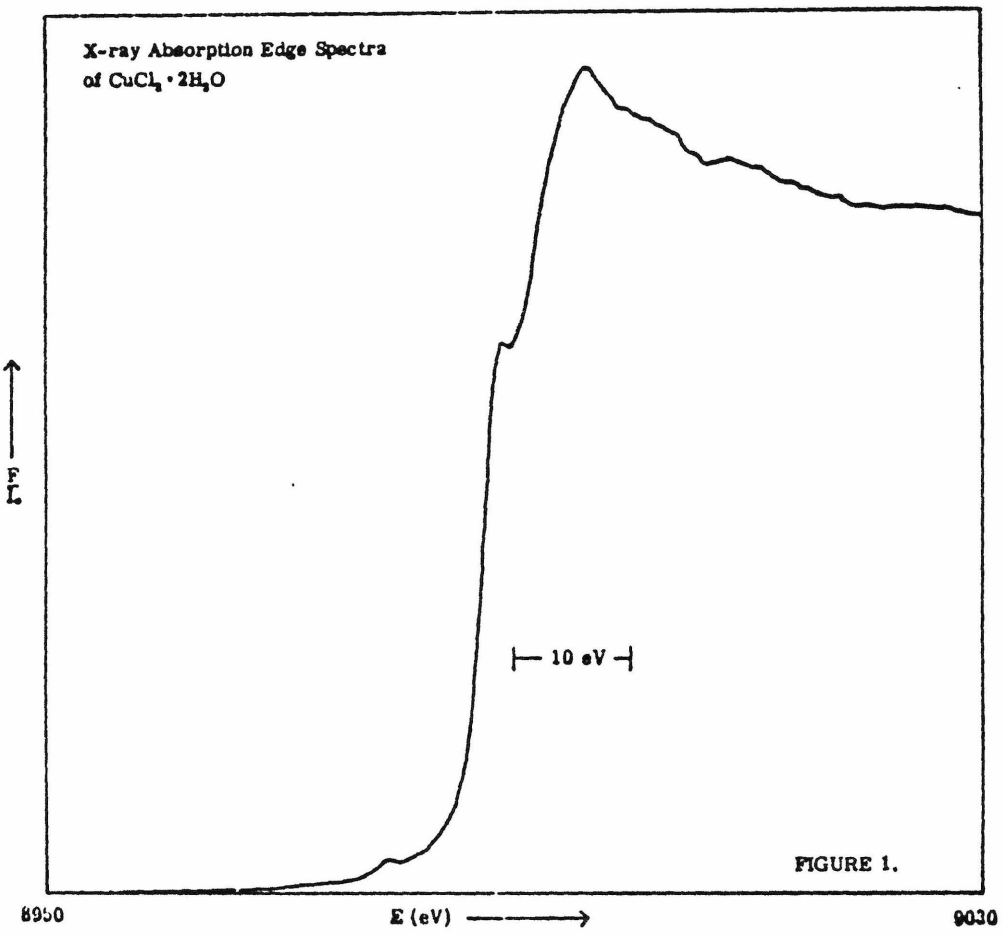

Figure 1. The EXAFS spectrum of crystalline $CuCl_2 \cdot 2H_2O$, courtesy of Chan et al., ref 2. Here each copper atom [Cu(II)] is octahedrally coordinated to four chlorines and two water molecules. This spectrum shows the three edge features typical of Cu(II) complexes.

absorption edge for a molecular system. We report calculations on excited states of the $CuCl_2$ molecule and Cu atom involving excitations from the 1s orbital of Cu, into the bound valence and virtual orbitals. $CuCl_2$ is a simple model that adequately demonstrates many of the features of the x-ray absorption edge to be found in other Cu(II) complexes. It has been observed in the gas phase[11] (although no EXAFS spectra have been reported). Details about the calculational methods used are in Section V.

II. Discussion

A. Copper Atom. We performed ab initio calculations involving excitations from the Cu 1s orbital as a benchmark with two purposes in mind. First, it has been proposed[9] that the splittings of the (1s) hole states of copper should be very similar to the splittings of the corresponding valence states of Zn atom (with the 1s doubly-occupied). We wished to test this hypothesis; and secondly, knowledge of the ab initio atomic splittings will be useful when considering the $CuCl_2$ complex in the next section.

Since Cu(II) complexes may often be considered as having $(3d)^9$ occupation on the metal, we calculated the 1s excitations of the corresponding Cu^{++} ion. The ground state of Cu^{++} is ^2D with a single 3d hole and no 4s electrons. The 1s excitations of Cu^{++} are compared with the corresponding valence and Rydberg states of Zn^{++} in Figure 2. Here we have chosen the $(1s)^1(3d)^{10}$ state of Cu^{++} and the $(1s)^2(3d)^{10}$ ground state of Zn^{++} as the zero in energy (the remaining n = 2 and n = 3 orbitals are filled). [To have consistent valence exchange interactions, we have compared the quartet excited states of Cu^{++} with the triplet states of Zn^{++}.] The SCF calculations are in good agreement with the five experimentally known Zn^{++} states. Considering the large excitation energies involved (10 to 40 eV above the ground state), the errors in our calculation (0.2 to 0.8 eV) are of minor importance.

Table I lists the results of calculations of the allowed Cu^{++} excitations from the 1s orbital to doublet excited states, along with the calculated oscillator strengths. Only the allowed electric dipole and electric quadrupole transitions are listed (there are no allowed magnetic dipole transitions from the 1s orbital). From these data we see that the lowest allowed electric dipole transition [(1s) → (4p)] is 87 times stronger than the allowed quadrupole transition [(1s) → (3d)].

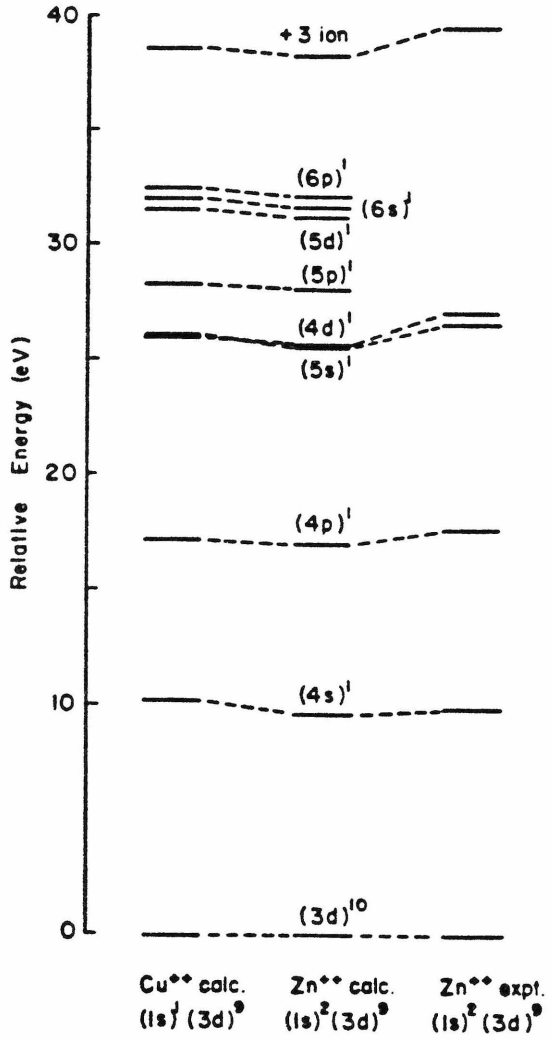

Figure 2. K-shell quartet excited states calculated for Cu^{++} as compared with the calculated and experimental[12] triplet valence excited states of Zn^{++}. In each case the remaining n = 2 and n = 3 levels are filled. The SCF calculations are described in Section V. The energies are the average of the five 3d hole states. Likewise, the experimental atomic states were averaged within each electronic configuration.

Table I. Low-Lying Electric Dipole and Quadrupole K-Shell Transitions of Cu^{++} from SCF Calculations

Term Symbol	Electron Configuration[a]	Transition	Excitation Energy (eV)	Oscillator Strength (f)
^2D	$(1s)^2(3d)^9$		-8894.14	ground state
^2S	$(1s)^1(3d)^{10}$	1s → 3d	0.0[b]	1.93×10^{-5}
^2D	$(1s)^1(3d)^9(4s)^1$	1s → 4s	10.43	0.0[c]
^2D			10.83	0.0[c]
^2P	$(1s)^1(3d)^9(4p)^1$	1s → 4p	16.85	0.00355
^2F			17.18	0.00583
^2F			17.38	0.00594
^2P			17.86	0.00149
			1s → 4p Total	0.01681
^2P	$(1s)^1(3d)^9(5p)^1$	1s → 5p	28.18	0.00130
^2F			28.29	0.00222
^2F			28.34	0.00202
^2P			28.48	0.00052
			1s → 5p Total	0.00606
^2P	$(1s)^1(3d)^9(6p)^1$	1s → 6p	32.39	0.00077
^2F			32.45	0.00165
^2F			32.46	0.00076
^2P			32.54	0.00027
			1s → 6p Total	0.00345

[a] The remaining orbitals of the n = 2 and n = 3 shells are filled.

[b] We choose the d^{10} excited state as the zero of energy.

[c] The transition to the 4s excited state is included as a reference; it is forbidden.

The splittings of the atomic Cu^{++} (1s) excitations are indeed quite similar to the splittings of the valence electronic states of Zn^{++}. In this sense the previous efforts[2, 9] to analyze the absorption edge features based on those Z = N + 1 atomic spectra cannot be faulted. However, in the following section, we will examine the differences in these states in a sample Cu(II) complex. There it will be shown that the ligands have a significant influence and introduce additional satellite transitions, not possible for the atomic ion. Also, in complexes, the charge on the Cu will tend to be closer to neutral, compressing the spectrum of Rydberg states into a smaller energy range.

B. $CuCl_2$. In this section we will describe the 1s excitations in the $CuCl_2$ system. Although this is a small complex with only two ligands, many of the ideas developed from the $CuCl_2$ calculations have direct application to larger transition metal complexes with more ligands and different metal centers. The ground state of $CuCl_2$ is $^2\Sigma_g^+$ and may be qualitatively considered as two chloride ions (Cl^-) along the z axis bound to a d^9 Cu^{++} atom (with the d_{z^2} orbital singly-occupied). In this discussion we will be concerned with the occupation of the Cu 1s and $3d_{z^2}$ orbitals as well as the highest occupied Cl ligand orbital of each symmetry. We will also be exciting into some of the unoccupied diffuse $CuCl_2$ orbitals (e.g., the 4s-like and 4p-like molecular orbitals). Hence, for the benefit of the reader we have constructed Table II which gives the occupation of these important orbitals in the ground state of $CuCl_2$ and in the various classes of excited states of interest.

Our calculated excitation energies for the lowest K shell excitations of $CuCl_2$ are listed in Table III. The calculated oscillator strengths of the allowed transitions are also shown in this table. As expected, the lowest energy transition corresponds to exciting the 1s electron into the 3d hole on the Cu. This

Table II. Occupation of the $CuCl_2$ Orbitals in Selected States[a]

State	Description	Orbitals Localized on Cu			Highest Cl 3p Orbitals			
		1s	$3d_{z^2}$	Rydberg	σ_g^+	σ_u^+	π_g	π_u
$^2\Sigma_g^+$	ground state	2	1	0	2	2	4	4
$^2\Sigma_g^+$	$1s \rightarrow 3d_{z^2}$	1	2	0	2	2	4	4
Shakedown Excitation	1s → Rydberg plus $\sigma_g^+ \rightarrow 3d_{z^2}$	1	2	1	1	2	4	4
Direct Excitation	1s → Rydberg	1	1	1	2	2	4	4

[a] The remaining n = 2 and n = 3 orbitals on Cu are doubly-occupied, as are the n = 1 and n = 2 orbitals on Cl. There are two doublet states arising from each three open-shell configuration.

Table III. Low-Lying K-Shell Excited States of $CuCl_2$ from Configuration Interaction Calculations

State	Description[a]	Excitation Energy (eV)	Oscillator Strength (f)
$^2\Sigma_g^+$	ground state	-8891.31	--
$^2\Sigma_g^+$	Cu 1s → $3d_{z^2}$	0.0[b]	1.92×10^{-5}
$^2\Sigma_g^+$	Cu 1s → 4s + shakedown	7.95[c]	0.0
		10.09[c]	0.0
$^2\Pi_u$	Cu 1s → $4p_\pi$ + shakedown	9.88	0.000204
		10.59	0.000071
$^2\Sigma_u^+$	Cu 1s → $4p_\sigma$ + shakedown	12.15	1.37×10^{-6}
		12.20	7.70×10^{-7}
$^2\Sigma_g^+$	Cu 1s → 4s	13.32[c]	0.0
		14.70[c]	0.0
$^2\Pi_u$	Cu 1s → $4p_\pi$	16.42	0.000595
		16.50	0.000721
$^2\Sigma_u^+$	Cu 1s → $4p_\sigma$	20.70	9.64×10^{-6}
		21.07	8.80×10^{-7}

[a] By $4p_\sigma$ and $4p_\pi$ we mean the low-lying Rydberg-like molecular orbitals of σ_g^+ and π_u symmetry that resemble the Cu 4p functions.

[b] We choose the d^{10} excited state as the zero of energy.

[c] The excitation energies into the 4s-like molecular orbital are from SCF calculations.

transition is electric dipole-forbidden but quadrupole-allowed. The oscillator strength[13] is small ($f = 1.92 \times 10^{-5}$), and almost identical to the value for the atomic ion. Experimentally, high resolution x-ray absorption edge spectra of Mn, Fe, Co, and Ni and Cu complexes all show a small feature on the low energy side of the main absorption edge (e.g., see Figure 1).[2, 9, 14] This has been previously identified as the $1s \rightarrow 3d$(-hole) transition. In fact, for $KFeF_3$ and K_2NaF_6 crystals, the EXAFS spectra of Shulman and co-workers[9] show both the $1s \rightarrow 3d_{t_2}$ and $1s \rightarrow 3d_e$ absorption features. The transition energies differ by approximately the value of 10 D_q for these complexes, as expected. It has been proposed that vibronic coupling serves to increase the intensity of these $(1s)^2d^n \rightarrow (1s)^1d^{n+1}$ transitions by mixing p character into the upper states. This would introduce an electric dipole component into the transition and increase its intensity. However, we find that the electric quadrupole transition moment calculated for $CuCl_2$ leads to an intensity comparable to the observed values without vibrational enhancement (of course, such enhancement may also be present). We will often use this transition (the lowest energy peak) as the relative zero of energy.

In the range of 8 to 12 eV (Table III) above the first $^2\Sigma_g^+$ excited state, there are four sets of states that can be termed shakedown transitions. To explain, we will first consider the ionization of $CuCl_2$ from the Cu 1s level. Our calculations show that when the 1s electron is removed and the wavefunction permitted to relax, the ground state changes from d^9 in $CuCl_2$ to d^{10} in $CuCl_2^+$. The electron that fills the d_{z^2} hole can come from any one of the highest occupied ligand orbitals. Table IV lists the energies of the states formed by ionization directly from the Cu (1s) and also the shakedown ionizations from the highest ligand orbitals of each symmetry. Note that all four of the shakedown d^{10} ions are 6 to 8 eV lower than the d^9 ion. This shakedown process is

Table IV. Calculated K-Shell Ionization Potentials of $CuCl_2$

State	Ligand Hole[a]	Ionization Potential (eV)	Relative Energy (eV)
$^3\Sigma_g^+$	Cu $3d_{z^2}$	8914.8	0
$^3\Sigma_g^+$	σ_g^+	8908.3	-6.5
$^3\Sigma_u^+$	σ_u^+	8907.9	-6.9
$^3\Pi_u$	π_u	8907.2	-7.6
$^3\Pi_g$	π_g	8906.9	-7.9

[a] In each case the ligand hole is the highest occupied molecular orbital of the indicated symmetry.

similar to a ligand-to-metal charge transfer, though the net charge on the Cu does not change appreciably (since the other valence orbitals polarize to neutralize any charge separation). These $CuCl_2^+$ results suggest that a Cu 1s-to-Rydberg transition plus a simultaneous shakedown in the form of a ligand-to-metal charge transfer should produce states lower in energy than the direct Cu 1s-to-Rydberg transition, without the shakedown. Our results (in Table III) confirm this analysis. There is a 5 to 9 eV separation between the corresponding direct and shakedown states in $CuCl_2$. This separation corresponds closely to the splitting (6 to 8 eV) of the d^9 and d^{10} ions of Table IV.

To illustrate, we will explicitly consider one set of the shakedown excitations--those where the highest σ_g ligand orbital is singly-occupied. This σ_g ligand orbital has the same symmetry as the Cu d_{z^2} orbital, so in this case we can consider that the d_{z^2} hole, which was localized on the Cu in the ground state has readjusted to become localized on the chlorines in the excited state. The lowest such shakedown state involves the Cu 1s excitation to a Cu 4s-like orbital. This 4s orbital is plotted in Figure 3 along with the atomic 4s orbital for Cu^{++}. We can see that the molecular orbital (of σ_g^+ symmetry) is more diffuse than the atomic orbital and has a significant amount of ligand character. This transition leads to two $^2\Sigma_g^+$ states, differing in the spin coupling of the three open-shell electrons. (These are separated by approximately twice the Cu $3d_{z^2}$ - 4s exchange interaction.) Both components are symmetry-forbidden, so that this 1s-to-4s shakedown transition is not to be observed.

The next higher shakedown state (with σ_g^+ ligand hole) involves the 1s-to-$4p_\pi$ transition ($4p_x$ or $4p_y$). In this case, the $4p_\pi$ orbitals are slightly larger than the atomic 4p orbitals (see Figure 3). This transition to the $^2\Pi_u$ excited state is symmetry-allowed, though we find that it is not very strong

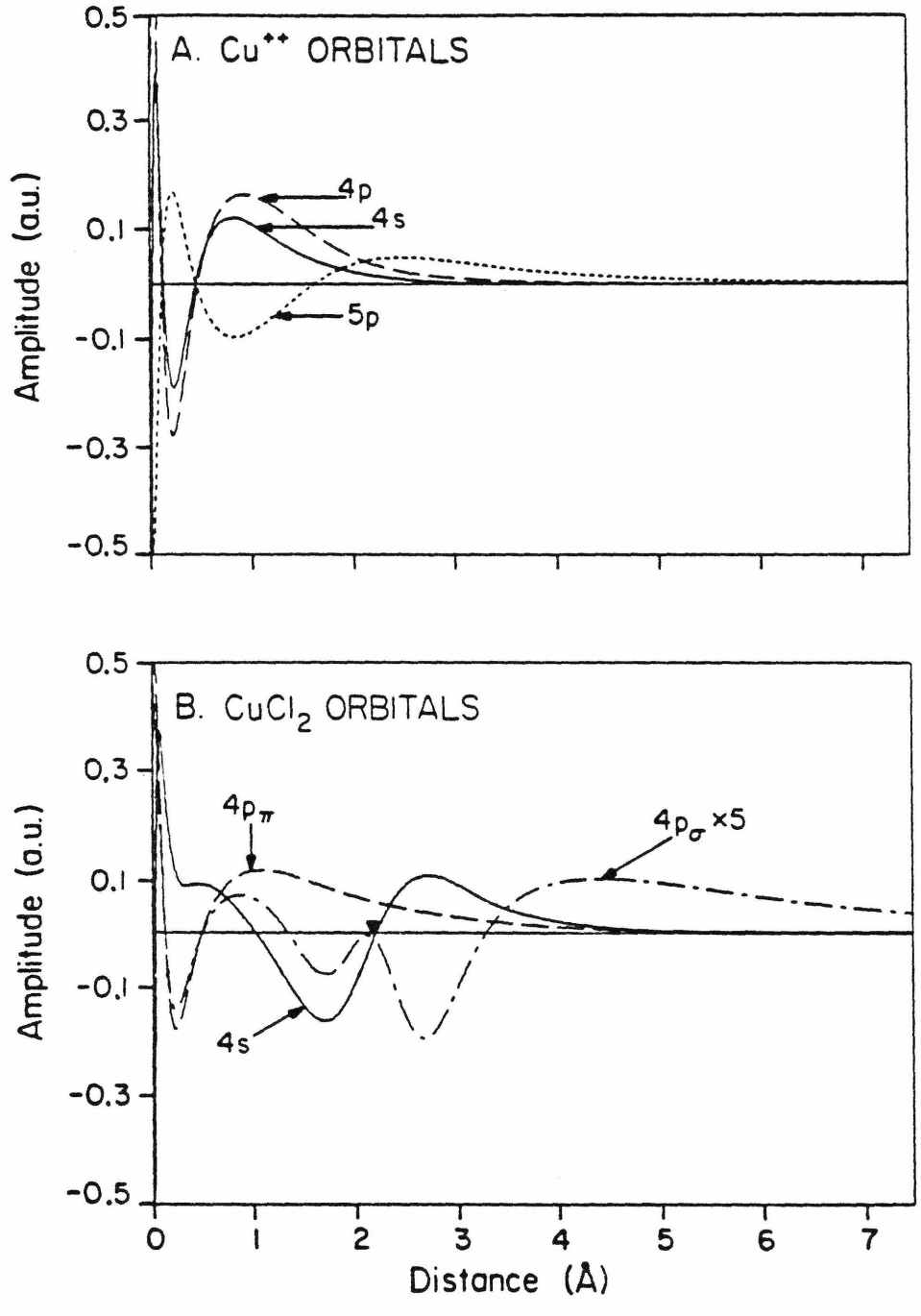

Figure 3. Orbital amplitudes as a function of distance from the Cu for the excited state 4s, 4p, and 5p orbitals of Cu^{++} (A) and the 4s, $4p_\pi$ and $4p_\sigma$ orbitals of $CuCl_2$ (B). For $CuCl_2$, the 4s and $4p_\sigma$ amplitudes are shown along the molecular axis, while the $4p_\pi$ amplitude is perpendicular to this axis.

($f = 2.7 \times 10^{-4}$, Table III). The reason it has a small oscillator strength lies in the nature of the shakedown process. Qualitatively, the transition moment for all these shakedown transitions varies as the transition moment from the 1s to the virtual orbital ($4p_\pi$ in this case) times the overlap of the d_{z^2} orbital of the ground state wavefunction with the singly-occupied ligand orbital in the excited state[15] (highest σ_g^+ in this case). For this reason the transition moments for the shakedown transitions are smaller than the direct transitions by a factor of this overlap. Also, only shakedown transitions involving the σ_g^+ ligand orbitals will have any intensity since only those ligand orbitals can overlap with the Cu d_{z^2} orbital. Note that the ground state $3d_{z^2}$ orbital can overlap the excited state σ_g^+ orbital since the excited state wavefunction is allowed to relax (self-consistently). The orbitals change shape in the excited state, leading to an overlap of ~ 0.37 in this case (the total many-electron wavefunctions do not, of course, overlap). The amplitudes of these two orbitals are plotted in Figure 4 ($\hat{a}$ is d_{z^2}, $\hat{b}$ is ligand σ_g).

The next shakedown state in this series is to a Cu 5s-like orbital. It is also forbidden. At 1.9 eV above the excitation to the $4p_\pi$ states we find the transition to the $4p_z$. This $4p_z$ orbital, plotted in Figure 3 together with the Cu^{++} atomic orbital, is strongly affected by the proximity of the occupied Cl orbitals and has been pushed higher in energy. This leads to the 1.9 eV splitting, which has implications for four- and six-coordinated complexes, as discussed later. Also, the more diffuse nature of the $4p_z$ orbital reduces the strength of this transition, relative to the corresponding $4p_\pi$ state.

We assign these (1s → 4p) shakedown transitions (both $4p_\pi$ and $4p_\sigma$) to the absorption peak commonly identified as the 1s → "4s" direct transition (see Figure 1). There are two factors to consider in reassigning this absorption edge feature. The first is intensity. We find that the 1s-to-4p shakedown is

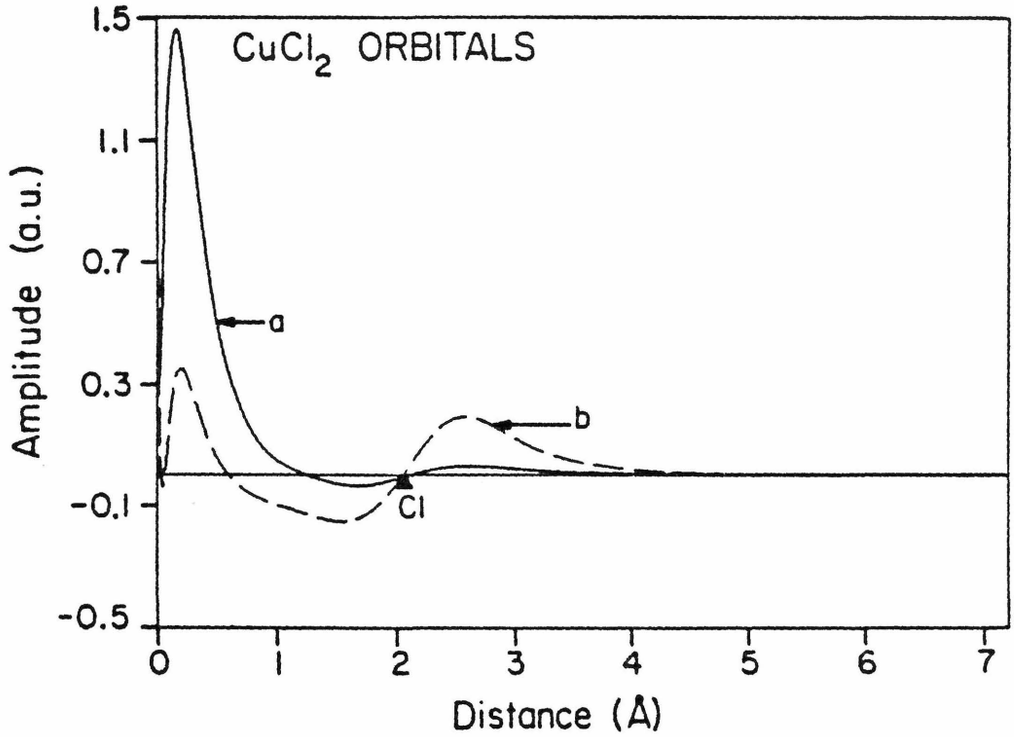

Figure 4. Orbital amplitudes as a function of distance along the $CuCl_2$ molecular axis. The solid line (a) is the amplitude of the singly-occupied $3d_{z^2}$ orbital in the ground state. The dashed line (b) is the amplitude of the singly-occupied ligand σ_g^+ orbital in the shakedown excited states. Note the overlap of these two orbitals.

80% weaker than the 1s-to-4p direct transition, whereas the 1s-to-4s direct transition is symmetry-forbidden. Even in complexes with low symmetry, considerable p character would have to be built into the lowest unoccupied molecular orbital (about 14%) for the intensity to rival that of our $1s \rightarrow 4p$ shakedown transition. The second factor is energy position. We find that although the 1s-4s transition is ~ 6.6 eV below $1s \rightarrow 4p$ in Cu^{++} ions, it is displaced in $CuCl_2$ to be only 2.2 eV below $1s \rightarrow 4p$ (due to interactions of the excited orbital with the ligands). We find the $1s \rightarrow 4p$ shakedown transition at ~ 7.5 eV below the $1s \rightarrow 4p$ direct; about the same location as observed experimentally. Empirical evidence in favor of our reassignment can be obtained from studies of the first-row transition metal fluorides.[9] Shulman et al.[9] find that the difference in energy between the 1s-to-"4s" (1s-to-4p plus shakedown in our assignment) and 1s-to-4p is nearly constant for the divalent elements Mn(II) through Ni(II). This result is consistent with either assignment. However, the 1s-to-4s assignment predicts a large (10 eV) "4s"-4p splitting for the corresponding Fe(III) complex in the next higher oxidation state. Here our assignment would predict a smaller increase in the splitting of the 1s-to-4p + shakeup, versus the 1s-to-4p direct states. This splitting is just the difference in energy between the $L_e^4 d^n$ configuration (where L_e is the highest ligand e level) and the $L_e^3 d^{n+1}$ configuration resulting from the shakedown process, which is expected to be approximately constant with changes in oxidation state of the metal. Thus the 7 eV splitting observed[9] for K_2NaFeF_6 is more consistent with our assignment. Similar arguments apply to the analysis of the higher states in this series. The transitions to s- or d-like unoccupied orbitals are forbidden and those to p-like orbitals are allowed.

Shakedowns from the other three high ligand orbitals (see Table II) give the same ordering of states in the same energy range (Table V) and will not

Table V. Calculated K-Shell Excited States Involving Shakedown for $CuCl_2$

Rydberg Orbital Occupied in Excited State	Excited State Energy (eV) for Each Ligand Hole[a]			
	σ_g^+	σ_u^+	π_g	π_u
4s	7.95, 10.09	7.12, 9.69	6.62, 6.80	6.90, 7.15
$4p_\pi$	9.88, 10.59	9.62, 9.73	8.26-9.56	8.52-9.74
$4p_\sigma$	12.15, 12.20	11.60, 11.67	10.68, 10.74	10.98, 11.04

[a] Using the $(1s)^1(3d)^{10}$ state as the zero of energy.

be discussed separately. However, these transitions are symmetry-forbidden from the ground state.

Finally, at 13 eV above the lowest excited state ($^2\Sigma_g^+$) we calculate the first direct transition from the Cu 1s to the 4s-like unoccupied molecular orbital. This transition is forbidden. The next state, a transition to the $4p_\pi$ is allowed and occurs 6.2 eV above the corresponding shakedown state. The $4p_\sigma$ ($4p_z$) level occurs 4.4 eV above the $4p_\pi$ level. This splitting is caused by the axial ligands, and would be much smaller in tetrahedrally or octahedrally coordinated Cu^{II} complexes. The $5p_\pi$ states occur 3.1 eV above the n = 4 levels and are expected to be much weaker, since the intensity of this transition falls off rapidly as the size of the np orbital increases. Similarly, the $5p_\sigma$ state is 1 eV above the $4p_\sigma$ state, though the $5p_\sigma$-like orbital is so diffuse that our description of this particular state is less accurate than the others.

We find that the oscillator strength of the atomic 1s-to-4p transitions is decreased by a factor of 12 in $CuCl_2$ (Tables I and III). The molecular 4p orbitals are more diffuse than atomic 4p orbitals and indeed are comparable in size to atomic 5p orbitals. Since the 1s-to-5p atomic transition is a factor of 2.8 weaker than 1s-to-4p, this size difference could account for a major part of the decrease in intensity in the molecular transition. In addition, the $CuCl_2$ excited 4p orbital has character on the ligands, further decreasing the intensity (for the transition from Cu 1s).

On the other hand, the direct transitions are 4.8 times as strong as the shakedown transitions. From the overlap of the ground state $3d_{z^2}$ orbital and the shakedown excited state open-shell ligand sigma orbital (S = 0.37), we would expect a factor of 7.1. Thus, qualitatively, the transition moment from the 1s to the 4p is similar, and the difference in intensity arises primarily from the overlap term introduced by the shakedown.

In conclusion, our $CuCl_2$ calculations allow us to make assignments of the common three absorption edge features of Cu^{II} EXAFS spectra. The lowest energy transition is a weak quadrupole-allowed Cu 1s – 3d transition. The next absorption corresponds to the dipole-allowed 1s-to-4p plus ligand-to-metal shakedown, and the most intense peak is the direct 1s-to-4p transition. It is important to note that in each case the spectral feature has been assigned to an allowed transition. This differentiates our assignment of the middle peak from previous work and has implications about the x-ray absorption edge spectroscopy of the transition metals, as illustrated in the next section.

III. Applications to Other Systems

In this section we will consider the application of our ideas about Cu II systems to the other transition metals in the Cu row. Also, we will briefly discuss the effects of mixed ligands and low symmetry. First we examine the divalent transition metal fluorides, KMF_3, where the metal occupies an octahedral site.

The EXAFS spectra are available[9] for Mn^{II} through Zn^{II}, with the exception of Cu. Of these, Mn^{II} through Cu^{II} all have an unfilled e_g-type metal d orbital. Thus we expect to observe at least three transitions on the absorption edge. At low energy there is an electric quadrupole-allowed 1s → 3d transition with low intensity. In the metals with an unoccupied t_2-type d orbital (as in V^{II} through Co^{II}), the 1s → 3d transition may be split into 1s → $3d_e$ and 1s → $3d_{t_2}$ components. The energy separation is approximately 10 D_q for the corresponding complex containing the metal of the next higher atomic number.[17] Then, about 5-7 eV higher there is a shoulder,[9] representing a 1s → 4p plus shakedown transition of intermediate intensity. Finally, at the apex of the edge, there is a strong 1s → 4p transition.

For Zn^{II}, there are no d holes so we do not expect either 1s → 3d or shakedown transitions. It would then be consistent to assign the lowest energy feature to the 1s → 4p. However, two peaks are observed at the top of the absorption edge.[9] Even assuming strong vibrational coupling, the lower energy peak appears much stronger than would be reasonable for a 1s → 4s transition. Therefore we tentatively reassign the lower energy peak to the 1s → 4p, which should be a strong transition. There are several possibilities for the origin of the higher energy transitions, including (1) a 1s → 4p plus shakeup state (where this shakeup would involve a transition from a 3d orbital to a virtual orbital of the same symmetry) or (2) the 1s → 5p transition.

Now, considering the first part of the row (Ti^{II} through Cr^{II}), we expect the trifluoride crystals to have qualitatively the same absorption edge features as for Mn^{II} through Cu^{II}, with one notable exception. This exception is Cr^{II}, which is formally d^4. For this metal the ligand-to-metal shakedown has two nondegenerate components. Since the Cr^{II} 3d e_g level has only one electron, the electron that comes from the ligand e_g orbital into the 3d e_g level may be either singlet- or triplet-coupled to the single 3d electron already there. Both of these 3d spin configurations may be coupled to the remaining 1s and 4p singly-occupied orbitals to produce an overall quintet excited state. This splitting should be about twice the 3d exchange integral (for the excited state), around 1.2 to 1.9 eV. Thus, in the Cr^{II} trihalide crystal, the EXAFS experiment is predicted to show two shakedown transitions. This experiment, if performed, may serve to differentiate our assignment of the second peak from the 1s → 4s assignment made previously. The 1s → 4s transition is also split into two components; however, the energy difference is only twice the 3d-4s exchange interaction, which is smaller, about 0.4 to 0.6 eV.

Now we consider the qualitative features of the edge spectra of mixed ligand complexes for the first transition series. Here, each chemically different ligand may give rise to a shakedown transition of a different energy. This transition can be described as a metal 1s → 4p plus a ligand-to-metal charge transfer involving the ligand lone-pair sigma bonding to the metal and the metal d orbital(s) oriented sigma to this ligand orbital. If there are several ligands of the same type, a particular shakedown transition may be enhanced. Of course this analysis applies best to ionic bonds. Covalently bound ligands may have such satellite transitions that are actually higher in energy than the corresponding direct transition. In addition,

the 4p virtual orbitals are not degenerate in complexes with low symmetry. In fact, our $CuCl_2$ calculations show a 2-4 eV splitting, probably an extreme. Because of this splitting, it may be possible to observe the components of both the 1s→4p shakedown and the 1s→4p direct transitions. This would provide some supportive information about bond angles and molecular symmetry. Along this vein, we have initiated calculations to compare square planar and tetrahedral conformations of a model Cu complex.

IV. Summary

We have carried out ab initio SCF and configuration interaction calculations on the $CuCl_2$ system and related our results to the K edge x-ray absorption spectra of transition metal complexes. The three common features on the K edge were described by our calculations. The assignment of the 1s → 3d and 1s → 4p transitions agrees with previous assignments. We have reassigned the 1s → "4s" transition as an allowed 1s-to-4p transition with a concurrent ligand-to-metal shakedown. This shakedown involves the ligand orbital sigma to the metal and a d-hole sigma to the ligand.

V. Details of the Calculations

A. Basis Set. All of the calculations used the Cu (^{2}S) gaussian basis set of Wachters[18] with the first six s functions, the first five p functions, and the first four d functions contracted to form a single final s, p, and d basis function, respectively. The remaining functions were left uncontracted. This contraction system allows more flexibility in the Cu core functions than the usual double zeta contraction of Wachters functions. We felt that this extra flexibility was necessary to adequately describe the core electronic relaxation after 1s excitation. In addition, we replaced the two 4s functions of the Wachters basis with four gaussians having exponents of 0.3324, 0.1108, 0.03166, and 0.008442 in order to also describe both 4s-like and 5s-like orbitals. Similarly, we replaced the outer two 4p functions with four gaussians (0.2099, 0.05998, 0.01714, and 0.004570) in order to describe both 4p-like and 5p-like orbitals. We also added two diffuse d functions with gaussian exponents of 0.1168 and 0.0329. Altogether, this gives a basis size of 62 final functions on the metal and more than double zeta quality (only the innermost 1s, 2p, and 3d functions contracted). For the Cl atoms in the $CuCl_2$ calculations, we used an effective potential[19] to replace the Ne core of Cl. This potential reduces the Cl basis set to those functions describing the valence orbitals. This double zeta Cl basis was contracted[20] to a minimum basis set by explicit optimization of the contraction for $CuCl_2$. Thus, our final Cl basis consisted of four functions, with the contraction optimized for $CuCl_2$. The CuCl bond distance of 2.17 Å was taken from SCF calculations[21] (double zeta basis) on $CuCl_2$. (The experimental bond distance is not known.)

VI. Wavefunctions

To calculate the atomic excitation energies, we carried out SCF calculations using the fully-optimized open-shell Hartree-Fock wavefunctions. For the atomic wavefunctions with $(3d)^9$ occupation, we solve for an average d^9 state in the same manner as reported previously.[22] Here the variational hamiltonian (Fock operator) was derived from the average energy of the five possible d holes. Some of the excited state atomic wavefunctions were constructed using the improved virtual orbital (IVO) method.[23] In general, all the Rydberg states could be obtained from a single SCF calculation for the lowest Rydberg state and a set of IVO's providing an orthogonal set of Rydberg orbitals. We checked these IVO results by performing additional SCF calculations on the Cu^{++} ion. The largest error for any state in Figure 2 was 0.06 eV. The Rydberg states were calculated as high-spin (quartets) and we performed a small CI calculation to obtain the energies for the low-spin (doublet) states. Indeed, the manifold of states arising from the quartet SCF + IVO calculations is energetically almost the same (0.03 eV difference) as the average of the corresponding doublet states from the CI, thus justifying this straightforward approach. (This result is expected since the exchange interactions between the 1s and open-shell valence orbitals are small.) The atomic oscillator strengths were determined by calculating the (length-form) transition moments between the ground and excited state SCF wavefunctions, allowing electronic relaxation,[24] and including the correct excited state spin-coupling as optimized in the CI. Again, since the excited doublet and quartet states are so close in energy, we could use the SCF orbitals from the quartet state to describe the doublet states.

For the $CuCl_2$ complex, the same kind of open-shell SCF calculations were carried out, but without averaging the 3d hole. Here we found an accurate,

simple method for obtaining the spectrum of excited states for the direct and shakedown transitions. For those states with an occupied Rydberg orbital, we removed the Rydberg electron and calculated the corresponding positive ion wavefunction by SCF methods. Then we froze the occupied orbitals, replaced the Rydberg electron, and calculated the spectrum of orthogonal Rydberg orbitals. These results agreed within 0.007 eV of the fully relaxed SCF results for the several cases we tested. Again, as for the atom, we obtained the Rydberg states as quartets, and performed a small CI to get the doublet energies. The oscillator strengths were calculated by two different methods. First we calculated the moments between the ground and excited state SCF wavefunctions, allowing electronic relaxation and including the correct excited state spin coupling for the three open-shell electrons (as we did for Cu^{++}). The second method used the entire set of occupied orbitals from the ground and excited state in a larger CI. This orbital set included the 22 orbitals of the ground state SCF wavefunctions, the 23 orbitals of the $(1s)^1(4p_x)^1$ plus shakedown excited state, and the $4p_z$ virtual orbital (all orthogonalized). The CI configuration list included the ground state configuration, the four excited state configurations (shakedown and direct to $4p_x$ and $4p_z$), and all single excitations from these four configurations requiring that the 1s orbital be singly-occupied. This configuration list was adequate to describe the ground state, the 1s → 3d transition, and the 1s → 4p transitions (both shakedown and direct). The oscillator strengths were then calculated for these states of the CI. The results for both methods are presented in Table VI. This table shows that both approaches produce similar oscillator strengths. The agreement for the lower energy excited states is much better than for the higher ones. However, our aim was to determine the relative strength of these transitions, which we accomplished with a set of simple and consistent wavefunctions. Certainly this purpose was achieved,

Table VI. Comparison of Excitation Energies and Oscillator Strengths of $CuCl_2$ Transitions Calculated by SCF and CI Methods

State	SCF Excitation Energy (eV)	SCF Oscillator Strength (f)	CI Excitation Energy (eV)	CI Oscillator Strength (f)
$^2\Sigma_g^+$ [a]	0.0	1.92×10^{-5}	0.0	1.92×10^{-5}
$^2\Pi_u$	10.03	1.28×10^{-4}	9.88	2.04×10^{-4}
	11.04	3.67×10^{-5}	10.59	7.13×10^{-5}
$^2\Sigma_u^+$	12.47	2.10×10^{-6}	12.15	1.37×10^{-6}
	12.55	1.09×10^{-6}	12.20	2.70×10^{-7}
$^2\Pi_u$	15.74	5.35×10^{-4}	16.42	5.95×10^{-4}
	15.88	2.79×10^{-4}	16.50	7.21×10^{-4}
$^2\Sigma_u^+$	18.91	1.85×10^{-5}	20.70	9.64×10^{-6}
	18.95	2.05×10^{-7}	21.07	8.80×10^{-7}

[a] This is the Cu $(1s)^1(3d)^{10}$ excited state.

although in an absolute sense, oscillator strengths often vary (systematically) from the true value by a factor of 2 to 3 for such wavefunctions.

Acknowledgments

The author gratefully acknowledges support provided by a traineeship from the National Institutes of Health. Computing assistance was obtained from the Health Sciences Computing Facility of the University of California, Los Angeles, supported by the National Institutes of Health Research Resources Grant RR-3. This work was partially supported by NIH Research Grant GM-23971 from the National Institute of General Medical Sciences. Some of the calculations were carried out on the Dreyfus-NSF Chemistry Department DEC VAX 11/780 Computer, funded by grants from the Camille and Henry Dreyfus Foundation and from the National Science Foundation.

References and Notes

(1) R. G. Shulman, P. Eisenberger, and B. M. Kincaid, Annu. Rev. Biophys. Bioeng., 7, 559 (1978).

(2) S. I. Chan, V. W. Hu, and R. C. Gamble, J. Mol. Struct., 45, 239 (1978).

(3) V. W. Hu, S. I. Chan, and G. S. Brown, Proc. Natl. Acad. Sci. U. S. A., 74, 3821 (1977).

(4) T. D. Tullius, P. Frank, and K. O. Hodgson, Proc. Natl. Acad. Sci. U.S.A., 75, 4069 (1978).

(5) W. E. Blumberg, J. Peisach, P. Eisenberger, and J. A. Fee, Biochemistry, 17, 1842 (1978).

(6) J. H. Sinfelt, G. H. Via, and F. W. Lytle, J. Chem. Phys., 68, 2009 (1978).

(7) P. Eisenberger and B. M. Kincaid, Chem. Phys. Lett., 36, 134 (1977).

(8) G. Martens, P. Rabe, N. Schwentner, and A. Werner, Phys. Rev. B, 17, 1481 (1978).

(9) R. G. Shulman, Y. Yafet, P. Eisenberger, and W. E. Blumberg, Proc. Natl. Acad. Sci. U.S.A., 73, 1384 (1976).

(10) F. A. Cotton and C. J. Ballhausen, J. Chem. Phys., 25, 617 (1956).

(11) C. W. DeKock and D. M. Gruen, J. Chem. Phys., 44, 4387 (1966); 49, 4521 (1968).

(12) C. E. Moore, "Atomic Energy Levels", National Bureau of Standards Circular, Vol. II, 1971.

(13) For the electric quadrupole transitions, our oscillator strengths are: $f = \frac{2}{3}(\Delta E^3/C^2)M^2$, where M is the electric quadrupole transition moment between the two states of interest, c is the speed of light, and all quantities are in atomic units.

(14) R. G. Shulman, P. Eisenberger, B. K. Teo, B. M. Kincaid, and G. S. Brown, J. Mol. Biol., 124, 305 (1978).

(15) Not allowing the wavefunction to relax, the 1s-to-$4p_z$ oscillator strength is

$$f = \tfrac{2}{3}\Delta E \langle \phi_{1s} | \underset{\sim}{z} | \phi_{4p} \rangle^2,$$

where ϕ_{1s} and ϕ_{4p_z} are the 1s and $4p_z$ orbitals of the frozen wavefunction. However, allowing the wavefunction to relax upon excitation introduces additional overlap factors. Most of the overlaps are very nearly 1, so they can be ignored here. However, in $CuCl_2$, the ground state is d^9 with the d_{z^2} singly-occupied and the shakedown excited state is d^{10} with a singly-occupied ligand orbital. This introduces a factor of the overlap of the ground state $3d_{z^2}$ orbital, $\phi_{3d_{z^2}}$ and the excited state ϕ'_L singly-occupied ligand orbital. Thus, in this case,

$$f = \tfrac{2}{3}\Delta E \left[\langle \phi_{1s} | x | \phi'_{4p_z} \rangle \langle \phi_{3d_{z^2}} | \phi'_L \rangle\right]^2,$$

where the overlap is ~ 0.37.

(16) M. A. Hepworth, K. H. Jack, R. D. Peacock, and G. J. Westland, Acta Crystallogr., 10, 63 (1957).

(17) This splitting is shown clearly in the iron-fluoride spectra of Shulman and coworkers, ref 14.

(18) A. J. Wachters, J. Chem. Phys., 52, 1033 (1970).

(19) A. K. Rappé, T. A. Smedley, and W. A. Goddard III, manuscript in preparation.

(20) A. K. Rappé and W. A. Goddard III, unpublished results.

(21) A. F. Voter and W. A. Goddard III, unpublished results.

(22) R. A. Bair and W. A. Goddard III, J. Am. Chem. Soc., 99, 3505 (1977).

(23) W. J. Hunt and W. A. Goddard III, Chem. Phys. Lett., 3, 414 (1969).

(24) Our transition moments were calculated from separate SCF wavefunctions for the ground and excited states. This makes the actual evaluation of the moments much more difficult, but it is necessary since there is so much relaxation in the wavefunction in the (1s) hole states.

Part B:

ELECTRON CORRELATION CONSISTENT CALCULATION OF BOND DISSOCIATION ENERGIES

PREFACE

A detailed knowledge of the thermochemistry of reaction intermediates is fundamental to the understanding of microscopic reaction mechanisms. Experimental thermochemical data are available for some chemical species; however, many (most) intermediates are difficult, if not impossible, to observe experimentally. The research discussed in Part B of this thesis describes a systematic theoretical method for accurate ab initio calculation of bond dissociation energies.

The method described herein is directly applicable to the calculation of bond energies of large systems, for example, the central C-C bond of $(CH_3)_3C\text{-}C(CH_3)_3$ with our "standard" electronic structure programs. The research results are divided into three sections. The first section is a paper describing the method as it applies to the calculation of the R-H bonds of the first-row hydrides: CH_4, NH_3, OH, and FH. The second paper discusses the calculation of the R-R bond strengths of C_2H_6, N_2H_4, H_2O_2, and F_2. These two papers compare our results with well-known experimental dissociation energies. These benchmark comparisons establish the validity of our approach. In the third paper, we calculate all of the O-O, O-C, and O-H bond dissociation energies of the three hydro- and methyl peroxides: H_2O_2, CH_3OOH, and CH_3OOCH_3. As supporting work, we also report calculations of the C-O bond energies of CH_3OH and CH_3O^-; the O-H bond energies of $[OH]_3^-$, CH_3OH, and C_2H_5OH; and the electron affinities of F, OH, and CH_3O. Overall, the calculations produced very good results. The errors are small and systematic, so that accurate determinations of substituent effects could be made. Finally, a fourth paper describing calculations of the equilibrium structures of HOOH, CH_3OOH, CH_3OOCH_3, $HOO\cdot$, and $CH_3OO\cdot$ is included as an Appendix.

Chapter 1:

Application to Calculation of the R-H Bond Energies of CH_4, NH_3, H_2O, and HF

I. Introduction

A systematic theoretical method for accurate calculation of bond dissociation energies would be a useful tool for the thermochemical study of competing pathways of organic reaction mechanisms. In this paper we present the structure of our method, as it applies to R-H bonds for the first-row hydrides: CH_4, NH_3, H_2O, and HF. These simple species span a range from rather covalent bonds (e.g., CH_4) to rather ionic bonds (e.g., HF). Good experimental thermochemical data are available for these molecules and the corresponding radicals: CH_3, NH_2, OH, and F. This allows us to readily assess the validity of the calculations and to determine any systematic errors. The results of the calculations, in Table I, show very good agreement between the experimental and theoretical studies. Our errors range from 2.5 to 3.5 kcal (average value 2.9), systematically lower than the experimental values.

Table I. Theoretical and Experimental R-H Bond Dissociation Energies (kcal). Calculated Values are from DC-CI.

Molecule	$\Delta H^0_{f_{298°K}}$ (R-H)		D_0 (R-H)		D_e (R-H)		Difference
	Calc.	Expt.	Calc.	Expt.	Calc.	Expt.	Expt.-Calc.
CH_4	101.3	104.8	99.8	103.3	108.8	112.3	3.5
NH_3	104.9	107.4	103.5	106.0	112.9	115.4	2.5
H_2O	116.4	119.4	115.1	118.1	122.6	125.6	3.0
HF	133.4	136.1	132.4	135.1	138.3	141.0	2.7

II. Calculational Method

In this section we will outline a general scheme for calculating bond energies. Details of the calculations are given in the following section. Of course, the proper treatment of electron correlation is essential in correctly describing bond dissociation. However, we will concentrate on including only those correlation modes that are important in describing the bond of interest, rather than trying to retrieve the maximum amount of correlation energy. This is an important distinction, as it shifts the emphasis from calculation of the best possible electronic energy for each species to calculation of consistent bond energies with easily analyzed wavefunctions.

Throughout we use a localized orbital description of the wavefunctions. In our calculations we first solve self-consistently for the generalized valence bond (GVB) orbitals, where each valence electron has its own optimized orbital (including lone pairs). The orbital plots are shown in Figures 1-8. For example, the GVB wavefunction for H_2O can be written as

$$\psi = \frac{1}{N} \mathcal{A}\{[\phi(1s)\phi(1s)\alpha\beta][\phi_{\ell}(OH_1)\phi_r(OH_1)(\alpha\beta - \beta\alpha)]$$
$$\times [\phi_{\ell}(OH_2)\phi_r(OH_2)(\alpha\beta - \beta\alpha)][\phi_{in}(LP_1)\phi_{out}(LP_1)(\alpha\beta - \beta\alpha)]$$
$$\times [\phi_{in}(LP_2)\phi_{out}(LP_2)(\alpha\beta - \beta\alpha)]\}$$

or in natural orbital form

$$\psi = \frac{1}{N'} \mathcal{A}\{[\phi(1s)^2][\phi_a(OH_1)^2 - \lambda_1\phi_b(OH_1)^2]$$
$$\times [\phi_a(OH_2)^2 - \lambda_2\phi_b(OH_2)^2][\phi_a(LP_1)^2 - \lambda_3\phi_b(LP_1)^2]$$
$$\times [\phi_a(LP_2)^2 - \lambda_4\phi_b(LP_2)^2](\alpha\beta\alpha\beta\alpha\beta\ldots)\},$$

Figure 1. GVB Orbitals of CH_3

C-H Bond Pair

(One of three equivalent C-H bonds)

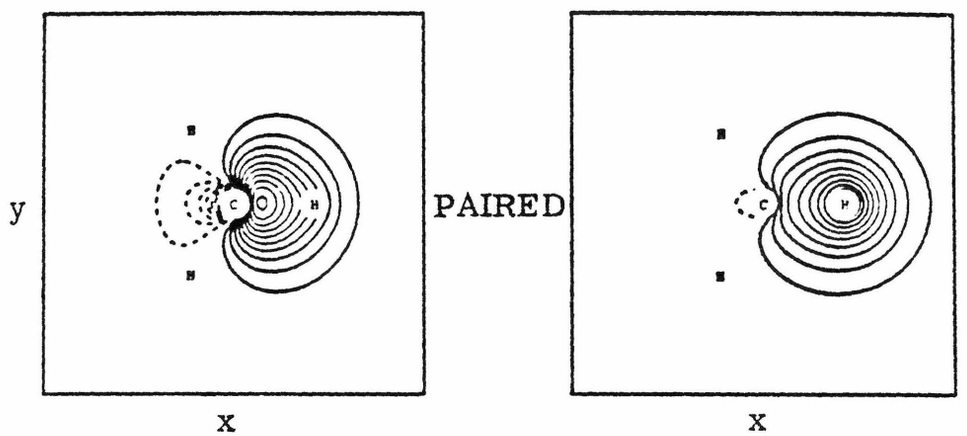

C Radical Orbital

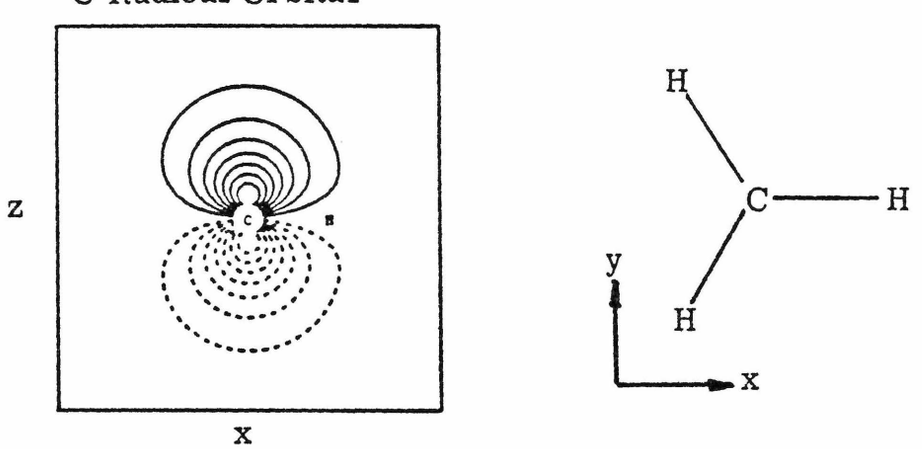

N-H Bond Pair

(One of two equivalent N-H bonds)

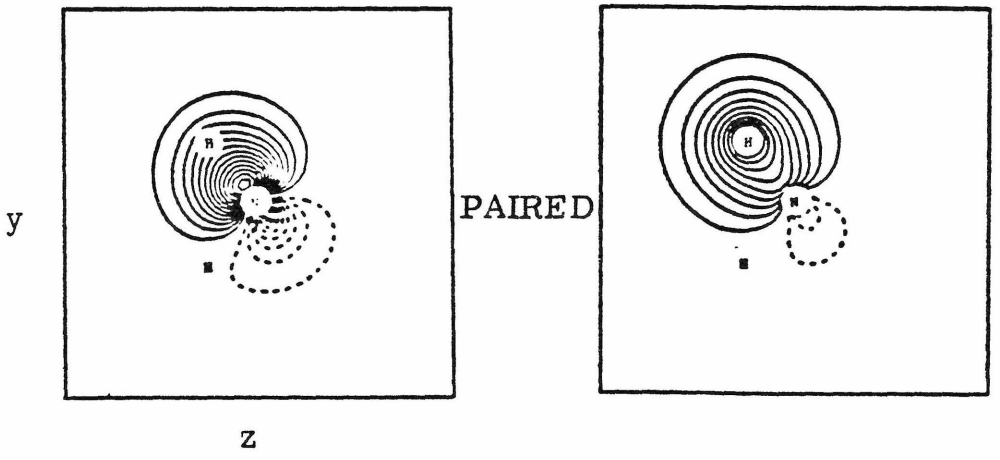

N Lone Pair

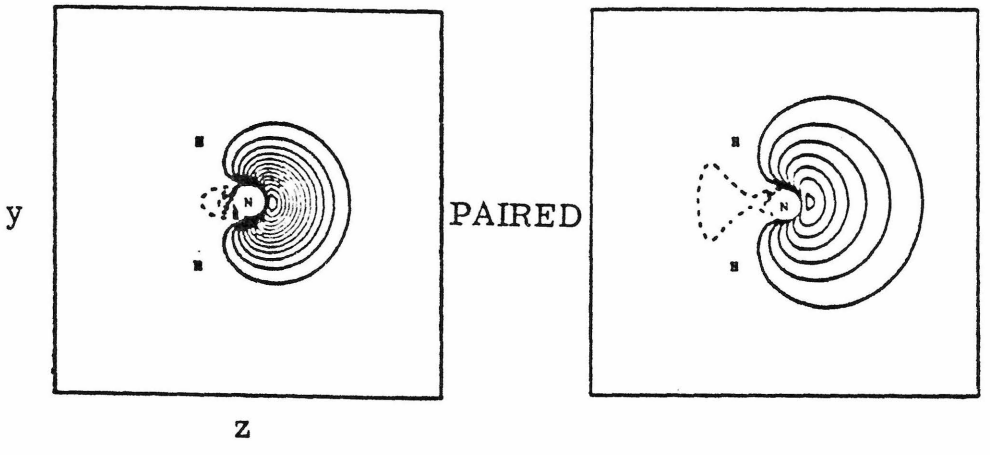

N Radical Orbital

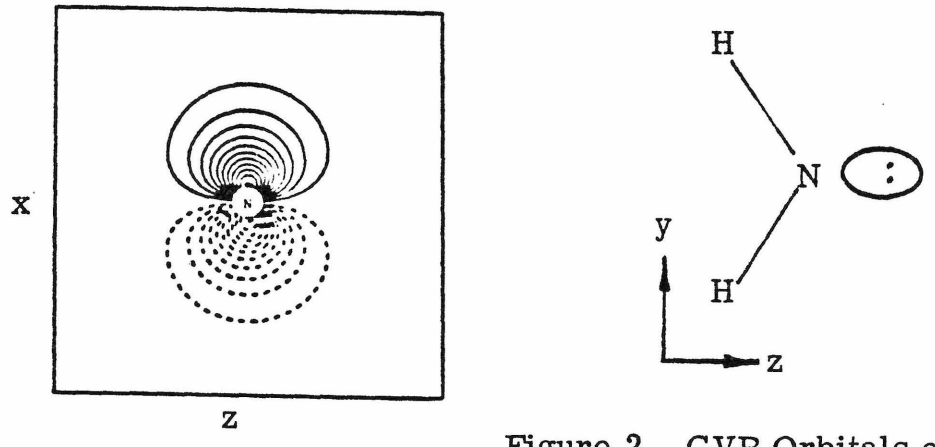

Figure 2. GVB Orbitals of NH_2.

Figure 3. GVB Orbitals of OH

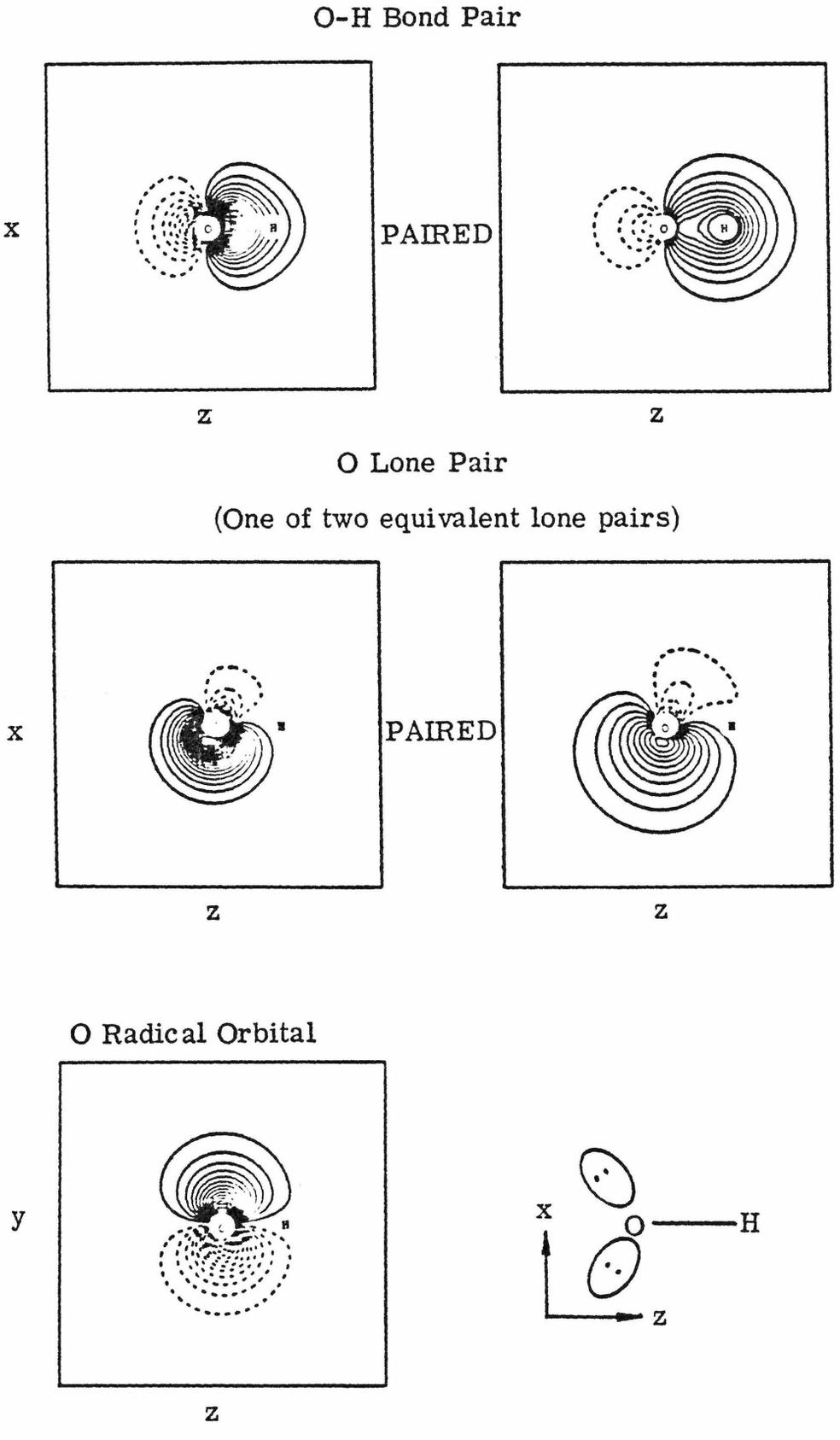

Figure 4. GVB Orbitals of F

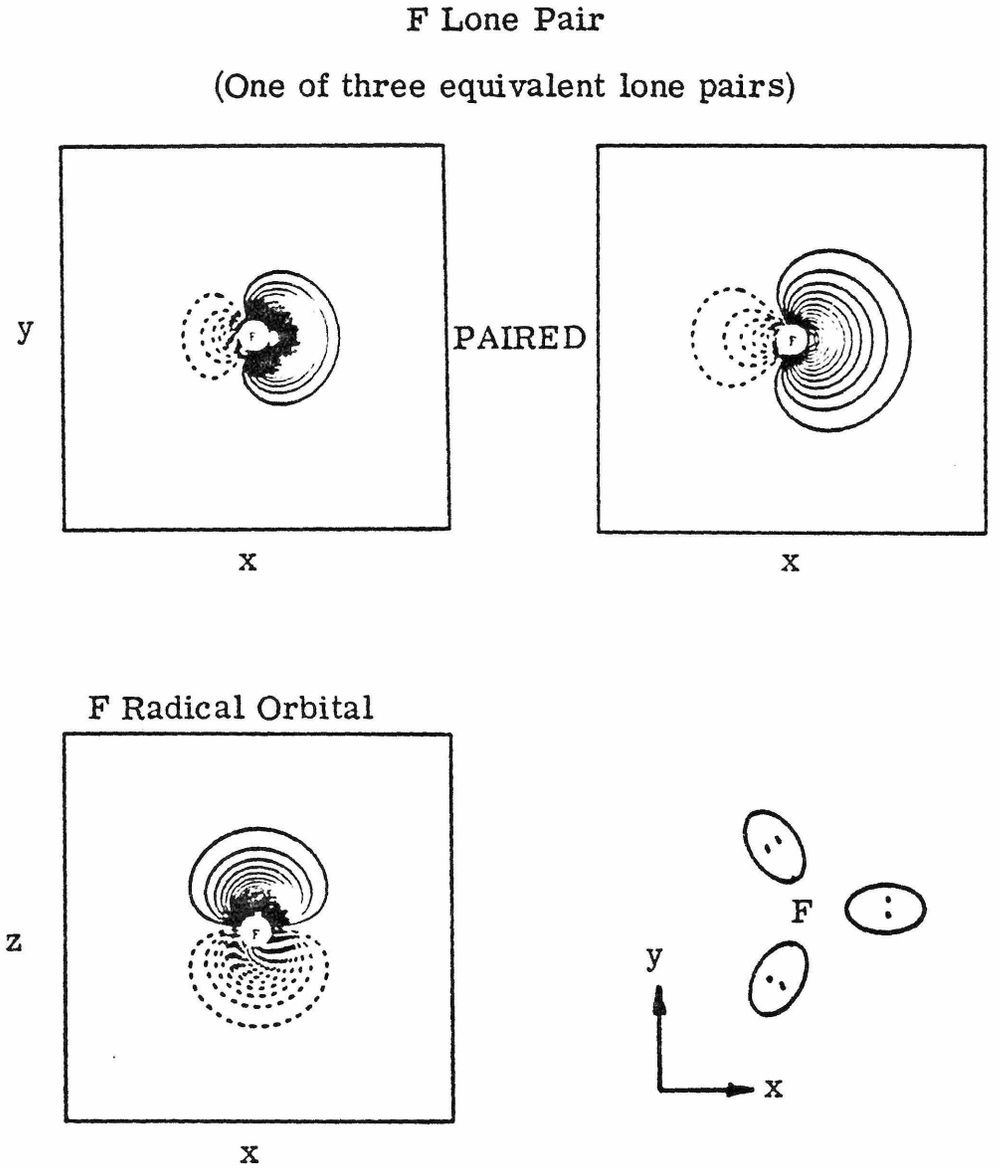

Figure 5. GVB Orbitals of CH_4.

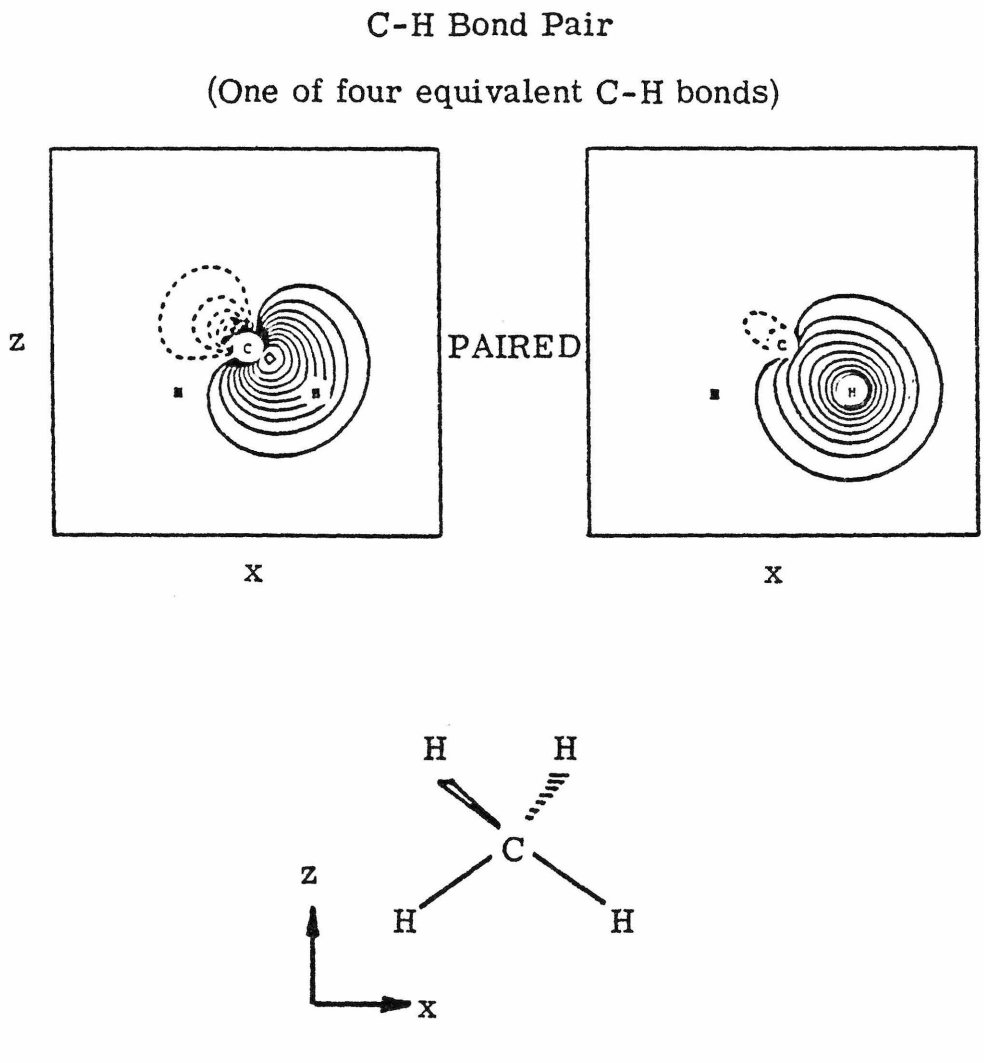

Figure 6. GVB Orbitals of NH_3

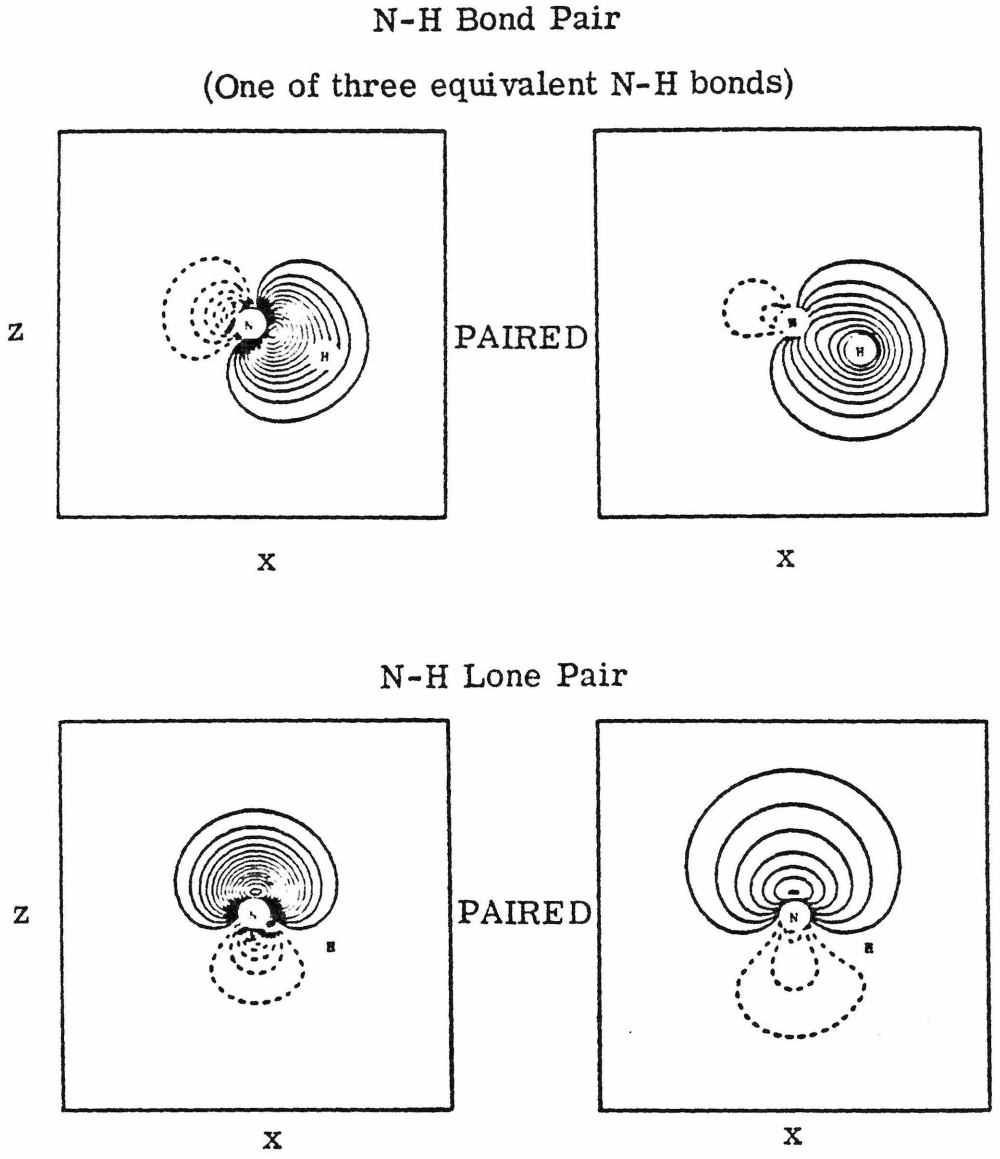

Figure 7. GVB Orbitals of H_2O.

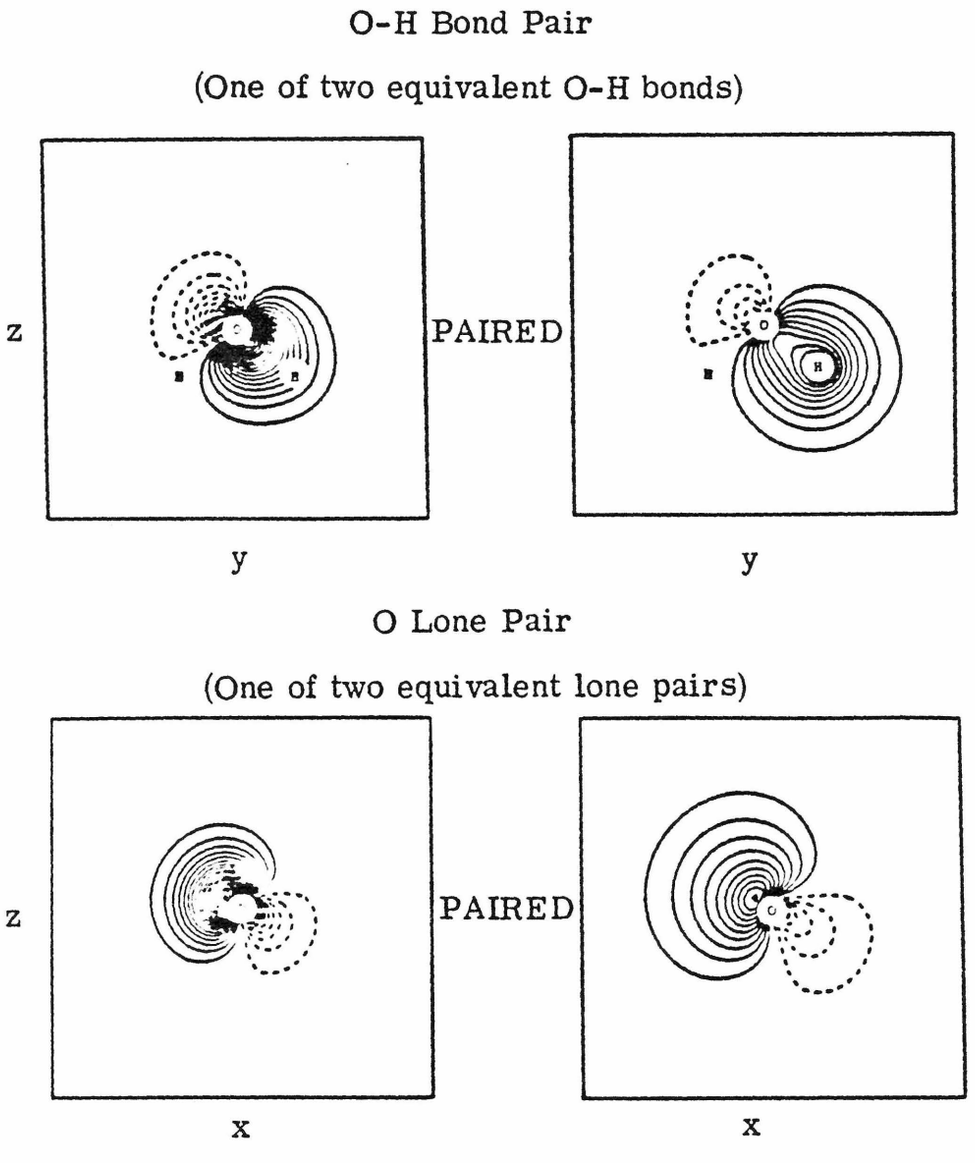

Figure 8. GVB Orbitals of FH

F-H Bond Pair

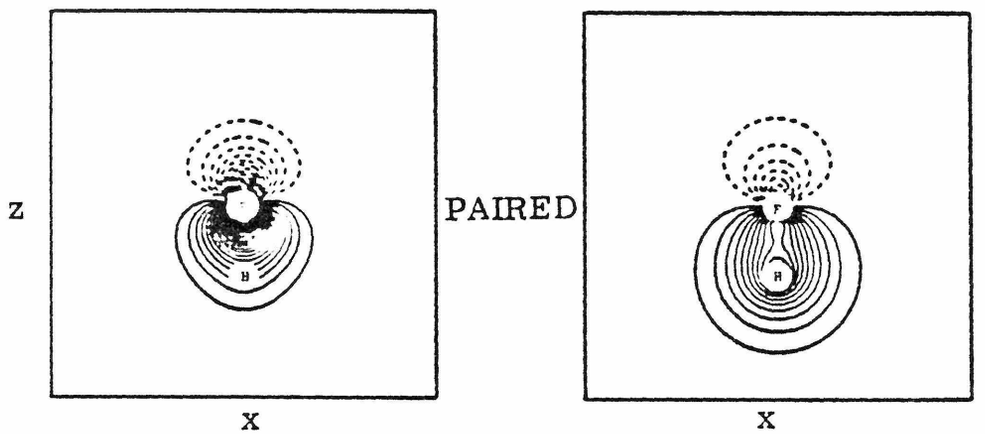

F Lone Pair

(One of three equivalent lone pairs)

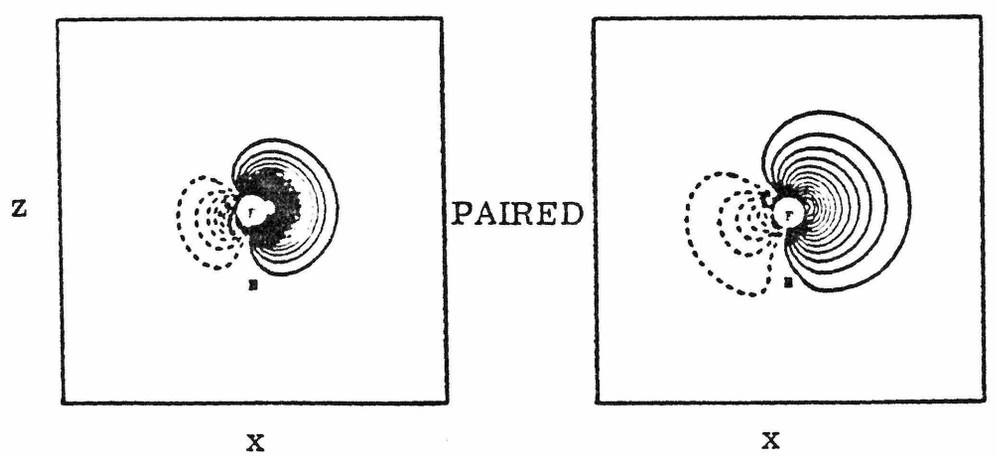

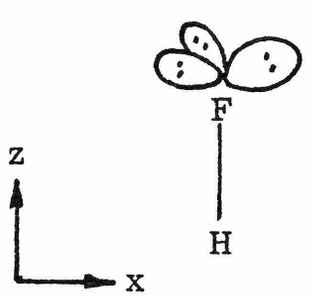

where LP_1 and LP_2 are the two lone pairs and N is a normalization factor. This simple wavefunction includes the dominant left/right correlation in each pair (left/right for bonds, in/out for lone pairs) and gives much more accurate charge distributions than does the Hartree-Fock wavefunction. In addition, a given level of electron correlation can almost always be described with a far smaller configuration space using these localized GVB orbitals, rather than a delocalized Hartree-Fock reference states. We will use the natural orbital representation of the GVB orbitals in our calculations, as they are orthogonal.

At this point we can divide the localized orbitals into two distinct sets, the active space, including the two GVB orbitals describing the bond being broken, and the semi-active space, including the GVB orbitals of the remaining bonds to the two centers being dissociated. For an R-H dissociation, there are two active orbitals and six semi-active orbitals (the remaining three R-H bonds or lone pairs). Once the bond is broken, the R$\cdot$ species has only one active orbital but retains the six semi-active orbitals. There are both electronic and structural relaxations in the R$\cdot$ fragment, so we solve self-consistently for this wavefunction also. The H$\cdot$ fragment has one active orbital with no electron correlation and does not make a differential contribution to the bond energies. Note that the number of variational orbitals does not change as the bond is broken. Thus we term the GVB orbital basis as dissociation-consistent.

To describe angular correlation of the active bond, we will add functions of higher angular momentum to the orbital basis used in the CI. These virtual orbitals will be used in the configuration interaction (CI) part of the calculation. Polarization functions are included on all atoms with one set of five d functions on the heavy center and one set of three p functions on

each hydrogen. All basis functions are allowed to enter the GVB wavefunctions; those on centers not involved in the bond scission are not otherwise explicitly utilized until the CI. Thus the CI basis for the R-H dissociation consists of two active orbitals, six semi-active orbitals, five d virtual orbitals, and three p virtual orbitals on the hydrogen being dissociated, for a total of 16 orbitals. The corresponding radical molecular fragment has one active orbital, six semi-active orbitals, and five d virtual orbitals, for a total of 12 orbitals. The hydrogen atom accounts for the remaining four orbitals (one active and three p virtual). Thus the basis used in the CI maps directly into the basis for the separated fragments as the bond is broken. Consequently, we refer to this as a dissociation-consistent CI basis.

In the CI, we want to include a good description of the electron correlation involving the active electrons, plus any differential terms involving the semi-active electrons (i.e., terms leading to correlation effects that are different for the molecular case than for the separated fragments R• and H•). At the same time, we maintain dissociation consistency in the CI configuration space. That is, we require that the molecular CI configuration space dissociate into the corresponding CI configuration space of the two fragments. Specifics concerning the configurations chosen are in the following section; however, the organization of the configuration list will be given here. The orbital space of the CI is divided into three parts: the active orbitals, the semi-active orbitals, and the virtual orbitals. The configuration list is logically divided into sections, each section being the product of excitations involving the active orbitals times excitations involving the semi-active orbitals. Also, each section describes certain specific kinds of electron correlation and orbital readjustments. This approach maintains the dissociation consistency of the CI configuration basis.

III. Calculational Details

Basis Sets. For C, N, O, and F we used the (9s, 5p) gaussian basis set of Huzinaga,[1] contracted to valence double zeta level by Dunning (3s, 2p).[2] To this we added a set of single exponent gaussian d functions optimized for bond correlation use. Details of the optimization are in Appendix A. The exponents are listed in Table II. Also, the addition of diffuse s and p exponents was tested. These were optimized for the corresponding negative ions, at the GVB level. For wavefunctions with localized orbitals, we found that both s and p diffuse functions were needed. The exponents are listed in Table III. Coincidentally, our p exponents are nearly the same as those of Dunning,[2] although optimized differently. In Table IV we give the calculated values of D_e(R-H) with and without the diffuse functions. It can be seen that the diffuse functions increase all bond energies except H-CH_3. D_e(H-NH_2) increases by 0.2 kcal, D_e(H-OH)increases by 0.8 kcal, while D_e(H-F) increases by 2.0 kcal. This is the expected trend since F has a greater electron affinity (78 kcal) than OH (42 kcal).[3,4] The final calculations in Table I all have basis sets including the diffuse functions. For hydrogen, we used the (3/1/1) triple zeta contraction of Huzinaga's five primitive gaussian basis (unscaled).[1] The triple zeta basis removes the need for scale factors that might bias the calculations.

Geometries. In each case we used the experimental equilibrium geometries for our calculations. The chosen structures are in Table V.[5,6] For well-established structures like these, further geometry optimization can only change the bond energies by small fractions of a kcal and therefore is not significant.

Self-Consistent Field Wavefunctions. For each of the species and fragments, the ground state was solved self-consistently with the GVB2.5

TABLE II. Gaussian Bond Correlation Exponents for First Row Atoms.

Atom	Molecule Optimized	Calculated d Exponent	Calculated p Exponent for H
C	CH_4	0.64[b]	0.91
	CH_4	0.65	a
N	NH_3	0.76[b]	1.16
	NH_3	0.76	a
O	H_2O	0.95[b]	1.35
	H_2O	0.94	a
	H_2O_2	1.01	a
F	HF	1.34[b]	1.45
	HF	1.26	a
	F_2	1.42	

[a] These cases were optimized without p exponents on hydrogen.

[b] Recommended value for general use.

TABLE III. Gaussian Diffuse Exponents for First Row Negative Ions.[a]

Atom	State Optimized	Calculated s Exponent	Calculated p Exponent
C^-	^4S	0.045	0.034
N^-	^3P	0.066	0.045
O^-	^2P	0.088	0.060
F^-	^1S	0.112	0.076

[a] These functions are to be added to the normal (9s,5p) basis and were optimized from GVB calculations on the negative ion.

TABLE IV. Dependence of the Calculated R-H Bond Dissociation Energies (From DC-CI), D_e (kcal), upon Diffuse s and p Functions on the Heavy Atom.

Molecule	Without Diffuse Functions	With Diffuse Functions
CH_4	108.8	108.8
NH_3	112.6	112.8
H_2O	121.8	122.6
HF	136.3	138.3

TABLE V. Experimental Equilibrium Geometries Used for Calculated Species.

Molecule	r_{RH} (Å)	θ_{HRH}	ref.
CH_4	1.094	109.5	5
NH_3	1.012	106.7	5
H_2O	0.9575	104.5	5
HF	0.9168		6
CH_3	1.079	120.0	5
NH_2	1.024	103.3	5
OH	0.9697		6

program developed at Caltech.[7] Each of the closed-shell molecules, CH_4, NH_3, H_2O, and HF, was first solved with four GVB pairs, each pair having two natural orbitals (Figure 1). This includes one GVB pair for each bond and each lone pair. The corresponding calculation was done on each fragment for the ground state where there are three GVB pairs and one open-shell orbital.

Configuration Interaction Basis. For the closed-shell cases, the virtual part of the CI basis was generated by separately Schmidt-orthogonalizing the five correlating d functions on the heavy center and the three correlating p functions on the active hydrogen to the occupied GVB orbitals (which also have some d and p character). Then these two sets of orbitals were symmetrically orthogonalized to each other, giving eight orthogonal virtual orbitals. Angular correlation will be included in the CI, using these eight virtual orbitals. Thus the closed-shell CI calculations had a basis of four GVB pairs (eight orbitals), plus eight virtual orbitals for angular correlation and polarization. The C, N, O, and F 1s orbitals were obtained self-consistently (for the GVB wavefunction) but were always filled and need not be included in discussing the CI basis.

For the radical fragments, the CI basis consisted of the seven occupied orbitals from the ground state (three GVB pairs and an open-shell p orbital), excluding the 1s. The set of five d virtual orbitals was Schmidt-orthogonalized to the seven occupied orbitals. More extensive MCSCF calculations gave essentially the same virtual orbitals since the total virtual space is limited.

Spatial Configurations for CI. In the process of developing this method, many different lists of spatial configurations were tested; the results reported here represent the smallest list of spatials that gave

results free of systematic errors. The CH_3, NH_2, OH, and F fragment CI calculations used a small basis of 12 orbitals, previously described. We will express each term in the CI as the product of the semi-active CI, on the left, times the active CI, on the right:

$$[\text{semi-active CI}] \times [\text{active CI}] .$$

The notation will be explained as it is used. The CI of the fragment radical species consisted of the following:

i) [GVB-PP(2)] × [1/1]: We started with all double excitations from the dominant configuration of the GVB wavefunction but with the requirement that the two electrons of each GVB pair remain in the two natural orbitals defining the pairs and not permitting any orbital except the radical p orbital to be singly-occupied. These configurations are usually called GVB perfect-pairing configurations, hence the notation GVB-PP(2) for all such double excitations. These configurations allow left/right bond correlation and in/out lone-pair correlation. We multiply this set of configurations by all single excitations from the active orbital, denoted 1/1, since excitation to any empty or singly-occupied orbital is allowed.

ii) [GVB-RCI(1)] × [1/1]: To the above configurations we added all single excitations, with the requirement that the two electrons of a GVB pair remain within the two natural orbitals defining the pair. This is called a GVB restricted-CI, and allows spin optimization between bonds and between bond pairs and the radical orbital. Again, we multiply these configurations by all single excitations from the active orbital, allowing shape readjustments.

iii) All single and double excitations from the active to the semi-active orbitals and from the semi-active to the active orbitals. These

configurations relax the strong orthogonality of the GVB pairs. The total number of spatial configurations, including these three types of excitation, is 90 (126 spin eigenfunctions and 162 determinants).

The CH_4, NH_3, H_2O, and HF spatial configurations were constructed so that the R-H bond CI would dissociate into the fragment spatial list, plus a hydrogen atom. This CI included

i) [GVB-PP(2)] × [2/2]: All GVB perfect-pairing doubles in the semi-active orbitals times all single and double excitations from the active orbital. This term dissociates into the first term of the fragment CI.

ii) [GVB-RCI(1)] × [2/2]: All GVB restricted-CI singles times all single and double excitations from the active orbital. This term dissociates into the second term of the fragment CI.

iii) All single and double excitations from the active to the semi-active orbitals and vice versa. This term also dissociates correctly into the third term of the fragment CI.

This spatial list has 637 configurations (847 spin eigenfunctions and 2062 determinants).

This spatial list emphasizes correlation of the active pair of electrons, while including the minimal set of excitations required among the semi-active orbitals. Various tests indicated that this is the minimal level of calculation that systematically includes all differential terms for all four cases. For example, increasing the size of the semi-active CI to include GVB perfect-pairing quadruples and GVB restricted-CI doubles produces a significant decrease in the total energies (CH_4 = 4.2 kcal, NH_3 = 9.5 kcal, H_2O = 12.6 kcal), FH = 12.3 kcal) but does not change the bond energies significantly (C-H = 0, N-H = -0.3 kcal, O-H = +0.3 kcal, F-H = 0). These additional terms

primarily increase the level of pair/pair correlation among the semi-active electron pairs (e.g., left on bond 1 simultaneously with right on bond 2, etc.). These terms are not differential. The important pair/pair correlations involving the active bond were already included in the smaller list of configurations. Of course, many other such tests were made, many with much larger lists of spatial configurations. The calculations described here represent what we feel is a quantitatively accurate method that can be applied to much larger molecules.

IV. Summary

We have presented a systematic method for ab initio calculation of the R-H bond dissociation energies of the first-row hydrides, CH_4, NH_3, H_2O, and HF. The method is dissociation-consistent in both the orbital basis and CI configuration space and is referred to as DC-CI for dissociation-consistent CI. We make full use of the localized GVB bond and lone pairs to reduce the size of the CI configuration lists.

In order to compare with experiment, we have included zero point energies to obtain D_0 dissociation energies and have included the temperature dependence of the enthalpies to obtain bond energies at 298°K (see Table VI[3,4,6,8-10] for these corrections). The results are in very good agreement with experiment.

The principles of our approach can be extended to more complex bonds and substituted systems without incurring large scale factors in the CI studies. Partitioning of the GVB wavefunction (with its localization of orbitals into active, semi-active, and inactive sets) plus a CI based on this partition to selectively include those correlation effects influencing the bond energy are the keys to reducing the calculational costs. The most important electrons are then given the most emphasis while still considering the important secondary correlation and substituent effects.

Acknowledgments

The author wishes to thank the U. S. Department of Energy for partial support of this work under Contract No. DE-AC03-76SF00767, Project Agreement No. DE-AT03-80ER10608.

TABLE VI. Corrections for Heat Capacity and Zero Point Energy in R-H Bonds (kcal).

Molecule	$\Delta H^0_{f_{298°K}}$(R-H)	$\Delta H^0_{f_{298°K}} - \Delta H^0_{f_0}$	Zero Point Energy	D_e	Ref.
CH_4	104.8	1.5	9.0	112.3	3,8,9
NH_3	107.4	1.4	9.4	115.4	3,9,10
H_2O	119.4	1.3	7.5	125.6	3,4,6,8
HF	136.1	1.0	5.9	141.0	6

TABLE VII. Total Energies for Calculated Wavefunctions (hartrees).

Species	Hartree-Fock	GVB	DC-CI
CH_4	-40.2082	-40.2685	-40.2890
NH_3	-56.2121	-56.2755	-56.3033
H_2O	-76.0492	-76.1114	-76.1468
HF	-100.0502	-100.1051	-100.1471
$\cdot CH_3$	-39.5684	-39.6116	-39.6158
$\cdot NH_2$	-55.5754	-55.6203	-55.6236
$\cdot OH$	-75.4083	-75.4490	-75.4516
$\cdot F$	-99.3956	-99.4249	-99.4269
$\cdot H$	-0.49981	-0.49981	-0.49981

Appendix A: Calculation of Gaussian Bond Correlation Exponents

For each molecule in Table II, the GVB wavefunctions were first solved without any d functions on the heavy center or p functions on the hydrogens. After the SCF, a set of five single gaussian d functions was added to the basis of the heavy center and three p functions to one hydrogen. These two sets were separately Schmidt-orthogonalized to the existing occupied orbitals and then symmetrically orthogonalized to each other. This step removes much of the dependence of one set of exponents upon the other. The CI basis consisted of all eight valence GVB orbitals plus the five d and three p orbitals. The CI spatial configurations included

i) all GVB-PP quadruples among the four GVB pairs,

ii) all single and double excitations from the four bonds to the correlating d orbitals,

iii) all single and double excitations from the special R-H bond (the H having the p functions) to the p orbitals, and

iv) the cross terms having one excitation from any of the four bonds to the d orbitals times one excitation from the special R-H bond to the p orbitals.

This CI calculation (284 spatial configurations, 407 spin eigenfunctions, or 1026 determinants) was repeated with different values of the d and p exponents until a minimum in energy was found. The configuration space has been chosen to allow both shape readjustment of the orbitals and optimal angular correlation of the selected R-H bond. For H_2O_2 and F_2, an analogous CI was done, but with d functions on both heavy centers.

Appendix B: Calculation of Gaussian s and p Negative Ion Exponents

The goal of this optimization was to find s and p diffuse gaussian exponents to describe the diffuse character present in ionic bonds at the GVB level. In Hartree-Fock calculations, only diffuse p exponents may be needed to describe negative ion character, but the GVB orbitals are hybrids and require both s and p diffuse character. Our exponents were optimized for the negative ions of C, N, O, and F. Each negative ion calculation had as many GVB pairs as there were doubly-occupied valence orbitals. The diffuse s and p exponents were varied and the wavefunction was solved self-consistently at each point until an energy minimum was found. The optimum exponents are given in Table III.

References and Notes

(1) Huzinaga, S. J. Chem. Phys. 1965, 42, 1293.

(2) Dunning, T. H., Jr.; Hay, P. J. In "Modern Theoretical Chemistry: Methods of Electronic Structure Theory"; Schaefer, H. F., III, Ed.; Plenum Press: New York, 1977; Vol. 3, Chapter 1, p 23.

(3) "JANAF Thermochemical Tables", 2nd ed.; NSRDS-NBS 37; U. S. Government Printing Office: Washington, D.C., 1970.

(4) Chase, M. W.; Curnutt, J. L.; Hu, A. T.; Prophet, H.; Syverud, A. N.; Walker, L. C. J. Phys. Chem. Ref. Data 1974, 3, 311.

(5) Callomon, J. H.; Hirota, E.; Kuchitsu, K.; Lafferty, W. J.; Maki, A. G.; Pote, C. S. "Structure Data of Free Polyatomic Molecules", Landolt-Börnstein, New Series, Group II, Vol. 7; Springer-Verlag: New York, 1976.

(6) Huber, K. P.; Herzberg, G. "Molecular Spectra and Molecular Structure", Vol. 4; Van Nostrand Reinhold Co.: New York, 1979.

(7) GVB2.5 was written by R. A. Bair in 1977. This program is an extensively rearranged version of GVBTWO, written by F. W. Bobrowicz and W. R. Wadt in 1973, which avoids the extensive I/O requirements for cases with larger numbers of GVB pairs.

(8) "Tables of Molecular Vibrational Frequencies, Consolidated Volume I", Shimanouchi, T., Ed.; NSRDS-NBS 39; U. S. Government Printing Office: Washington, D.C., 1972.

(9) Surratt, G. T.; Goddard, W. A., III, Chem. Phys. 1977, 23, 39.

(10) Bohme, D. K.; Hemsworth, R. S.; Rundle, H. J. Chem. Phys. 1973, 59, 77.

Chapter 2:

Application to Calculation of the R-R Bond Energies of C_2H_6, N_2H_4, H_2O_2, and F_2

I. Introduction

In a previous paper, we outlined a systematic method (dissociation-consistent CI or DC-CI) for accurate calculation of bond dissociation energies and applied the method to R-H where

$$R = CH_3,\ NH_2,\ OH, \text{ and } F.$$

In this paper we extend this scheme to describe the dissociation of the more general R-R′ single bonds. Together these calculational methods can provide useful and accurate thermochemical information about chemical species that are inaccessible experimentally. In other cases the calculations can supply strong evidence for assigning thermochemical parameters where the experiments are uncertain or conflicting.

For the current study we have selected the following molecules: C_2H_6, N_2H_4, H_2O_2, and F_2. Each has a homonuclear bond between the two heavy centers. The structures of these molecules, and their corresponding radical fragments, CH_3, NH_2, and OH, are known with good accuracy. Heats of formation have also been obtained experimentally, allowing us to compare our calculated bond energies with accepted values and to assess the accuracy of our calculations. We are especially interested in ensuring that our method produces only small systematic errors. Hence, this series of molecules provides good comparisons. The R-R bond energies vary from 97 kcal for ethane to only 38 kcal for F_2. The results of the calculations, displayed in Table I, show very good agreement between the experimental and theoretical studies.

Table I. Theoretical and Experimental Dissociation Energies (kcal). Calculated values are from DC-CI.

Molecule	$\Delta H^{o}_{f298°K}$(R-R)		D_0 (R-R)		D_e (R-R)		Difference
	Calc.	Expt.	Calc.	Expt.	Calc.	Expt.	Expt. -Calc.
H_3C-CH_3	89.7	89.8 ± 2	87.5	87.6	96.6	96.7 ± 3	0.1
H_2N-NH_2	69.0	65.8 ± 2	67.2	64.0	74.4	71.2 ± 3	-3.2
HO-OH	53.3	51.5 ± 1	51.5	49.7	56.8	55.0 ± 2	-1.8
F-F	36.9	37.7 ± 1	36.1	36.9	37.4	38.2 ± 1	0.8

Table II. Corrections for Heat Capacity and Zero Point Energy (kcal).

Molecule	$\Delta H^{o}_{f298°K}$(R-R)	$\Delta H^{o}_{f298°K} - \Delta H^{o}_{f0°K}$	Zero Point Energy	D_e(R-R)	Ref.
H_3C-CH_3	89.8 ± 2	2.2	9.1	96.7 ± 3	1-4
H_2N-NH_2	65.8 ± 2	1.8	7.2	71.2 ± 3	1,5
HO-OH	51.5 ± 1	1.8	5.3	55.0 ± 2	1,6-8
F-F	37.7 ± 1	0.8	1.3	38.2 ± 1	1,8

II. Results

Our calculations produce D_e(R-R). To calculate $\Delta H^0_{f0°K}$(R-R) we have used the experimental vibrational frequencies to determine the zero point energies (Table II[1-8]). To obtain $\Delta H^0_{f298°K}$ we have used standard heat capacity corrections. Of the four molecules, the experimental dissociation energy of F_2 is certainly the most accurate. Of the remaining three, the H_2N-NH_2 bond has the most uncertainty, and we estimate at least a 2 kcal uncertainty in the $H^0_{f298°K}$ (H_2N-NH_2). Also, our calculations of D_e from the experimental data have an additional uncertainty of up to 1 kcal from the use of ground state vibrational frequencies to determine the zero point contributions. Thus, overall there are 1-3 kcal uncertainties when comparing the experimental D_e values with our calculated values. Keeping this in mind, our calculated dissociation energies are in very good agreement with the experiments. Our average error is only 1.5 kcal for the four molecules. Hydrazine shows the most deviation, its D_e being 3.2 kcal greater than the experimental bond energy. We estimate a ±3 kcal uncertainty in the D_e calculated from the experimental data. Thus, our calculations are still in good agreement with the observed data. Of the remaining molecules, we calculate the R-R bond dissociation of H_2O_2 to be 1.8 kcal greater than the experimental value, while C_2H_6 and F_2 are smaller than experiment, by 0.1 and 0.8 kcal, respectively. These three values certainly fall within the range of uncertainty for the experimental D_e values.

The following sections explain our calculational method. First we will describe the strategy of the method as it applies to R-R′ bond dissociation, and then we will discuss in detail the calculations reported herein.

II. Calculational Method

As the C-C bond in ethane is stretched to dissociation, both structural and electronic changes occur. At the separated limit, the methyl radicals are planar and the C-H bond lengths have decreased from 1.111 to 1.079 Å. These structural changes are accompanied by changes in the electronic wavefunction. The amounts and importance of the major modes of electronic correlation also vary dramatically between ethane and two methyl radicals. In F_2 there is no structural relaxation as the F-F bond is lengthened, yet very similar electronic changes occur. F_2 is best described as having two sets of three staggered lone pairs on each fluorine, analogous to the CH bond pair distribution in ethane. At the separated limit, each fluorine radical has a singly-occupied 2p orbital and three coplanar lone pairs, each 120° apart (as are the CH bonds in methyl radical).

Thus, it is important that the important modes of correlation be included in our calculations for both the molecule of interest and its radical fragments. On the other hand, a consistent description of the bond dissociation is necessary so that the calculation performed on the radical fragments is precisely the limit of the molecular calculation at inifinite separation. For example, a common type of configuration interaction (CI) calculation is to allow all single and double excitations from a Hartree-Fock (HF) reference state, but to do this for both ethane and methyl radical would be inconsistent since double excitations on both methyl radicals would involve numerous quadruple excitations when viewed as a dissociated ethane. Thus this approach necessarily favors the radical, where a lower level of correlation will retrieve a greater proportion of the correlation energy. Of course, a CI containing all possible spatial and spin configura-

tions is consistent, but impractical for systems with more than several electrons.

When a bond is broken, the most important differential correlation effects involve correlations of the electrons in the bond being broken. We denote this bond as the active bond. Also of importance are any other bonds to the centers of the active bond (the active centers), which change significantly upon dissociation or correlate with the active bond. We will call these the semi-active bonds. The remaining bonds in the molecule are referred to as inactive bonds if their description does not change appreciably upon dissociation of the active bond.

The important differential electron correlation usually occurs in the vicinity of the active bond so that a localized description of the bonds is a calculational advantage. As such, we first solve self-consistently for the generalized valence bond (GVB) orbitals in our calculations. Here, each valence electron has its own optimized orbital. This MCSCF includes the dominant correlation terms: left/right correlation of bond pairs and in/out correlation of lone pairs. The GVB orbitals also have the property of dissociating correctly to the proper energy of the separated species. In addition, the ratio of covalent to ionic character in the bonds is more accurately represented than for HF orbitals. We will use the natural orbital representation of the GVB orbitals in our calculations since they are orthogonal but still localized.

For the general R-R′ dissociation we can divide the localized valence orbitals into four groups:

i) active orbitals (two for an R-R′ single bond);

ii) semi-active orbitals of R (two for each remaining valence electron pair of the active center of R, generally leading to a total of six);

iii) semi-active orbitals of R′ (generally another six); and

iv) inactive orbitals of R and R′.

For example, ethane has 14 valence electrons divided into two active orbitals, six semi-active orbitals on one carbon, and six on the other. For dissociation of the central C-C bond of

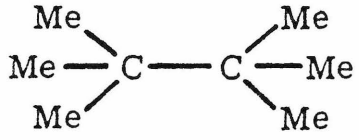

there would again be two active orbitals and 12 semi-active; however, there would also be 36 electrons in inactive valence orbitals.

The R• fragments are also solved self-consistently. Each fragment has

i) an active orbital (the radical orbital),

ii) semi-active orbitals [same as (ii) above], and

iii) inactive orbitals.

Thus, each methyl radical has one active orbital and six semi-active orbitals. Note that the sum of the number of active and semi-active orbitals for the two methyl fragments is the same as the respective number of active and semi-active orbitals of ethane. Consequently, the GVB orbital basis is dissociation-consistent.

In each case, the GVB calculation is followed by a CI calculation to determine the final energies of each species. For the molecular species the orbital basis for the CI calculation consists of

i) the two active orbitals,

ii) all of the semi-active orbitals, and

iii) polarization functions on each active center (referred to as virtual orbitals).

Ethane has 14 active and semi-active orbitals. To this basis we add a set of five d polarization functions centered on each carbon. These d orbitals are needed to describe angular correlation of the C-C bond, but they were also present in the SCF to describe polarization of the valence orbitals. This leads to a total of 24 orbitals in the CI calculation.

For the radical species, the CI orbital basis includes

i) the active orbital,

ii) all of the semi-active orbitals, and

iii) polarization functions on the active center.

Thus the CI basis for methyl radical has seven active and semi-active orbitals plus five d polarization functions on the carbon for a total of 12 orbitals. Two methyl radicals would account for 24 orbitals, which is precisely the size of the ethane CI basis. In fact, each orbital in the ethane CI basis maps directly into one of the methyl radical orbitals. Thus the dissociation-consistent nature of the GVB basis is preserved at the CI level also.

It is necessary to carefully consider the modes of electron correlation needed to describe bond dissociation when selecting spatial configurations for the CI calculations. To be dissociation-consistent, we require that the molecular CI configuration space is a product of the corresponding CI configuration spaces of the two fragments. Here is where the use of localized GVB orbitals becomes imperative. Many kinds of correlation (left/right, radial, angular, spin polarization) are well described from a few spatial configurations if the basis is localized. Thus the list of spatial configurations for the fragments can be relatively short (90 for methyl radical) and the product of the two fragment lists is still a very tractable size (4200 for ethane). Despite

the fact that quadruple excitations are explicitly included, the criteria in selecting the correlation modes to be included are twofold: (a) first, emphasis is placed on including a good description of the active electron correlation plus any other semi-active correlation and coupled modes that are differential, and (b) second, the configurations to be included must be systematic and not dependent upon the importance of particular configurations for a particular case. A correlation mode is differential if it alters significantly the bond energy being calculated. Total energy is not a criterion since we seek the most compact list of spatial configurations that adequately describe the dissociation. Specific information about the configurations actually used is in the following section.

In summary, we have extended the method for describing R-H bond dissociation to the more general R-R′ species. In each case we divide the localized GVB orbitals into groups, according to their importance in the dissociation process:

i) active GVB orbitals [the bond(s) being broken];

ii) semi-active GVB orbitals (the other bonds to the active centers);

iii) virtual orbitals associated with the active centers (polarization functions); and

iv) inactive SCF orbitals (substituent orbitals not associated with the active centers, core orbitals, etc.).

The CI basis consists of the first three groups, each of which dissociates cleanly into two groups of fragment orbitals, with a one-to-one mapping. The CI calculation also maintains dissociation consistency in the spatial configurations used. As the active bond is stretched, the molecular CI becomes precisely two fragment CI's.

IV. Calculational Details

A. Basis Sets

For C, N, O, and F we used the (9s, 5p) gaussian basis of Huzinaga[9] contracted to valence double zeta level by Dunning (3s, 2p).[10] To this we added a set of single exponent gaussian d functions optimized for correlated wavefunctions. Also, diffuse s and p functions were added to the active centers (optimized for GVB wavefunctions of the corresponding negative ions). Details of these optimizations are given in an earlier paper.[11] For hydrogen, we used the (3/1/1) triple zeta contraction of Huzinaga's unscaled five-gaussian basis.[9] In all cases a set of single gaussian p polarization functions was added to each hydrogen. These p functions were optimized independently for each X-H bond in an earlier paper.[11]

B. Geometries

For each species except H_2O_2 we used the experimental equilibrium geometries for our calculations. The chosen structures are in Table III.[8, 12-14] These structures are known well enough that further optimization would not significantly alter the bond energies. There are experimental uncertainties in assigning the H_2O_2 structure, so we optimized it along with some other peroxides. This work is detailed in another publication.[14]

C. Self-Consistent Field Wavefunctions

The ground state of each molecule and each fragment was solved self-consistently with the GVB2.5 program. For C_2H_5, N_2H_4, H_2O_2, and F_2 there were seven GVB pairs, each consisting of two natural orbitals for a total of 14 valence GVB orbitals. Orbital contour plots are shown in Figures 1 to 4. For the fragments CH_3, NH_2, OH, and F, there were three GVB pairs

Table III. Equilibrium Geometries Used for Calculated Species.[a]

Molecule	r_{AA}	r_{AH}	θ_{AAH}	θ_{HAH}	ϕ	Ref.
C_2H_6	1.533	1.111	111.4	107.3	60.0	12
N_2H_4	1.447	1.008	109.2	113.3	88.9	13
HOOH	1.462	0.965	100.0		120.0	14
FF	1.417					8
CH_3		1.079		120.0		12
NH_2		1.024		103.3		12
OH	0.9697					8

[a] Lengths are in Ångstroms, angles are in degrees, and ϕ is the dihedral angle.

Table IV. Total Energies for Calculated Wavefunctions (hartrees).

Molecule	HF	GVB	DC-CI
C_2H_6	-79.2479	-79.3557	-79.3856
N_2H_4	-111.2112	-111.3240	-111.3657
H_2O_2	-150.8189	-150.9426	-150.9938
F_2	-198.7329	-198.8631	-198.9134
CH_3	-39.5684	-39.6116	-39.6158
NH_2	-55.5754	-55.6203	-55.6236
OH	-75.4083	-75.4490	-75.4156
F	-99.3956	-99.4249	-99.4269

Figure 1. GVB Orbitals of C_2H_6.

C-C Bond Pair

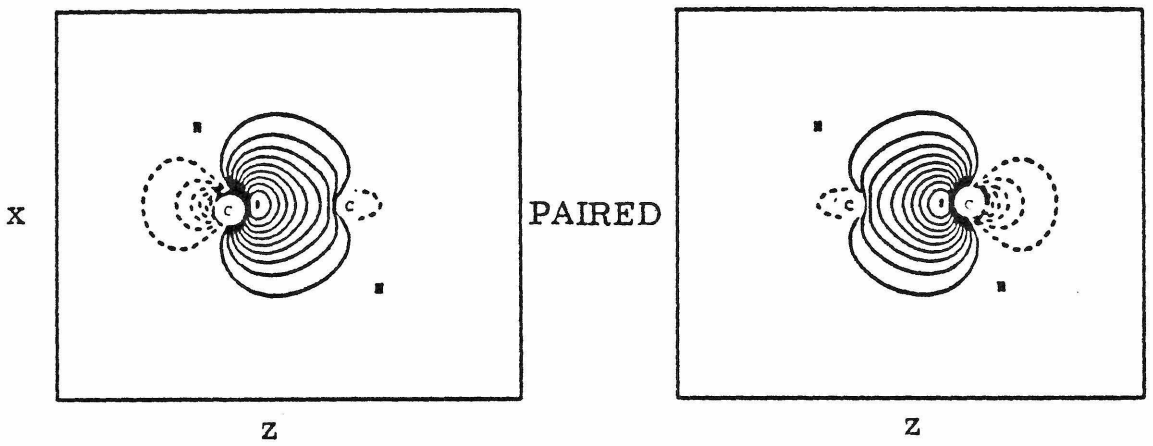

C-H Bond Pair

(One of six equivalent C-H bonds)

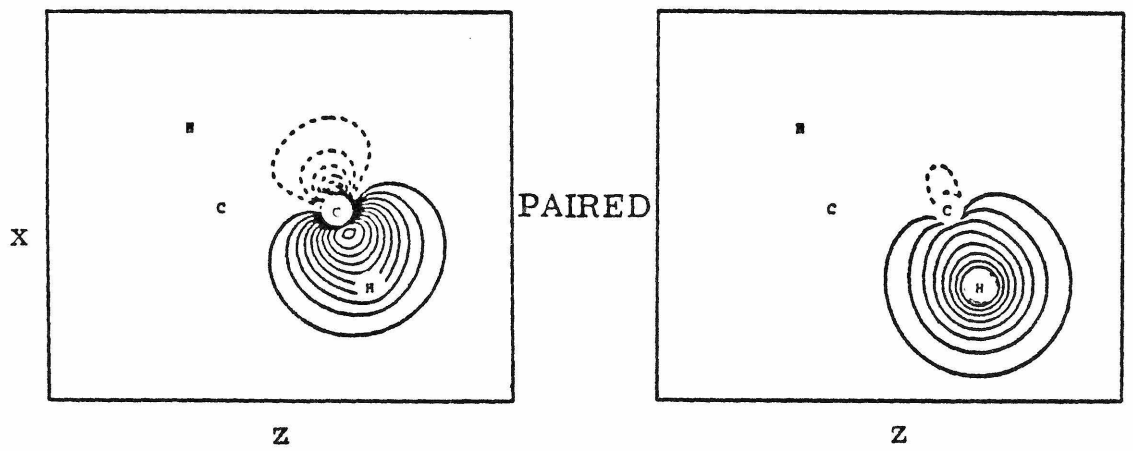

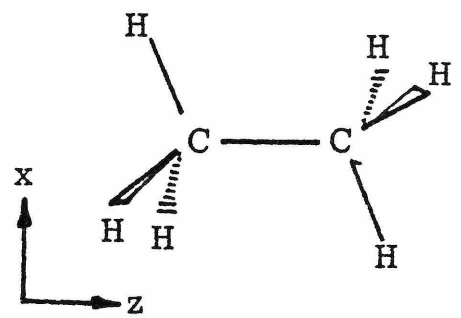

Figure 2a. GVB Orbitals of N_2H_4

N-N Bond Pair

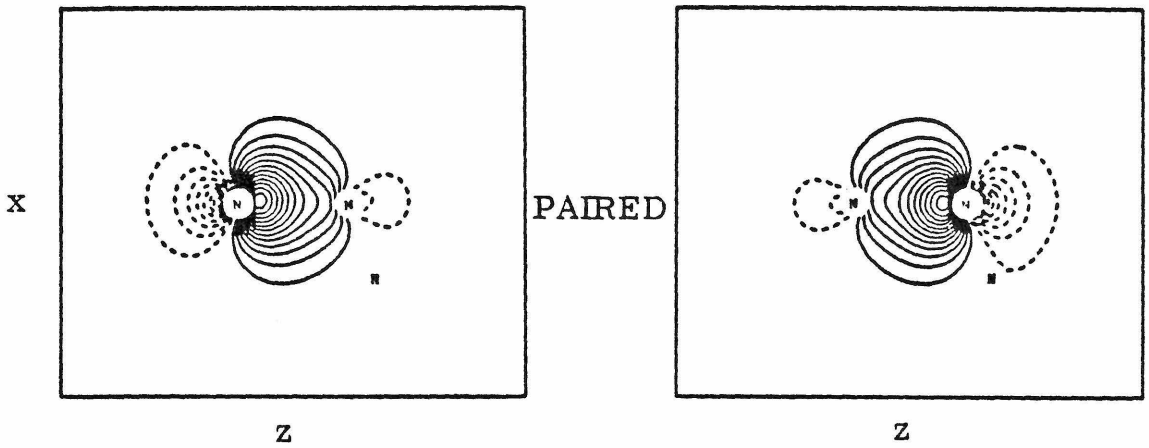

N-H Bond Pair

(One of four equivalent N-H Bonds)

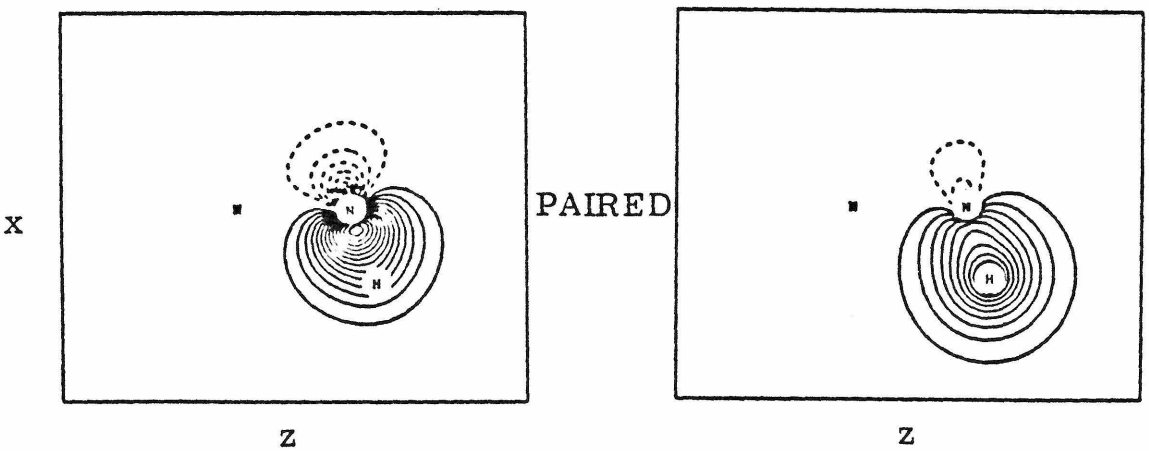

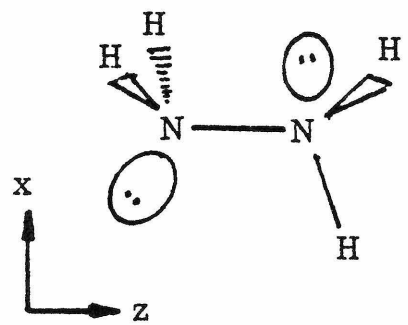

Figure 2b. GVB Orbitals of N_2H_4.

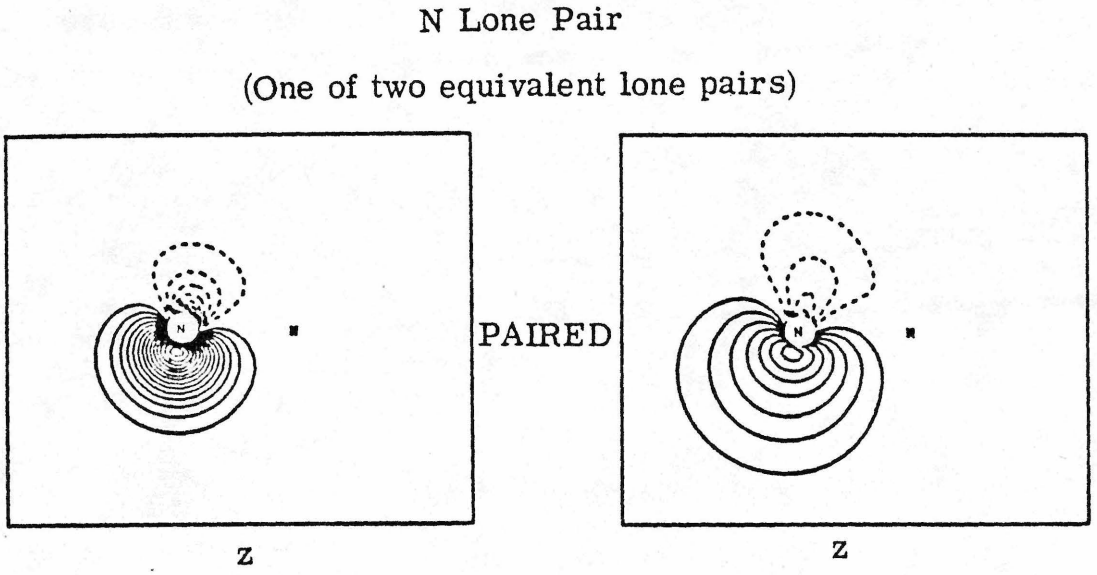

Figure 3a. GVB Orbitals of H_2O_2.

O-O Bond Pair

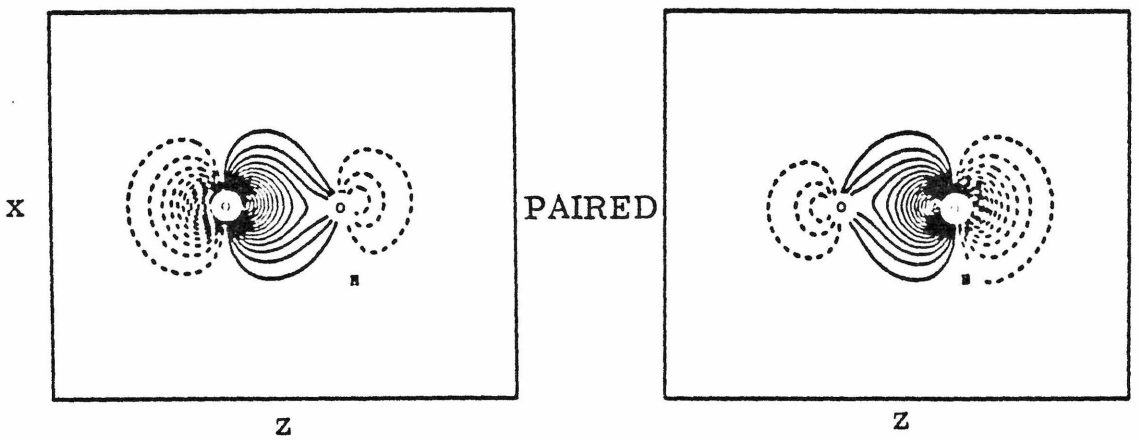

O-H Bond Pair

(One of two equivalent O-H bonds)

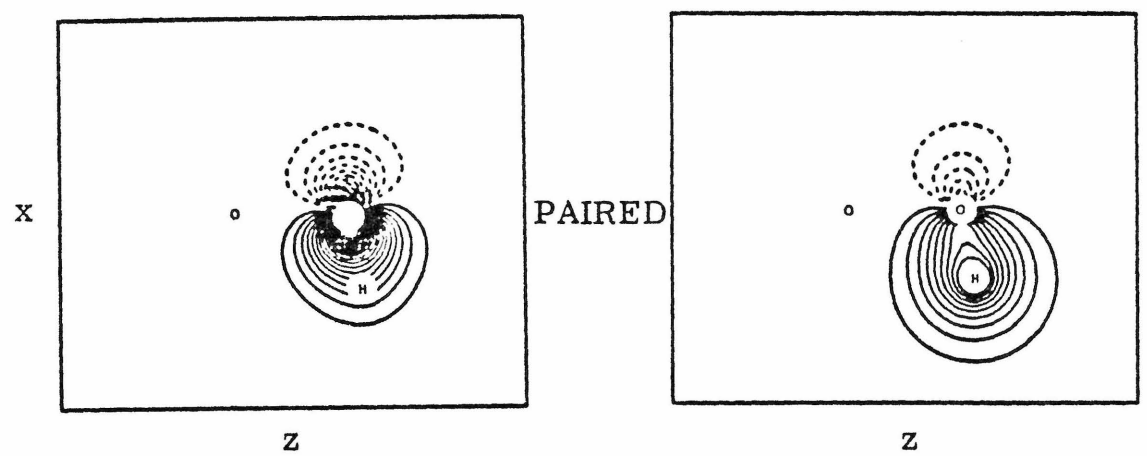

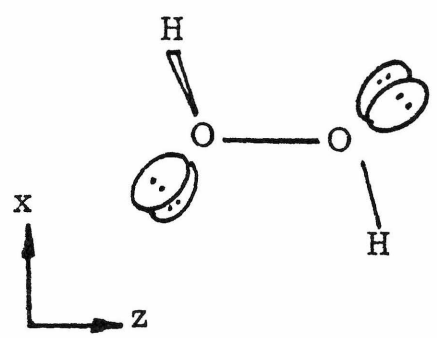

Figure 3b. GVB Orbitals of H_2O_2.

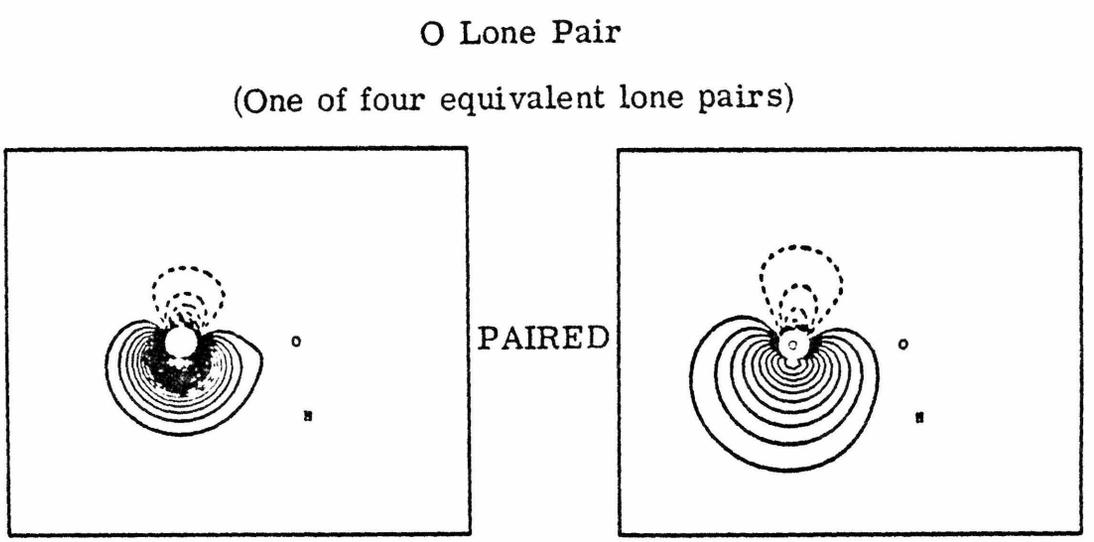

Figure 4. GVB Orbitals of F_2.

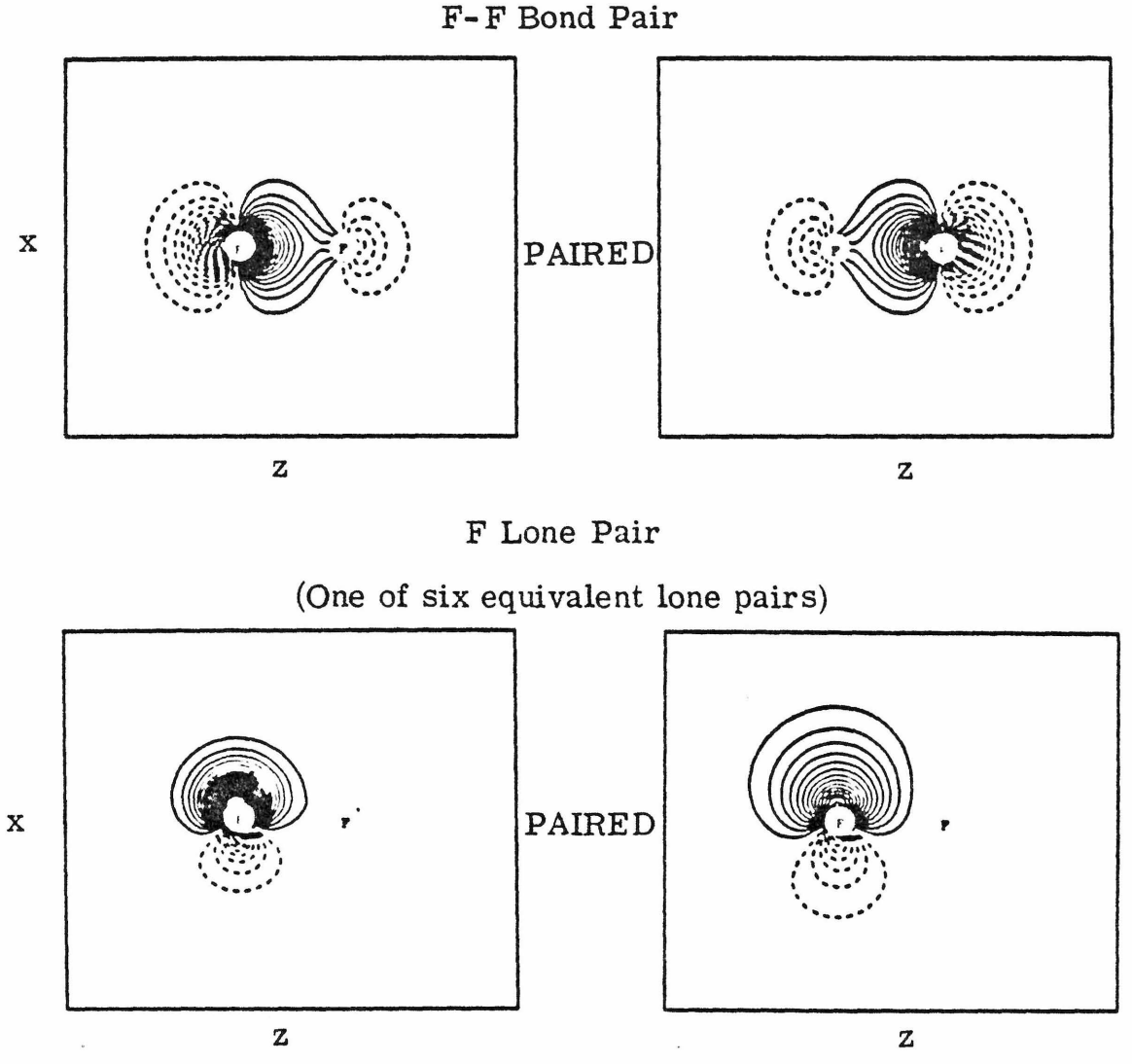

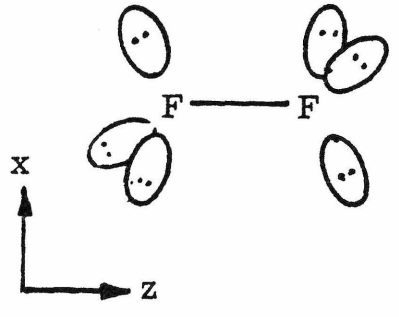

and a radical orbital, leading to a total of seven valence GVB orbitals. The 1s orbitals were also included in the SCF but left invariant in the CI calculations.

D. Configuration Interaction Basis

For each molecule the five correlating d functions on each active center were Schmidt-orthogonalized to the occupied orbitals (which included some d character). The two sets of five d-like functions were then symmetrically orthogonalized to each other. This process produces a localized and symmetric set of correlating virtual orbitals. The d orbitals on the fragments were simply orthogonalized to the occupied orbitals. The full molecular CI basis consisted of 14 GVB natural orbitals (two active, 12 semi-active) and ten d-like correlating orbitals, totalling 24 orbitals. The corresponding CI basis for the fragments consisted of the six GVB natural orbitals (semi-active), the radical orbital (active), and five d-like correlating orbitals, totalling 12 orbitals.

We did not optimize the d orbitals self-consistently since there was only one function of each type. For multiple sets of polarization basis functions, an MCSCF calculation could be used to generate a set of correlating orbitals for the molecules and fragments.

E. CI Spatial Configurations

The CI wavefunctions were evaluated with the CI2.5 program. We will express each term in the fragment CI as the product ot the semi-active CI, on the left, times the active CI, on the right,

$$[\text{semi-active CI}] \times [\text{active CI}].$$

The spatial list is the same for each fragment, and it is the same as the

list used in calculating the R-H bond dissociation energies, reported previously.[11] The notation will be explained as it is used.

i) [GVB-PP(2)] × [1/1]: We started with all double excitations from the dominant configuration of the GVB wavefunction with with the requirement that the two electrons of each GVB pair remain in the two natural orbitals defining the pairs and not permitting any orbital except the radical p orbital to be singly-occupied. These configurations are usually called GVB perfect-pairing configurations; hence the notation GVB-PP(2) for all such double excitations. These configurations allow left/right bond correlation and in/out lone-pair correlation. We multiply this set of configurations by all single excitations from the active orbital, denoted 1/1 since excitation to any empty or singly-occupied orbital is allowed.

ii) [GVB-RCI(1)] × [1/1]: To the above configurations we added all single excitations with the requirement that the two electrons of a GVB pair remain within the two natural orbitals defining the pair. This is called a GVB restricted-CI, and it allows spin optimization between bonds and between bond pairs and the radical orbital. Again we multiply these configurations by all single excitations from the active orbital, allowing shape readjustments.

iii) All single and double excitations from the active to the semi-active orbitals and from the semi-active to the active orbitals. These configurations relax the strong orthogonality of the GVB pairs.

This spatial list had 90 configurations (126 spin eigenfunctions or 162 determinants).

The molecular CI is much more complex since the product of two radical spatial lists produces many cross terms. We will express each term as a triple product:

[left semi-active CI] × [active CI] × [right semi-active CI] ,

where left and right denote the semi-active orbitals of the two active centers. The terms for this CI are:

i) [GVB-PP(2)] × [2/2] × [GVB-PP(2)]: All GVB perfect-pairing doubles in the semi-active orbitals of the left center times all single and double excitations from the active orbital times all GVB perfect-pairing doubles in the semi-active orbitals of the right center.

ii) [GVB-RCI(1)] × [2/2] × [GVB-RCI(1)]: All GVB restricted-CI singles in the left semi-active orbitals times all single and double excitations from the active orbital times all GVB restricted-CI singles in the right semi-active orbitals.

iii) [GVB-PP(2)] × [2/2] × [GVB-RCI(1)] + [GVB-RCI(1)] × [2/2] × [GVB-PP(2)]: The cross-terms analogous to (i) and (II). Terms (i) through (iii) dissociate into terms (i) and (ii) of the fragment CI.

iv) All single and double excitations from the active to the semi-active orbitals and vice versa. This term dissociates correctly into the third term of the fragment CI.

This product of the two radical CI lists emphasizes correlation of the active electrons yet includes the important semi-active correlations and cross-terms also. The entire list contains 4200 spatial configurations (10188 spin eigenfunctions or 34377 determinants). All excitations that were greater than quadruples with respect to the dominant configuration have been eliminated, as tests show that they do not contribute significantly to the total energy (less than 0.1 kcal for ethane).

V. Summary

We have extended the ab initio theoretical method of our previous work to describe the general R-R′ bond dissociation. The H_3C-CH_3, H_2N-NH_2, HO-OH, and F-F bond energies are calculated and found to be in very good agreement with experimental values (Table I). The calculational method is termed dissociation-consistent, since both the orbital basis and CI configuration space dissociate correctly to the corresponding fragment calculations. Our method can be readily extended to substituted systems without large scaling penalties. Two factors contribute to the compactness of the calculation:

1) the use of localized GVB natural orbitals and
2) the partition of these orbitals into active, semi-active, and inactive sets in the CI calculations to selectively include only those correlation effects that influence the bond energy.

Acknowledgments

The author wishes to thank the U. S. Department of Energy for partial support of this work under Contract No. DE-AC03-76SF00767, Project Agreement No. DE-AT03-80ER10608.

References and Notes

(1) "JANAF Thermochemical Tables", 2nd ed.; NSRDS-NBS 37; U. S. Government Printing Office: Washington, D. C., 1970.

(2) Benson, S. W. "Thermochemical Kinetics", 2nd ed.; John Wiley and Sons: New York, 1976.

(3) Surratt, G. T.; Goddard, W. A., III, Chem. Phys. 1977, 23, 39.

(4) "Tables of Molecular Vibrational Frequencies, Consolidated Volume I", Shimanouchi, T., Ed.; NSRDS-NBS 39; U. S. Government Printing Office: Washington, D. C., 1972.

(5) Bohme, D. K.; Hemsworth, R. S.; Rundle, H. J. Chem. Phys. 1973, 59, 77.

(6) Chase, M. W.; Curnutt, J. L.; Hu, A. T.; Prophet, H.; Syverud, A. N.; Walker, L. C. J. Phys. Chem. Ref. Data 1974, 3, 311.

(7) Shimanouchi, T. J. Phys. Chem. Ref. Data 1977, 6, 993.

(8) Huber, K. P.; Herzberg, G. "Molecular Spectra and Molecular Structure", Vol. 4; Van Nostrand Co.: New York, 1979.

(9) Huzinaga, S. J. Chem. Phys. 1965, 42, 1293.

(10) Dunning, T. H., Jr., Hay, P. J. In "Modern Theoretical Chemistry: Methods of Electronic Structure Theory"; Schaefer, H. F., III, Ed.; Plenum Press: New York, 1977; Vol. 3, Chap. 1, p. 23.

(11) Bair, R. A.; Goddard, W. A., III, manuscript in preparation.

(12) Callomon, J. H.; Hirota, E.; Kuchitsu, K.; Lafferty, W. J.; Maki, A. G.; Pote, G. S. "Structure Data of Free Polyatomic Molecules"; Landolt-Börnstein, New Series, Group II; Springer-Verlag: New York, 1976; Vol. 7.

(13) Tsunekawa, S. J. Phys. Soc. Jpn. 1976, 41, 2077.

(14) Bair, R. A.; Goddard, W. A., III, manuscript in preparation.

Chapter 3:

Application to Calculation of the O-O, O-C, and O-H Bond Energies of HOOH, CH_3OOH, and CH_3OOCH_3

I. Introduction

A detailed description of the microscopic reaction mechanisms of combustion is essential for development of detailed kinetic models that would be utilized in designing and optimizing real combustion systems. Such detailed understanding requires accurate estimates of the ΔH and ΔS for competing reactions. Unfortunately, accurate experimental data are not available for many of the probable intermediates in combustion. This research is designed to extend the available thermochemical information to systems that can be used to estimate ΔH for combustion intermediates.

As such, the first phase of this research was directed toward developing theoretical methods to accurately calculate the bond energies of organic species. In order to develop ab initio methods that would be practical for large molecules, we have determined which electronic correlation effects change upon dissociation of a particular bond and have designed a general procedure for automatically including all such correlation effects. Our method employs ab initio generalized valence bond (GVB) wavefunctions and dissociation-consistent configuration interaction (DC-CI) methods to directly calculate bond energies. To test our method, we selected two benchmark series of compounds, where the experimental bond energies were well known. The first series[1] included calculation of the R-H bond dissociation energies of CH_4, NH_3, H_2O, and FH. The calculated bond energies are low by 3.5, 2.5, 3.0, and 2.7 kcal/mol. The second series[2] included calculation of the R-R bond dissociation energies of C_2H_6, N_2H_4, H_2O_2, and F_2. Here the calculated bond energies are low by 0.1, -3.2, -1.8, and 0.8 kcal/mol, respectively (note that there is some uncertainty in the experimental value for $H_2N\text{-}NH_2$). Since the DC-CI method includes all correlation effects

associated with a particular bond, it should give accurate results for substituent effects [like D(CH_3O-H) versus D(C_2H_5O-H)], despite the fact that the substituent effect may be only 1 kcal/mol, while the absolute error in the total bond energy is 3 kcal/mol.

Peroxides and peroxy radicals are thought to be important intermediates in the low temperature combustion of alkanes. From the few known heats of formation and bond dissociation energies of peroxides, Benson and co-workers[3] have estimated the ΔH_f^0 of CH_3OOH, CH_3OO, and numbers of related systems. To obtain a better understanding of the thermochemistry of these species, we have calculated all of the O-O, O-C, and O-H bond dissociation energies of HOOH, CH_3OOH, and CH_3OOCH_3. Our calculated bond energies, plus the known heats of formation, allow us to calculate the ΔH_f^0 values for the remaining species.

To calculate these bond energies, we have applied the DC-CI method to substituted molecules. In addition, we have calculated the CH_3-OH, CH_3O-H, and C_2H_5O-H bond energies to provide comparisons between the bonds of peroxides and alcohols. The following sections describe our results and the details of the calculations.

II. Results

Tables I through IV list the calculated bond energies, along with the experimental values. Our calculations produce $D_e(A\text{-}B)$. To calculate $\Delta H^0_{f0^\circ K}(A\text{-}B)$ we have used experimental vibrational frequencies to determine zero point energy corrections (Tables V,[3-15] VI,[3-6,8,9,11-16] VII,[3-6,10-12,15,17] and VIII[3,4,6,11,12,14,15,18]). Where the vibrational frequencies were not available, we either used frequencies from similar compounds and our own calculations or we used zero point corrections for the same bond in another molecule. These exceptions are detailed in the footnotes of the tables. To obtain $\Delta H^0_{f298^\circ K}$ we have used the experimental heat capacity corrections, $\Delta H^0_{f298^\circ K} - \Delta H^0_{f0^\circ K}$, when available and standard heat capacity corrections for rotational and translational contributions to C_p in the remaining cases.

A. C-O Bonds. Table I contains the results of our calculations of the C-O bond dissociation energies of CH_3OOH, CH_3OOCH_3, and CH_3OH. The $\Delta H^0_{f298^\circ K}$ for CH_3OOH is not known. In Tables I-VIII we have used the average

$$\begin{aligned}\Delta H^0_{f298^\circ K}(CH_3OOH) &= \tfrac{1}{2}[\Delta H^0_{f298^\circ K}(HOOH) + \Delta H^0_{f298^\circ K}(CH_3OOCH_3)] \\ &= \tfrac{1}{2}[-32.53 - 30.0] \qquad (1) \\ &= -31.3 \text{ kcal/mol},\end{aligned}$$

as suggested by Benson.[19] The use of this average assumes that

$$\Delta H^0_f(CH_3O\text{-}OH) = \tfrac{1}{2}[\Delta H^0_f(HO\text{-}OH) + \Delta H^0_f(CH_3O\text{-}OCH_3)] \qquad (2)$$

$$\Delta H^0_f(CH_3\text{-}OOH) \approx \Delta H^0_f(HOO\text{-}H) \qquad (3)$$

and

$$\Delta H^0_f(CH_3\text{-}OOH) \approx \Delta H^0_f(CH_3\text{-}OOCH_3)\,. \qquad (4)$$

TABLE I: Theoretical and Experimental Bond Dissociation Energies (kcal). Calculated Values are from DC-CI.

Bond	$\Delta H^{0}_{f298°K}$ (C-O)		D_0 (C-O)		D_e (C-O)		Difference Expt. - Calc.
	Calc.	Expt.	Calc.	Expt.	Calc.	Expt.	
CH_3-OOH	72.3	71.0	69.9	68.7	76.4	75.2	-1.2
CH_3-$OOCH_3$	70.8	71.0	68.4	68.6	74.9	75.1	0.2
CH_3-OH	94.4	92.4	92.4	90.4	100.2	98.2	-2.0
CH_3-O^-	92.7	92.0	91.0	90.3	95.4	94.8	-0.6

TABLE II: Theoretical and Experimental O-H Bond Dissociation Energies (kcal). Calculated Values are from DC-CI.

Bond	$\Delta H^{0}_{f298°K}$ (O-H)		D_0 (O-H)		D_e (O-H)		Difference Expt. - Calc.
	Calc.	Expt.	Calc.	Expt.	Calc.	Expt.	
HOO-H	86.9	89.6	85.7	88.4	93.2	95.9	2.7
CH_3OO-H	85.7	89.6	84.2	88.1	91.7	95.6	3.9
HO-H	116.4	119.4	115.1	118.1	122.6	125.6	3.0
CH_3O-H	106.1	104.0	104.8	102.7	112.0	109.9	-2.1
C_2H_5O-H	106.1	104.2	105.3	103.4	112.8	110.9	-1.9

TABLE III: Theoretical and Experimental O-O Bond Dissociation Energies (kcal). Calculated Values are from DC-CI.

Bond	$\Delta H^0_{f298°K}$ (O-O)		D_0 (O-O)		D_e (O-O)		Difference Expt. - Calc.
	Calc.	Expt.	Calc.	Expt.	Calc.	Expt.	
HO-OH	53.3	51.5	51.5	49.7	56.8	55.0	-1.8
CH_3O-OH	50.0	43.2	47.9	41.1	52.1	45.3	-6.8
CH_3O-OCH_3	47.1	37.6	44.7	35.2	47.8	38.3	-9.5

TABLE IV: Theoretical and Experimental Electron Affinities (kcal). Calculated Values are from DC-CI.

Neutral Species	$\Delta H^0_{f298°K}$ (A) - $\Delta H^0_{f298°K}$ (A-)		$\Delta H^0_{f0°K}$ (A) - $\Delta H^0_{f0°K}$ (A-)		Equilibrium Electron Affinity		Difference Expt. - Calc.
	Calc.	Expt.	Calc.	Expt.	Calc.	Expt.	
F	77.7	79.9	76.2	78.4	76.2	78.4	2.2
OH	39.4	43.8	37.8	42.2	38.0	42.4	4.4
CH_3O	32.4	36.7	30.8	35.1	29.4	33.7	4.3

TABLE V: Corrections for Heat Capacity and Zero Point Energy in O-C Bonds (kcal).

Bond	$\Delta H^0_{f298°K}$ (C-O)	$\Delta H^0_{f298°K} - \Delta H^0_{f0°K}$	Zero Point Energy	D_e	Reference
CH_3-OOH	71.0	2.4 [a,b]	6.5 [c]	75.1	3,4-9
CH_3-$OOCH_3$	71.0	2.4 [b]	6.5 [c]	75.1	3,4-7,10
CH_3-OH	92.4	2.0	7.8	98.2	4,7,11-13
CH_3-O^-	92.0	1.7 [d,e]	4.5	94.8	4,7,14,15

[a] $\Delta H^0_{f0°K}(HOO) - \Delta H^0_{f298°K}(HOO) = 0.75$ kcal, estimated from standard translational and rotational contributions to C_p.

[b] $\Delta H^0_{f298°K} - \Delta H^0_{f0°K} = 2.4$ kcal, estimated as in note [a].

[c] Insufficient vibrational data available. Zero point correction from CH_3-OCH_3 used.

[d] $\Delta H_{f0°K}(CH_3O) - \Delta H_{f298°K}(CH_3O) = 1.8$ kcal, estimated as in note [a].

[e] Zero point energy of CH_3O estimated from CH_3F vibrational frequencies and ref. 15.

TABLE VI: Corrections for Heat Capacity and Zero Point Energy in O-H Bonds (kcal).

Bond	$\Delta H^0_{f298°K}$ (O-H)	$\Delta H^0_{f298°K} - \Delta H^0_{f0°K}$	Zero Point Energy	D_e	Reference
HOO-H	89.6	1.2[a]	7.5	95.9	3-5, 8, 9, 14
CH_2OO-H	89.6	1.5[b]	7.5[c]	95.6	3, 5, 6, 14
HO-H	119.4	1.3	7.5	125.6	6, 11, 12, 14
CH_3O-H	104.0	1.3	7.2[d]	109.9	3, 5, 13-15
C_2H_5O-H	104.2	0.8[e]	7.5[f]	110.9	5, 6, 14, 16

[a] $\Delta H^0_{f0°K}$ (HOO) - $\Delta H^0_{f298°K}$ (HOO) = 0.75 kcal, estimated from standard translational and rotational contributions to C_p.

[b] Estimated from standard translational and rotational contributions to C_p.

[c] Insufficient vibrational data available. Zero point correction from HOO-H used.

[d] $\Delta H_{f0°K}$ (CH_3O) - $\Delta H_{f298°K}$ (CH_3O) = 1.8 kcal, estimated as in note a.

[e] $\Delta H^0_{f0°K}$ C_2H_5O = -0.2, estimated.

[f] Zero point correction estimated from available vibrational data for C_2H_5F, $C_2H_5OC_2H_5$, CH_3OH, and HOOH.

TABLE VII: Corrections for Heat Capacity and Zero Point Energy in O-O Bonds (kcal).

Bond	$\Delta H^0_{f298°K}$ (O-O)	$\Delta H^0_{f298°K} - \Delta H^0_{f0°K}$	Zero Point Energy	D_e	Reference
HO-OH	51.5	1.8	5.3	55.0	4,5,11,12
CH_2O-OH	43.2	2.1[a]	4.2[b]	45.3	3,5,6,11,12,15
CH_3O-OCH_3	37.6	2.4[c]	3.1[d]	38.3	3,5,6,10,15,17

[a] $\Delta H_{f298°K} - \Delta H_{f0°K} = 2.1$, estimated from standard translational and rotational contributions to C_p.

[b] Zero point correction is average of that for HO-OH and CH_3O-OCH_3.

[c] $\Delta H_{f298°K} - \Delta H_{f0°K} = 2.4$, estimated as in note [a].

[d] Zero point correction estimated using experimental vibrational data for CH_3OCH_3 and HOOH, plus the calculated CH_3O-OCH_3 stretching frequency (716 cm^{-1}).

TABLE VIII: Corrections for Heat Capacity and Zero Point Energy in Electron Affinities (kcal).

Neutral Species	$\Delta H_{f298°K}(A) - \Delta H_{f298°K}(A^-)$	$\Delta H_{f298°K}(A - A^-) \Delta H_{f0°K}(A - A^-)$	Zero Point Correction	Equilibrium Electron Affinity	Reference
F	79.9	1.5	0	78.4	4, 11
OH	110.7	1.6	5.6[a]	115.3	11, 12, 14
CH_3O	36.7	1.6[b]	-1.4[c]	33.7	3, 6, 15, 18

[a] Calculated vibrational frequency used for HO^- (3924 cm^{-1}).

[b] Estimated using value for OH.

[c] $CH_3O\cdot$ has more zero point energy than CH_3O^-. See ref. 18.

TABLE IX: Bond energies in kcal/mol at 298°K using $\Delta H^0_{f298°K}(CH_3OO)$ = 4.7 versus 6.2 kcal/mol.

Our calculations in Table I show that (4) is not quite correct. We find that the CH_3-OOH bond is 1.5 kcal stronger than the CH_3-$OOCH_3$ bond. Even with this uncertainty, the C-O bond strengths are in excellent agreement with the experimental values.

The C-O bond strength of methanol was also calculated as a further calibration point. The ΔH_f^0 are well established for methanol, CH_3, and OH. Thus our small 2.1 kcal error in the CH_3-OH bond energy gives additional support to the validity of the calculated values for the peroxides. In fact, we expect that the error in the difference of the CH_3-OOH and CH_3-$OOCH_3$ bond energies should be much smaller, about 0.5 kcal maximum.

B. O-H Bonds. The results of our calculations of the O-H bond energies of HOOH, CH_3OOH, H_2O, CH_3OH, and C_2H_5OH are in Table II. The difference between methanol and ethanol involves the substitution of a methyl group for an alkyl hydrogen. We calculate this substituent effect to be 0.8 kcal (D_e), in very good agreement with the experimental difference of 1.0 kcal. Note that ethanol has the stronger O-H bond. The zero point and heat capacity corrections cancel out this difference, so that at 298° K the bond strengths are nearly equal. We calculate both of these bonds to be about 2 kcal stronger than the experimental values. On the other hand, calculations of the R-H bonds of CH_4, NH_3, H_2O, and FH average 2.9 kcal lower than the experimental values. In the Discussion section, we will propose means of resolving this discrepancy.

The difference between HOOH and CH_2OOH also involves the substitution of a methyl group for a hydrogen. In estimating the $\Delta H^0_{f298°K}$ for many hydrogen and alkyl peroxides, Benson[3] has assumed that $\Delta H^0_{f298°K}$ (ROO-H) is a constant 89.6 ± 2 kcal, which is the experimental value for HOO-H (Table II). We find this substituent effect to be 1.5 kcal,

with the HOO-H bond stronger than the CH_3OO-H bond. The accuracy of this difference is supported by the relative accuracy of our methanol and ethanol calculations. This 1.5 kcal substituent effect for ROO-H bonds is the same as calculated for the ROO-CH_3 bonds, showing the self-consistency of our method. The overall agreement with experiment is good, the HOO-H bond is calculated to be 2.7 kcal weaker than experiment, and the CH_3OO-H bond to be 3.9 kcal weaker than the indirect experimental value. At this point we have shown that Eqs. (3) and (4) are good approximations, but not precisely accurate, since our calculations show small but significant substituent effects of 1.5 kcal in both cases.

C. O-O Bonds. Table III compares the calculated and experimental bond energies for the three peroxides. The calculated HO-OH bond energy is in very good agreement with the experimental value (1.8 kcal high), but the substituted cases show major differences. This is surprising since we have very good agreement between the theoretical and experimental values for the O-C and O-H bonds previously discussed. The calculated strength of the CH_3O-OH bond is about 5 kcal stronger than expected, while the CH_3O-OCH_3 bond is 7.7 kcal stronger (assuming that they all would be 1.8 kcal high, as in HO-OH). We will discuss this discrepancy further in the Discussion section. It is interesting to note that the calculated strength of the CH_3O-OH bond (50.0 kcal) is almost exactly the average of the calculated HO-OH and CH_2O-OH bonds (50.2 kcal). Thus the assumption of Eq. (2) has proved to be very accurate.

III. Discussion

Our calculations agree fairly closely with the O-C and O-H bond dissociation energies of both the hydro- and methyl peroxides, using values derived from experimental heats of formation and group additivity concepts (Tables I and II). Experimentally, the $\Delta H^0_{f298°K}$ have not been determined for CH_3OOH and CH_3OO, and we have used Benson's estimates[3] in constructing our tables. Fortunately, our calculations provide direct information concerning the substituent effects in these peroxides that will enable us to suggest corrections of Benson's estimates of $\Delta H^0_{f298°K}$. We calculate that the CH_3OO-R (R = H, CH_3) bonds are 1.5 kcal weaker than the HOO-R bonds. The experimental columns of Tables I and II assume that there is no difference. To correct the experimental values, we can consider reducing $\Delta H^0_f(CH_3OO)$ by 1.5 kcal/mol, changing it from 6.2 kcal/mol to 4.7 kcal/mol. This change produces the correct substituent effects, while only altering the estimated $\Delta H^0_f(CH_3OO)$. The bond energies changed are compared in Table IX. Of course, this new estimate for $\Delta H_f(CH_3OO)$ also reduces the error of our calculation of the CH_3OO-H and CH_3OO-CH_3 bond energies. The CH_3OO-H error is reduced to 2.4 kcal (the bond energy is smaller than experiment), very similar to the 2.7 kcal deviation for HOO-H and the 3.0 kcal difference for HO-H. Also, the CH_3OO-CH_3 bond is calculated to be 1.3 kcal too large using $\Delta H^0_{f298°K}(CH_3OO)$ = 4.7 kcal, versus 0.2 kcal too small for $\Delta H^0_{f298°K}(CH_3OO)$ = 6.2 kcal. This now agrees with the direction of error in the calculated CH_3-OOH bond energy, which is 1.2 kcal too large. With these changes, the relative errors of these bonds are reduced to 0.1 kcal for CH_3-OOR bonds and 0.3 kcal for H-OOR bonds, well within our own 0.5 kcal estimate of the relative accuracy of the calculations for these similar bonds.

TABLE IX: Bond energies in kcal/mol at 298°K using $\Delta H^{o}_{f298°K}$ (CH_3OO) = 4.7 versus 6.2 kcal/mol.

Bond	Calc.	Experiment, using $\Delta H_f(CH_3OO) = 4.7$	Expt. -Calc.	Experiment, using $\Delta H_f(CH_3OO) =$ 6.2	Expt. -Calc.
CH_3OO-H	85.7	88.1	2.4	89.6	3.9
CH_3OO-CH_3	70.8	69.5	-1.3	71.0	0.2

Our calculated O-O bond energies for the methyl-substituted peroxides do not agree well with the experimental values. In fact, the difference is a function of the number of methyl groups. As previously discussed, the CH_3O-OH bond is calculated to be 5 kcal stronger than expected, and the CH_3O-OCH_3 bond is 7.7 kcal stronger than the experimentally measured dissociation energy.[17, 20] Recall that the heat of formation of CH_3OOH has been estimated by Benson from the average of the heats of formation of CH_3OOCH_3 and HOOH. Thus it is coupled to any change we make in ΔH_f (CH_3OOCH_3). Also, some of the strongest evidence for assigning $\Delta H^0_{f298°K}$ (CH_3O) = 3.8 kcal comes from the pyrolysis of CH_3OOCH_3 by Batt and McCulloch,[20] which directly determines $\Delta H^0_{f298°K}$(CH_3O-OCH_3) = 37.6 kcal, and the heat of formation of dimethyl peroxide measured by Baker et al.[10] as -30.0 kcal/mol. Thus, the heats of formation of CH_3O, CH_3OOH, and CH_3OOCH_3 are all interdependent from an experimental standpoint. Considering our results, the experimental measurement of the O-O dissociation energy would have to be changed to make the theory and experiment agree. A change of 8.4 kcal in the CH_3O-OCH_3 dissociation energy would be necessary, increasing the bond to 46.0 kcal. Since the ΔH_f(CH_3O) determination is dependent on this bond energy, the change necessitates the change of $\Delta H^0_{f298°K}$(CH_3O) from 3.8 kcal to 8.0 kcal. The O-O bond dissociation energy of CH_3OOH changes from 43.2 kcal to 47.4 kcal. This possible scheme is compared with the theoretical calculations in Table X. With these changes, the calculated O-O bond energies are 1.8, 2.6, and 1.1 larger than the altered experimental values for HOOH (unchanged), CH_3OOH, and CH_3OOCH_3, respectively. Even with the change in ΔH_f(CH_3O) we do not observe as much self-consistency in the relative errors of the theoretical calculations of the O-O bonds as we do in the calculations of the O-C and

TABLE X: Bond Energies in kcal/mol at 298°K using $\Delta H^{0}_{f298°K}$ (CH_3O) = 8.0 versus 3.8 kcal.

Bond	Calc.	Experiment, using $\Delta H_f(CH_3O) = 8.0$	Expt. -Calc.	Experiment, using $\Delta H_f(CH_3O) = 3.8$	Expt. -Calc.
CH_3O-OH	50.0	47.4	-2.6	43.2	-6.8
CH_3O-OCH_3	47.1	46.0	-1.1	37.6	-9.5

O-H bonds of the peroxides.

Other problems also exist. A change in the methoxy heat of formation would increase the O-H bond energy of methanol from 104.0 kcal to 108.2 kcal at 298° K. This would cause the calculated value to be low by 2.1 kcal, which is consistent with all of the other R-H bond energies calculated, except ethanol. In order to maintain the equivalence of the CH_3O-H and C_2H_5O-H bonds, we would have to increase the heat of formation of ethoxy radical by 4.2 kcal also. One experimental determination of the relative O-H bond energies of methanol and ethanol has been made by McIver and Miller.[21] They report the heterolytic bond dissociation energies

$$ROH = RO^- + H^+ , \qquad (7)$$

which can be combined with the heats of formation of ROH, H^+, and H to obtain the relative RO-H bond dissociation energies. For methanol, they have determined $\Delta H^0_{f298°K}(CH_3O^-) + \Delta H^0_{f298°K}(H^+) - \Delta H^0_{f298°K}(CH_3OH) =$ 378.1 kcal. However, independent measurement of the electron affinity of one of the alkoxy radicals is necessary to determine the absolute bond energies. This has been done by Janousek et al.[18] who measure EA ($CH_3O\cdot$) = 36.7 kcal at 300° K. Using these two values, plus IP (H) = 315.1 kcal, we get $\Delta H^0_{f298°K}(CH_3O\text{-}H)$ = 99.7 kcal, which disagrees with the calculations of Janousek et al., where they used IP(H) at 0° K instead of $[\Delta H^0_{f298°K}(H^+) - \Delta H^0_{f298°K}(H)] = IP_{298°K}(H)$. This result does not agree well with either the accepted value of 104.0 kcal or our calculation of 106.1.

We have also used our method to calculate electron affinities (Table IV). Our calculated electron affinity for OH is 4.4 kcal too low, whereas the calculated value for CH_3O is 4.3 kcal too low, entirely consistent with

the OH value. Here we have used the measurement of Janousek et al. for the methoxy electron affinity. Thus we agree with their experiment and therefore do not agree with the experiment of McIver and Miller. The theoretical results support $\Delta H^{0}_{f298^\circ K}(CH_3O\text{-}H)$ = 108.2 kcal and $\Delta H^{0}_{f298^\circ K}(C_2H_5O\text{-}H)$ = 108.4 kcal, using the experimental heats of formation of methanol and ethanol, plus 8.0 kcal for the $\Delta H^{0}_{f298^\circ K}$ of methoxy radical.

In conclusion, we are able to suggest a different heat of formation for CH_3OO by using our theoretical substituent effects upon the O-C and O-H bonds of the methyl and hydroperoxides. Even without this 1.5 kcal correction, the theoretical calculations agree very well with the experimental measurements. On the other hand, the O-O bond calculations suggest that the heat of formation of methoxy may be as much as 4.2 kcal larger than the accepted value of 3.8 kcal. Hopefully further research will resolve this issue.

IV. Calculational Method

The calculational methods used in this work are the same as those applied previously to R-H and R-R bond dissociation calculations, with extensions to properly include differential substituent interactions. We will briefly describe our approach here, including the necessary extensions for substituted molecules. These changes do not alter the calculations for unsubstituted molecules (e.g., H-OH, HO-OH).

When a bond is broken, the most important differential correlation effects involve correlations of the electrons in the bond being broken. We denote this bond as the active bond. Also of importance are any other bonds and lone pairs to the centers of the active bond (the active centers), which change significantly upon dissociation or correlate with the active bond. We will call these the semi-active electrons. The remaining electrons in the molecule are referred to as inactive electrons, if their description does not change appreciably upon dissociation of the active bond.

The important differential electron correlation usually occurs in the vicinity of the active bond so that a localized description of the bonds is a calculational advantage. As such, we first solve self-consistently for the GVB orbitals in our calculations. Here each valence electron has its own optimized orbital. This MCSCF includes the dominant correlation terms: left/right correlation of bond pairs and in/out correlation of lone pairs. The GVB orbitals also have the property of dissociating correctly to the proper energy of the separated species.

For the general R-R′ dissociation we can divide the localized valence orbitals into four groups:

i) active orbitals (two for an R-R′ single bond);

ii) semi-active orbitals of R (two for each remaining valence electron

pair of the active center of R, generally leading to a total of six);

iii) semi-active orbitals of R′ (generally another six, but there are none when R′ = H);

iv) inactive orbitals of R and R′.

For example, in calculating the O-O bond dissociation of CH_3OOH,

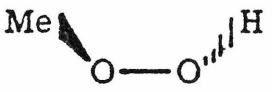

there are 20 valence electrons divided into two active orbitals (O-O GVB pair), six semi-active orbitals on the left oxygen (two lone pairs and an O-C bond pair), six semi-active orbitals on the right oxygen (two lone pairs and an O-H bond pair), and three inactive orbitals on the methyl group (doubly-occupied).

The R• fragments are also solved self-consistently. Each fragment has

i) an active orbital (the radical orbital),

ii) semi-active orbitals [same as (ii) above], and

iii) inactive orbitals.

In our previous example, the left oxygen has one active orbital, six semi-active orbitals, and three inactive valence orbitals; whereas the right oxygen has one active orbital and six semi-active orbitals. Note that the sum of the number of active and semi-active orbitals for the two fragments is the same as the respective number of active and semi-active orbitals of CH_3OOH. Consequently, the GVB orbital basis is dissociation-consistent.

In each case, the GVB calculation is followed by a CI calculation to determine the final energies of each species. For the molecular species, the orbital basis for the CI calculation consists of

i) the two active orbitals,

ii) all of the semi-active orbitals,

iii) polarization functions on each active center (referred to as virtual orbitals), and

iv) all of the inactive orbitals (except the 1s core orbitals).

For the radical species, the CI orbital basis included

i) the active orbital,

ii) all of the semi-active orbitals,

iii) polarization functions on the active center, and

iv) all of the inactive orbitals (except the 1s core orbitals).

The polarization functions for the active centers of the molecule map on a one-to-one basis into the polarization functions of the two radical fragments. This makes the CI orbital basis dissociation-consistent also.

It is necessary to carefully consider the modes of electron correlation needed to describe bond dissociation when selecting spatial configurations for the CI calculations. To be dissociation-consistent, we require that the molecular CI configuration space is a product of the corresponding CI configuration spaces of the two fragments. Here is where the use of localized GVB orbitals becomes imperative. Many kinds of correlation (left/right, radial, angular, spin polarization) are well described from a few spatial configurations if the basis is localized. Thus the list of spatial configurations for the fragments can be relatively short (90 for hydroxy radical) and the product of the two fragment lists is still a very tractable size (4200 for HO-OH) despite the fact that quadruple excitations are explicitly included. Emphasis is placed on (i) including a good description of the active electron correlation plus any other semi-active correlation and coupled modes that are differential, and (ii) insuring that the configurations to be included are systematic and not dependent upon the importance of particular configurations

for a particular case. Total energy is not a criterion since we seek the most compact list of spatial configurations that adequately describe the dissociation.

We will express each term in the fragment CI as the product of the semi-active CI, on the left, times the active CI, on the right

$$[\text{semi-active CI}] \times [\text{active CI}] .$$

The spatial list is the same for each fragment, and it is the same as the list used in calculating the R-H and R-R bond dissociation energies reported previously. The notation will be explained as it is used.

i) [GVB-PP(2)] × [1/1]: We started with all double excitations from the dominant configuration of the GVB wavefunction with with the requirement that the two electrons of each GVB pair remain in the two natural orbitals defining the pairs and not permitting any orbital except the radical p orbital to be singly-occupied. These configurations are usually called GVB perfect-pairing configurations; hence the notation GVB-PP(2) for all such double excitations. These configurations allow left/right bond correlation and in/out lone-pair correlation. We multiply this set of configurations by all single excitations from the active orbital, denoted 1/1 since excitation to any empty or singly-occupied orbital is allowed.

ii) [GVB-RCI(1)] × [1/1]: To the above configurations we added all single excitations with the requirement that the two electrons of a GVB pair remain within the two natural orbitals defining the pair. This is called a GVB restricted-CI, and it allows spin optimization between bonds and between bond pairs and the radical orbital. Again we multiply these configurations by all single excitations from the active orbital,

allowing shape readjustments.

iii) All single and double excitations from the active to the semi-active orbitals and from the semi-active to the active orbitals. These configurations relax the strong orthogonality of the GVB pairs.

iv) For cases with inactive valence orbitals (e.g., the molecular orbitals describing the C-H bonds of the $CH_3O\cdot$ fragment), we add all single and double excitations, allowing only excitations from the active to the semi-active, and from the inactive to the semi-active and active orbitals. This is equivalent to allowing the same excitations for the inactive orbitals as for the semi-active orbitals in term (iii). Of course, the inactive orbitals are delocalized molecular orbitals rather than GVB orbitals, so there are fewer possible excitations. These configurations are very important in correctly including the substituent effects. Our results indicate that only the inactive orbitals of the centers bonded to the active centers have important excitations. The SCF orbitals of large substituents can be localized to segregate these orbitals. For the unsubstituted $HO\cdot$ fragment, this spatial list has 90 configurations (126 spin eigenfunctions or 162 determinants). The CH_3O fragment has 156 configurations.

The molecular CI is much more complex since the product of two radical spatial lists produces many cross terms. We will express each term as a triple product:

$$[\text{left semi-active CI}] \times [\text{active CI}] \times [\text{right semi-active CI}] ,$$

where left and right denote the semi-active orbitals of the two active centers. The terms for this CI are:

i) $[\text{GVB-PP(2)}] \times [2/2] \times [\text{GVB-PP(2)}]$: All GVB perfect-pairing doubles

in the semi-active orbitals of the left center times all single and double excitations from the active orbital times all GVB perfect-pairing doubles in the semi-active orbitals of the right center.

ii) [GVB-RCI(1)] × [2/2] × [GVB-RCI(1)]: All GVB restricted-CI singles in the left semi-active orbitals times all single and double excitations from the active orbital times all GVB restricted-CI singles in the right semi-active orbitals.

iii) [GVB-PP(2)] × [2/2] × [GVB-RCI(1)] + [GVB-RCI(1)] × [2/2] × [GVB-PP(2)]: The cross-terms analogous to (i) and (II). Terms (i) through (iii) dissociate into terms (i) and (ii) of the fragment CI.

iv) All single and double excitations from the active to the semi-active orbitals and vice versa. This term dissociates correctly into the third term of the fragment CI.

v) For cases with inactive orbitals, we add all single and double excitations, allowing only excitations from the active to the semi-active and from the inactive to the semi-active and active orbitals. This term dissociates into the last term of the fragment CI.

This product of the two radical CI lists emphasizes correlation of the active electrons yet includes the important semi-active correlations and cross terms also. For the O-O bond of HOOH, the entire list contains 4200 spatial configurations (10188 spin eigenfunctions or 34377 determinants). For the same bond in CH_3OOH there are 4437 configurations. All excitations that were greater than quadruples with respect to the dominant configuration have been eliminated, as tests show that they do not contribute significantly to the total energy (less than 0.1 kcal for the C-C bond of ethane).

In summary, we have extended the method for calculating R-H and R-R′ bond dissociation to correctly describe substituted species [e.g., $(CH_3)_3C\text{-}C(CH_3)_3$ or $C_2H_5O\text{-}H$]. In each case we divide the orbitals for the molecule and its corresponding fragments into groups, according to their importance in the dissociation process:

i) active GVB orbitals [the bond(s) being broken];

ii) semi-active GVB orbitals (the other bonds and lone pairs associated with the active centers;

iii) virtual orbitals associated with the active centers (polarization functions); and

iv) inactive SCF orbitals (substituent orbitals).

The CI basis [groups (i) through (iii) plus substituent orbitals of (iv)] dissociates cleanly into two groups of fragment orbitals with a one-to-one mapping. The CI calculation also maintains dissociation consistency in the spatial configurations used. As the active bond is stretched, the molecular CI wavefunction becomes precisely two fragment CI wavefunctions.

V. Calculational Details

A. Basis Sets. For C, N, O, and F we used the (9s, 5p) gaussian basis of Huzinaga[22] contracted to valence double zeta level (3s, 2p) by Dunning.[23] To this we have added a set of single exponent gaussian d functions on each active center and all oxygens. These exponents were optimized for correlated wavefunctions. Also, diffuse s and p functions were added to the active centers and all oxygens (optimized for GVB wavefunctions of the corresponding negative ions). Details of these optimizations are given in an earlier paper.[24] For hydrogen we used the (3/1/1) triple zeta contraction of Huzinaga's unscaled five-gaussian basis.[22] When hydrogen was an active center and for all hydrogens bonded to oxygen, we added a set of single gaussian p polarization functions to the hydrogen.[24]

B. Geometries. The chosen structures are in Tables XI[24-27] and XII.[12,24-27] Whenever possible, we used experimental structures for our calculations. These experimental structures are known well enough that further optimization would not significantly alter the bond energies. We optimized the structures of HOOH, CH_3OOH, CH_3OOCH_3, CH_3O, and CH_3O^-, using the methods detailed in another publication.[24]

C. Self-Consistent Field Wavefunctions. The ground state of each molecule and each fragment was solved self-consistently with the GVB2.5 program. For the R-H bonds there were four GVB pairs, each pair consisting of two natural orbitals. The other R-R′ bond calculations had seven GVB pairs (14 natural orbitals). The substituent orbitals were optimized self-consistently as doubly-occupied orbitals. The R• fragments had three GVB pairs and a radical orbital, leading to a total of seven GVB orbitals.

TABLE XI: Structural Parameters Used for Closed-Shell Species in Bond Energy Calculations.[a]

Molecule	Structural Parameters			Ref.
HOOH	$r_{OO} = 1.464$	$\theta_{OOH} = 99.9$	$\phi = 119.1$	24
	$r_{OH} = 0.967$			
CH_3OOH[b]	$r_{OO} = 1.452$	$\theta_{OOH} = 99.6$	$\phi = 126$	24
	$r_{OH} = 0.967$	$\theta_{OOC} = 105.0$		
	$r_{OC} = 1.446$			
CH_3OOCH_3[b]	$r_{OO} = 1.450$	$\theta_{OOC} = 104.1$	$\phi = 180$	24
	$r_{OC} = 1.444$			
H_2O	$r_{OH} = 0.9575$	$\theta_{HOH} = 104.5$		25
CH_3OH[b]	$r_{OH} = 0.963$	$\theta_{COH} = 108.0$		26
	$r_{CO} = 1.421$			
C_2H_5OH	$r_{CO} = 1.431$	$\theta_{CCH} = 110.7$		26
	$r_{C_\alpha H} = 1.098$	$\theta_{COH} = 105.4$		
	$r_{CC} = 1.512$	$\theta_{CCH_a} = 110.1$		
	$r_{C_\beta H_a} = 1.091$	$\theta_{CCH_s} = 110.5$		
	$r_{OH} = 0.971$			
	$r_{C_\beta H_s} = 1.088$			
CH_3O^-	$r_{CO} = 1.401$	$\theta_{OCH} = 114.1$		this work
	$r_{CH} = 1.137$			

[a] Bond lengths are in Ångstroms, angles are in degrees, and ϕ are dihedral angles.

[b] Methyl groups as in dimethyl ether: $r_{CH_a} = 1.100$, $r_{CH_s} = 1.091$, $\theta_{OCH_a} = 110.8$, and $\theta_{OCH_s} = 107.2$; ref. 27.

TABLE XII: Structural Parameters Used for Radical Species in Bond Energy Calculations.[a]

Species	Structural Parameters		Ref.
$\cdot OH$	$r_{OH} = 0.9697$		12
$\cdot CH_3$	$r_{CH} = 1.079$	$\theta_{HCH} = 120.0$	25
$HOO\cdot$	$r_{OO} = 1.342$	$\theta_{OOH} = 104.2$	24
	$r_{OH} = 0.972$		
$CH_3O\cdot$	$r_{CO} = 1.410$	$\theta_{CH_a} = 111.1$	24
	$r_{CH_a} = 1.112$	$\theta_{CH_s} = 106.9$	
	$r_{CH_s} = 1.111$		
$CH_3OO\cdot$[b]	$r_{OO} = 1.339$	$\theta_{COO} = 110.2$	24
	$r_{OC} = 1.442$		
$C_2H_5O\cdot$[c]	$r_{CO} = 1.409$	$\theta_{OCH} = 110.7$	26
	$r_{C_\alpha H} = 1.098$	$\theta_{CCH_a} = 110.1$	
	$r_{CC} = 1.512$	$\theta_{CCH_s} = 110.5$	
	$r_{C_\beta H_a} = 1.091$		
	$r_{C_\beta H_s} = 1.088$		

[a] Bond lengths are in Ångstroms, and angles are in degrees.

[b] Methyl group as in dimethyl ether: $r_{CH_a} = 1.100$, $r_{CH_s} = 1.091$, $\theta_{OCH_a} = 110.8$, and $\theta_{CH_s} = 107.2$; ref. 27.

[c] Structure of C_2H_5O is not known, so the structure for C_2H_5OH was used, with C-O bond reduced from 1.431 to 1.409 Å.

D. Configuration Interaction Basis. For each molecule the five correlating d functions on each active center were Schmidt-orthogonalized to the occupied orbitals (which included some d character). The two sets of five d-like functions were then symmetrically orthogonalized to each other. This process produces a localized and symmetric set of correlating virtual orbitals. The d orbitals on the fragments were simply orthogonalized to the occupied orbitals. The full molecular CI basis consisted of 14 GVB natural orbitals (two active, 12 semi-active), ten d-like correlating orbitals, and any substituent SCF valence orbitals. For the O-O bond dissociation of HOOH, there were 24 orbitals in the CI, and for CH_3OOH there were 27 orbitals. The corresponding CI basis for the fragments consisted of the six GVB natural orbitals (semi-active), the radical orbital (active), five d-like correlating orbitals, and any substituent SCF valence orbitals. For example, the OH CI basis has 12 orbitals and the CH_3O CI basis had 15 orbitals.

TABLE XIII: Ab Initio Total Energies for Closed-Shell Wavefunctions Used in Bond Energy Calculations.

Molecule	Hartree-Fock	GVB	DC-CI
CH_3-OOH	-189.8486	-189.9800	-190.0207
CH_3-$OOCH_3$	-228.8547	-228.9859	-229.0266
CH_3-OH	-115.0762	-115.1845	-115.2272
CH_3-O^-	-114.4327	-114.5414	-114.5884
HOO-H	-150.8189	-159.9040	-150.9366
CH_3OO-H	-189.8249	-189.9090	-189.9420
HO-H	-76.0492	-76.1114	- 76.1468
CH_3O-H	-115.0463	-115.1095	-115.1456
C_2H_5O-H	-154.0742	-154.1380	-154.1743
HO-OH	-150.8185	-150.9426	-150.9938
CH_3O-OH	-189.8249	-189.9486	-190.0020
CH_3O-OCH_3	-228.8311	-228.9555	-229.0108
F^-	-99.4456	-99.5010	-99.5484
$[OH]^-$	-75.4030	-75.4680	-75.5122
CH_3O^-	-114.4327	-114.4950	-115.5382

TABLE XIV: Ab Initio Total Energies for Radical Wavefunctions (hartrees).

Species	Hartree-Fock	GVB	DC-CI
H·	-0.4998	-0.4998	-0.4998
·CH_3 (for CH_3-OH)	-39.5684	-39.6116	-39.6158
·CH_3 (for CH_3-O^-)	-39.5620	-39.6065	-39.6109
·CH_3 (for CH_3-OOH, CH_3-OOCH_3)	-39.5618	-39.6063	-39.6108
·OH	-75.4083	-75.4490	-75.4516
·F	-99.3956	-99.4249	-99.4269
CH_3O· (for CH_3O electron affinity)	-114.4444	-114.4850	-114.4913
CH_3O· (for CH_3O-H, CH_3O-OCH_3)	-114.4201	-114.4608	-114.4673
C_2H_5O·	-153.4477	-153.4882	-153.4947
HOO·	-150.2142	-150.2664	-150.2882
CH_3OO·	-189.2209	-189.2726	-189.2964

VI. Summary

Ab initio GVB and DC-CI methods are applied to calculations of the O-O, O-C, and O-H bond energies of HOOH, CH_3OOH, and CH_3OOCH_3. These results demonstrate the usefulness of our method in calculating substituent effects. Very good agreement is obtained between the calculated O-C and O-H bonds and experimental values. We suggest that the heat of formation of CH_3OO (298°K) is 1.5 kcal smaller than previous estimates (ΔH_f = 4.7 kcal) to account for the calculated substituent effects. A major discrepancy exists between the calculated O-O bond strengths of CH_3OOH and CH_3OOCH_3 and the current experimental values. One solution calls for an increase in the heat of formation of methoxy radical from 3.8 kcal to 8.0 kcal (298°K). However, this change conflicts with several experimental results and remains unresolved.

Acknowledgments

The author wishes to thank the U.S. Department of Energy for partial support of this work under Contract No. DE-AC03-76SF00767, Project Agreement No. DE-AT03-80ER10608.

References and Notes

(1) Bair, R. A.; Goddard, W. A., III, manuscript in preparation.

(2) Bair, R. A.; Goddard, W. A., III, manuscript in preparation.

(3) Nagia, P. S.; Benson, S. W. J. Phys. Chem. 1979, 83, 1138.

(4) "JANAF Thermochemical Tables", 2nd ed.; NSRDS-NBS 37; U. S. Government Printing Office: Washington, D. C., 1970.

(5) Shimanouchi, T. J. Phys. Chem. Ref. Data 1977, 6, 993.

(6) "Tables of Molecular Vibrational Frequencies, Consolidated Volume I", Shimanouchi, T., Ed.; NSRDS-NBS 39; U. S. Government Printing Office: Washington, D. C., 1972.

(7) Surratt, G. T.; Goddard, W. A., III, Chem. Phys. 1977, 23, 39.

(8) Blukis, U.; Kasai, P. H.; Myers, R. J. J. Chem. Phys. 1963, 38, 2753.

(9) Smith, D. W.; Andrews, L. J. Chem. Phys. 1974, 60, 81.

(10) Baker, G.; Littlefair, J. H.; Shaw, R.; Thynne, J. C. J. Int. J. Chem. Kinet. 1965, 1965, 6970.

(11) Chase, M. W.; Curnutt, J. L.; Hu, A. T.; Prophet, H.; Syverud, A. N.; Walker, L. C. J. Phys. Chem. Ref. Data 1974, 3, 311.

(12) Huber, K. P.; Herzberg, G. "Molecular Spectra and Molecular Structure", Van Nostrand Reinhold Company: New York, 1979; Vol. 4.

(13) Chen, S. S.; Wilhoit, R. C.; Zwolinski, B. J. J. Phys. Chem. Ref. Data 1977, 6, 105.

(14) Chase, M. W.; Curnutt, J. L.; Prophet, H.; McDonald, R. A.; Syverud, A.N. J. Phys. Chem. Ref. Data 1975, 4, 1.

(15) Engelking, P. C.; Ellison, G. B.; Lineberger, W. C. J. Chem. Phys. 1978, 69, 1826

(16) Domalski, E. S. J. Phys. Chem. Ref. Data 1972, 1, 221.

(17) Barker, J. R.; Benson, S. W.; Golden, D. M. Int. J. Chem. Kinet. 1977, 9, 31.

(18) Janousek, B. K.; Zimmerman, A. H.; Reed, K. J.; Brauman, J. I. J. Am. Chem. Soc. 1978, 100, 6142.

(19) Benson, S. W.; Shaw, R. In "Organic Peroxides", Swern, J., Ed.; Wiley-Interscience: New York, 1970; Vol. I, p. 126.

(20) Batt, L.; McCulloch, R. D. Int. J. Chem. Kinet. 1976, 8, 491.

(21) McIver, R. T.; Miller, J. S. J. Am. Chem. Soc. 1974, 96, 4323.

(22) Huzinaga, S. J. Chem. Phys. 1965, 42, 1293.

(23) Dunning, T. H., Jr., Hay, P. J. In "Modern Theoretical Chemistry: Methods of Electronic Structure Theory", Schaefer III, H. R., Ed.; Plenum Press: New York, 1977; Vol. 3, Chapter 1, p. 23.

(24) Bair, R. A.; Goddard, W. A., III; manuscript in preparation.

(25) Callomon, J. H.; Hirota, E.; Kuchitsu, K.; Lafferty, W. J.; Maki, A. G.; Pote, C. S. "Structure Data of Free Polyatomic Molecules", Landolt-Börnstein, New Series, Group II; Springer-Verlag: New York, 1976; Vol. 7.

(26) Harmony, M. D.; Laurie, V. E.; Koczkowski, R. L.; Schwendeman, R. H.; Ramsay, D. A.; Loras, F. J.; Lafferty, W. J.; Maki, A. G. J. Phys. Chem. Ref. Data 1979, 8, 619.

(27) Beers, Y.; Howard, C. J. J. Chem. Phys. 1976, 64, 1541.

Appendix:

Ab Initio Studies of the Structures of Peroxides and Peroxy Radicals

Introduction

Alkyl peroxides play an important part in hydrocarbon oxidation processes, yet few structural data are available, and reliable theoretical studies have previously been limited to the hydroperoxy species. In this study we have carried out ab initio generalized valence bond (GVB) and configuration interaction (CI) studies of the structures of the hydro and methyl peroxides, and the corresponding peroxy radicals:

$$HOOH,\ CH_3OOH,\ CH_3OOCH_3,\ HOO\cdot,\ CH_3OO\cdot$$

In all of these species it is necessary to include electron correlation in the wavefunction to determine an accurate equilibrium structure. Our calculations agree closely with the well-established experimental structures for HOOH and HOO·, giving strong support to the reliability of calculated structures for the remaining species.

Calculational Details

For carbon and oxygen, the (9s, 5p) gaussian basis of Huzinaga[1] was contracted using Dunning's coefficients to the valence double zeta (3s, 2p) level.[2] In addition, d polarization functions (α = 0.99) were added to the oxygen atoms. The hydrogen basis consisted of the Huzinaga (5s) gaussian basis contracted to three functions (but not scaled). Wherever hydrogen was bonded to oxygen, p polarization functions were added to the hydrogen (α = 1.25). This was found unnecessary for hydrogens bonded to carbon.

The C-H bond distances and O-C-H angles were chosen as those from the experimentally determined structure of dimethyl ether and not varied in our calculations. There is good support for this assumption since full optimization of the structure of $CH_3O\cdot$ led to essentially the same parameters (Table I). One would expect the methoxy radical to have larger C-H and O-C-H distortions than the other molecules in this study. Thus, in this study we optimized all the structural parameters for each molecule, except the C-H bond distances and O-C-H bond angles.

For each molecule the wavefunctions were solved self-consistently, using the GVB2.5 program.[3]
All of the valence electrons in the C-O, O-O, and H-O bonds were correlated (GVB pairs), allowing each electron to have its own optimized orbital. The oxygen lone pairs were also correlated as GVB pairs. For example, HOOH with its seven valence electron pairs was described with 14 localized GVB orbitals (and two core orbitals) optimized self-consistently. For $CH_3OO\cdot$ we correlated all nine valence electron pairs, including the C-H bonds. However, the results were not significantly affected by the correlation in the CH bonds, and, consequently, the C-H bonds were not correlated in CH_3OOH and CH_3OOCH_3.

TABLE I. Equilibrium Structure of $CH_3O\cdot$.

	r_{CO}	r_{CH_a}	r_{CH_s}	θ_{OCH_a}	θ_{OCH_s}
GVB + CI	1.410	1.112	1.111	111.1	106.9
Experimental[a] (CH_3OCH_3)	1.410	1.100	1.091	110.8	107.2

[a] Reference 14.

The basis for CI calculations consisted of all of the GVB orbitals (two per bond or lone pair correlated). For the radicals, the singly-occupied orbital was included, along with an additional more diffuse p-like orbital projected from the virtual space and centered on the radical atom. Thus both HOOH and HOO• have a CI basis of 14 orbitals. The CI calculation consisted of all single and double excitations from the dominant configuration, plus all closed-shell quadruple excitations from the dominant configuration, restricting the electrons to remain within their respective GVB pairs. Of course, the radicals always had at least one open shell.

Results

HOOH: The structure of HOOH has been the focus of numerous experiments; however, these experiments do not provide an unambiguous structure. This is because there are four structural parameters to determine, but only three rotational constants for the microwave spectra. The geometry often quoted is

$$R_0(OH) = 0.950 \text{ Å}$$
$$R_0(OO) = 1.475$$
$$\theta(OOH) = 94.8°$$
$$\phi(\text{dihedral}) = 111°$$

which was obtained with the assumption that $R_{OH} = 0.950$ Å.[4] In 1979, Cremer and Christen[5] reanalyzed the existing microwave data and concluded that more reasonable structures result from the assumption that $R_0(OH) = 0.965$ or 0.967 Å. This leads to the following structures:

$$R_0(OH) = 0.965 \text{ Å}$$
$$R_0(OO) = 1.464 \text{ Å}$$
$$\theta = 99.4°$$

and

$$R_0(OH) = 0.967 \text{ Å}$$
$$R_0(OO) = 1.463 \text{ Å}$$
$$\theta = 99.3°.$$

Cremer and Christen also determined that the best choice for the dihedral angle was

$$\phi = 120.2°.$$

As indicated in Table II, this is in almost exact agreement with our results.

TABLE II. Theoretical and Experimental Equilibrium Geometries of Peroxides. Values in Parentheses were Assumed in the Calculations. Distances in Ångstroms and Angles in Degrees. ϕ is the Dihedral Angle.

	Method	r_{OO}	r_{OH}	r_{OC}	θ_{OOH}	θ_{OOC}	ϕ	Ref.
A.	HOOH							
	Experimental	1.464	0.965		99.4		120.2	5
	Ab Initio							
	Correlated (GVB + CI)	1.464	0.967		99.9		119.1	this work
	Correlated (RS-MP2)	1.451	0.967		99.3		119.3	6
	Uncorrelated (RHF)	1.390	0.943		102.9		111.2	6
	Semi-Empirical							
	MINDO/2	1.404	0.966		90.3		115.5	7
	INDO	1.22	1.04		83.5		108.8	8
B.	CH_3OOH							
	Ab Initio							
	Correlated (GVB + CI)	1.452	0.967	1.446	99.6	105.0	126	this work
	Semi-Empirical							
	MINDO/2	1.414	0.970	1.338	115.6	119.0		7
	CNDO/2	1.23	(0.96)	(1.44)	109	109		9
C.	CH_3OOCH_3							
	Experimental					105	~170[a]	11,13
	Ab Initio							
	Correlated (GVB + CI)	1.450		1.444		104.1	180.0	this work
	Semi-Empirical							
	MINDO/2	1.424		1.338		118.7	96.5	7

[a] See text.

We observe that the calculated O-O length is 0.01 Å shorter than in hydrogen peroxide, in spite of the fact that thermochemical estimates would place the CH_3O-OH bond 5 to 10 kcal weaker. Hence, the O-O bond strengths do not correlate with the bond lengths for these peroxides.

On the other hand, the dihedral angle has increased from 119° in HOOH to 126° in CH_3OOH. An analysis of the GVB wavefunctions leads to a reasonable interpretation of these results. The O-H bonds are polar, placing a small net positive charge on the hydrogen. Thus a small amount of stabilization can be gained by overlapping the hydrogens on one oxygen with the lone pairs on the other. In HOOH, the lowest energy conformation has each O-H bond nearly eclipsing a lone pair (Figure 1). In our calculations, the valence electrons are localized, so we are able to determine that the angle between the oxygen lone pairs on each oxygen is 140°. (The same angle is found for all three of the peroxides, while the angle is 123° in H_2O.) This makes the bond pair-lone pair angle 110°. Of course, the lone pairs on one oxygen will tend to repel those on the other, but there are two favorable hydrogen-lone pair interactions in HOOH and only one unfavorable interaction. For CH_3OOH there is only one favorable interaction because the lone pair-methyl interaction is repulsive, opening the dihedral angle by 7°. Relative to previous theoretical studies (all empirical) of methyl hydroperoxide,[7,9] our OOC and OOH bond angles are significantly smaller. No previous estimate of the dihedral angle has been available. However, the zero-point energy in the torsional mode is greater than the calculated inversion barrier height, so considerable fluctuation is expected in this mode (Figure 2). Indeed, experiments may have difficulty in detecting the nonplanarity of the COOH group.

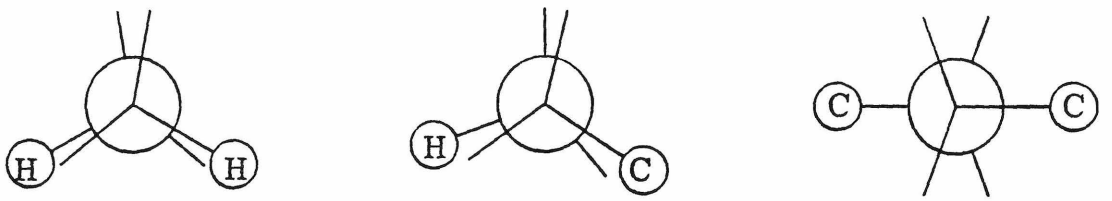

HOOH $\phi = 119°$

CH_3OOH $\phi = 126°$

CH_3OOCH_3 $\phi = 180°$

Figure 1. Calculated equilibrium structures of peroxides, projected along the O-O bond. Lone pairs are shown as lines with no atoms at the terminus. In each case the angle between the two lone pairs on an oxygen is 140°.

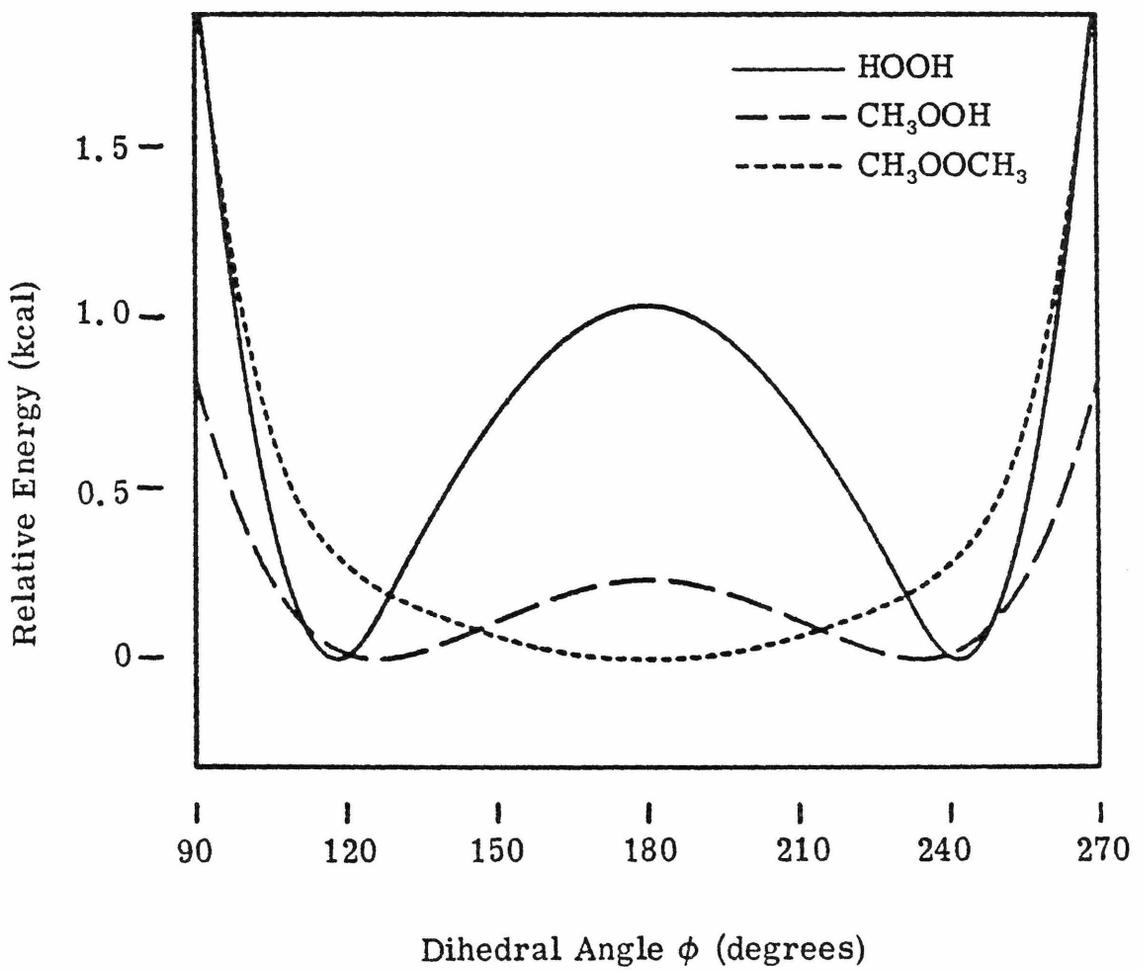

Figure 2. Calculated potential curves as a function of dihedral angle. All other structural parameters are fixed at the calculated equilibrium values.

$$R_0(OH) = 0.967 \text{ Å}$$
$$R_e(OO) = 1.464 \text{ Å}$$
$$\theta(OOH) = 99.9°$$
$$\phi = 119.1°.$$

Another set of ab initio correlated wavefunctions was calculated by Cremer (RS-MP2),[6] leading to geometries almost identical to ours except that the OO bond is 0.01 Å shorter (1.451 Å). This may be due to some residual bias in the RS-MP2 approach due to starting with uncorrelated wavefunctions. Uncorrelated wavefunctions (RHF) lead to an error of -0.07 Å in the OO bond, -0.02 Å error in the OH bond, +3.5° in the OOH angle, and -9° in the dihedral angle.

The results from semi-empirical and other approximate methods[7-10] lead to larger and nonsystematic errors, as indicated in Tables II and III. In general, MINDO/2 does fairly well for the bond distances of these species (except C-O bonds), but not very well for the bond angles, where errors of 10° or more are common. The INDO and CNDO/2 results are consistently poor. Our conclusion is that a proper description of electron correlation from ab initio calculations is essential to obtain accurate structural parameters.

CH_3OOH: No experimental structural data are available for methylhydroperoxide, and to our knowledge, these calculations represent the first reported ab initio studies done on this molecule. Our calculated equilibrium structure is

$$R(OC) = 1.446 \text{ Å}$$
$$R(OH) = 0.967 \text{ Å}$$
$$R(OO) = 1.452 \text{ Å}$$
$$\theta(OOC) = 105.0°$$
$$\theta(OOH) = 99.6°$$
$$\phi = 126°.$$

CH_3OOCH_3: The O-O-C bond angle of dimethyl peroxide was obtained in 1950 from electron diffraction measurements.[11] Our calculated angle of 104.1° is well within the bounds of the experimental value of 105 ± 3°. The electron diffraction data were not sufficient to determine the other structural parameters. The complete equilibrium structure calculated is

$$R(OC) = 1.444 \text{ Å}$$
$$R(OO) = 1.450 \text{ Å}$$
$$\theta(OOC) = 104.1°$$
$$\phi = 180°.$$

Our calculated O-O bond distance of 1.450 Å is essentially the same as that calculated for CH_3OOH (1.446 Å). Our calculated C-O bond length of 1.444 Å is 0.034 Å longer than is found experimentally for dimethyl ether.[12]

The most interesting aspect of the dimethyl peroxide structure is the 180° dihedral angle. The results of our calculations are supported by the photoelectron spectra of Rademacher and Elling.[13] They used the first two ionization potentials to obtain a rough estimate of 170° for this dihedral angle. They obtain 125° for HOOH, suggesting that their estimates are good to 5 or 10°, and hence their experimental results for CH_3OOCH_3 are consistent with our calculations. Figure 2 shows that the calculated potential curve for the torsional bending of CH_3OOCH_3 is quite flat at the minimum, allowing considerable rotational freedom. It is reasonable that CH_3OOCH_3 be planar since the OH-lone-pair interactions stabilizing the dihedral angle of CH_3OOH and HOOH are absent. The repulsive interactions between CH_3 groups and between CH_3 and lone pairs on different centers favor a 180° dihedral angle (staggered pairs on the two oxygens).

HO_2: The structure of HO_2

$$R_0(OH) = 0.977 \text{ Å}$$
$$R_0(OO) = 1.335 \text{ Å}$$
$$\theta_0(OOH) = 104.1°$$

is well established, having been obtained from microwave spectra of HO_2 and DO_2 by Beers and Howard.[14] In addition, many theoretical studies have been done on this molecule.[7-9, 15-17] Our calculated structure (Table II)

$$R_e(OH) = 0.972 \text{ Å}$$
$$R_e(OO) = 1.342 \text{ Å}$$
$$\theta_e(OOH) = 104.2°$$

is very close to the experimental one, demonstrating the accuracy of our GVB + CI calculations. Of course, we calculate equilibrium parameters; whereas experimentally, these parameters are measured for the zero quantum level. Thus perfect agreement is not to be expected.

CH_3O_2: This is another case where no experimental data are available and no previous ab initio calculations could be found. Structurally, CH_3OO is much like HO_2,

$$R_e(CO) = 1.442 \text{ Å}$$
$$R_e(OO) = 1.339 \text{ Å}$$
$$\theta_e(OOC) = 110.2° .$$

The O-O bond lengths are essentially the same, and in both cases the OOR bond angle increases 4-5° from the corresponding peroxide (Table II). The C-O bond length is the same as in the methyl peroxides.

TABLE III. Theoretical and Experimental Equilibrium Geometries of Peroxy Radicals. Values in parentheses were assumed in the calculations. Distances in Å and angles in degrees.

Method	r_{OO}	r_{OH}	r_{OC}	θ_{OOH}	θ_{OOC}	Ref.
HOO						
Experimental	1.335	0.977		104.1		14
Ab Initio Correlated						
GVB + CI	1.342	0.972		104.2		this work
Ab Initio Uncorrelated						
RHF	1.31	0.95		104		15
Semi-Empirical						
MINDO/2	1.349	0.972		117.6		7
INDO	1.19	1.05		110.7		8
CNDO/2	1.19	(0.96)		111		9
CH_3OO						
Experimental						
Ab Initio Correlated						
GVB + CI	1.339		1.442		110.2	this work
Semi-Empirical						
MINDO/2	1.335		1.335		122.1	7
INDO	1.20		1.38		112.5	10
CNDO/2	1.19		(1.44)		111	9

Summary

These calculations are the first reported ab initio studies of the equilibrium structures of CH_3OOH, CH_3OOCH_3, and CH_3OO. The calculated structural parameters of HOOH and HOO are very close to those obtained experimentally, demonstrating the accuracy of the GVB + CI approach.

The dihedral angles of the peroxides are calculated to vary from 119° in HOOH, to 126° in CH_3OOH, and 180° in CH_3OOCH_3, giving new insight into the gas phase structures of peroxides.

Acknowledgments

The author wishes to thank the U. S. Department of Energy for partial support of this work under Contract No. DE-AC03-76SF00767, Project Agreement No. DE-AT03-80ER10608.

Figure 3a. GVB Orbitals of H_2O_2.

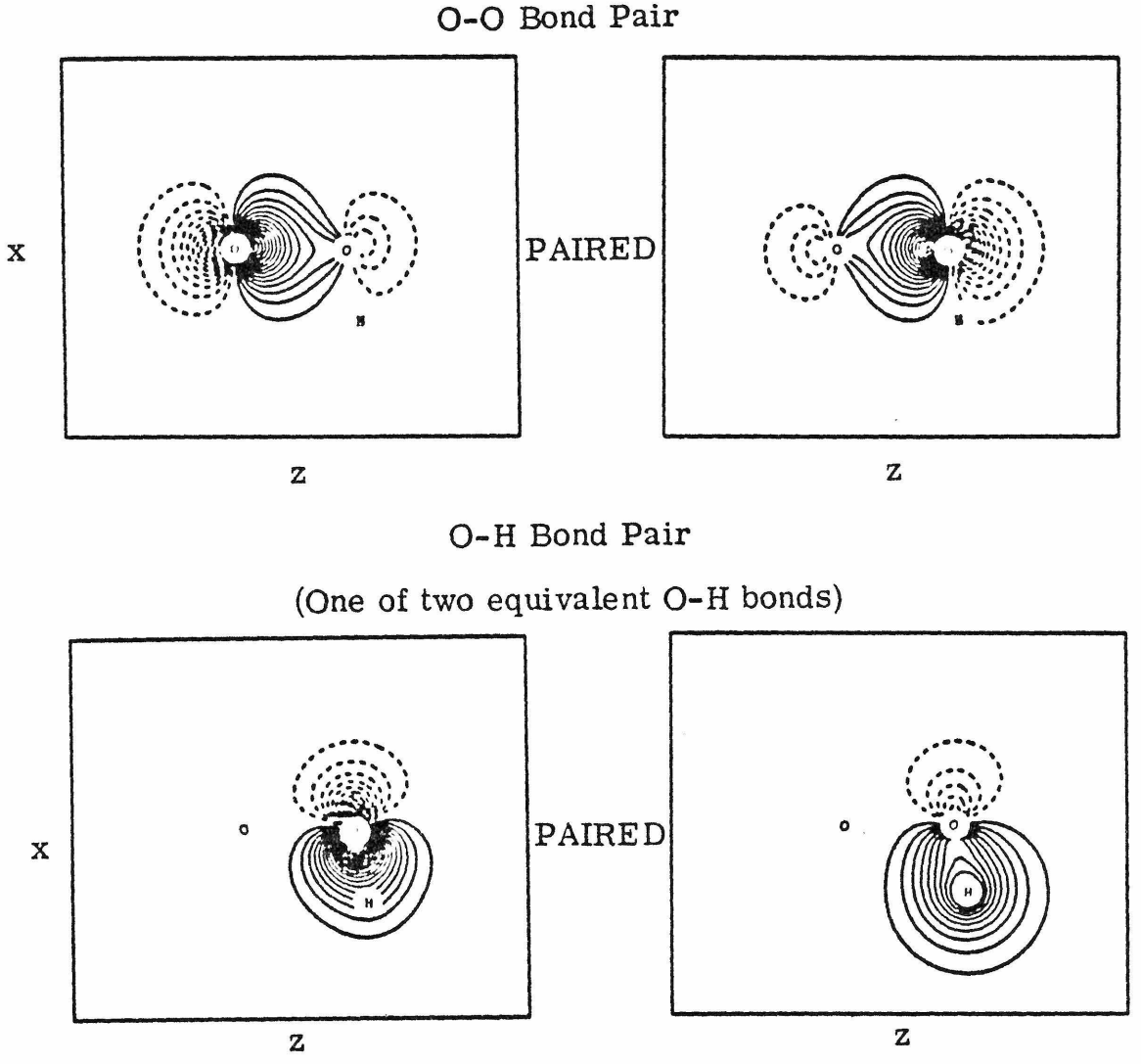

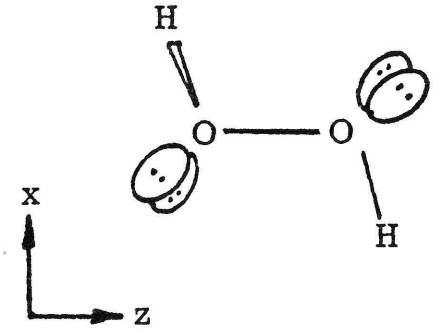

Figure 3b. GVB Orbitals of H_2O_2.

O Lone Pair

(One of four equivalent lone pairs)

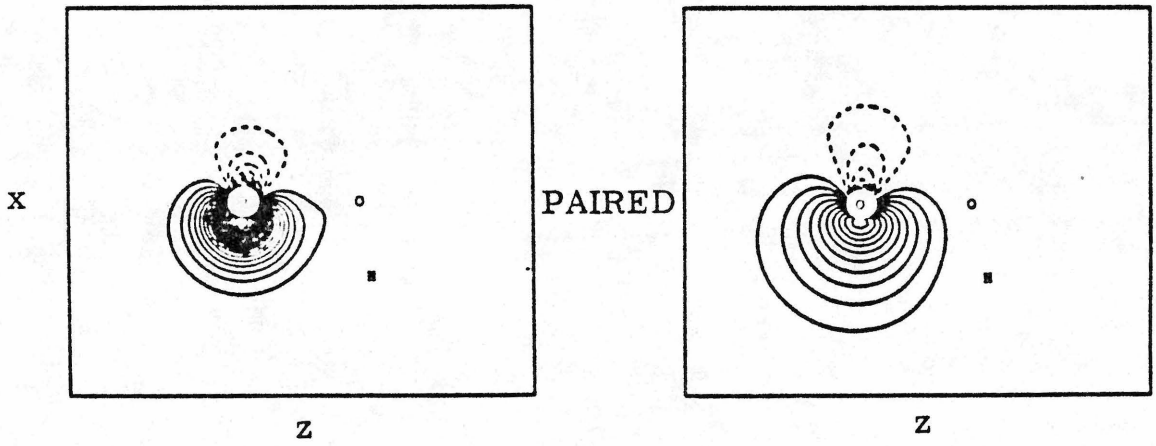

Figure 4a. GVB Orbitals of CH_3OOH.

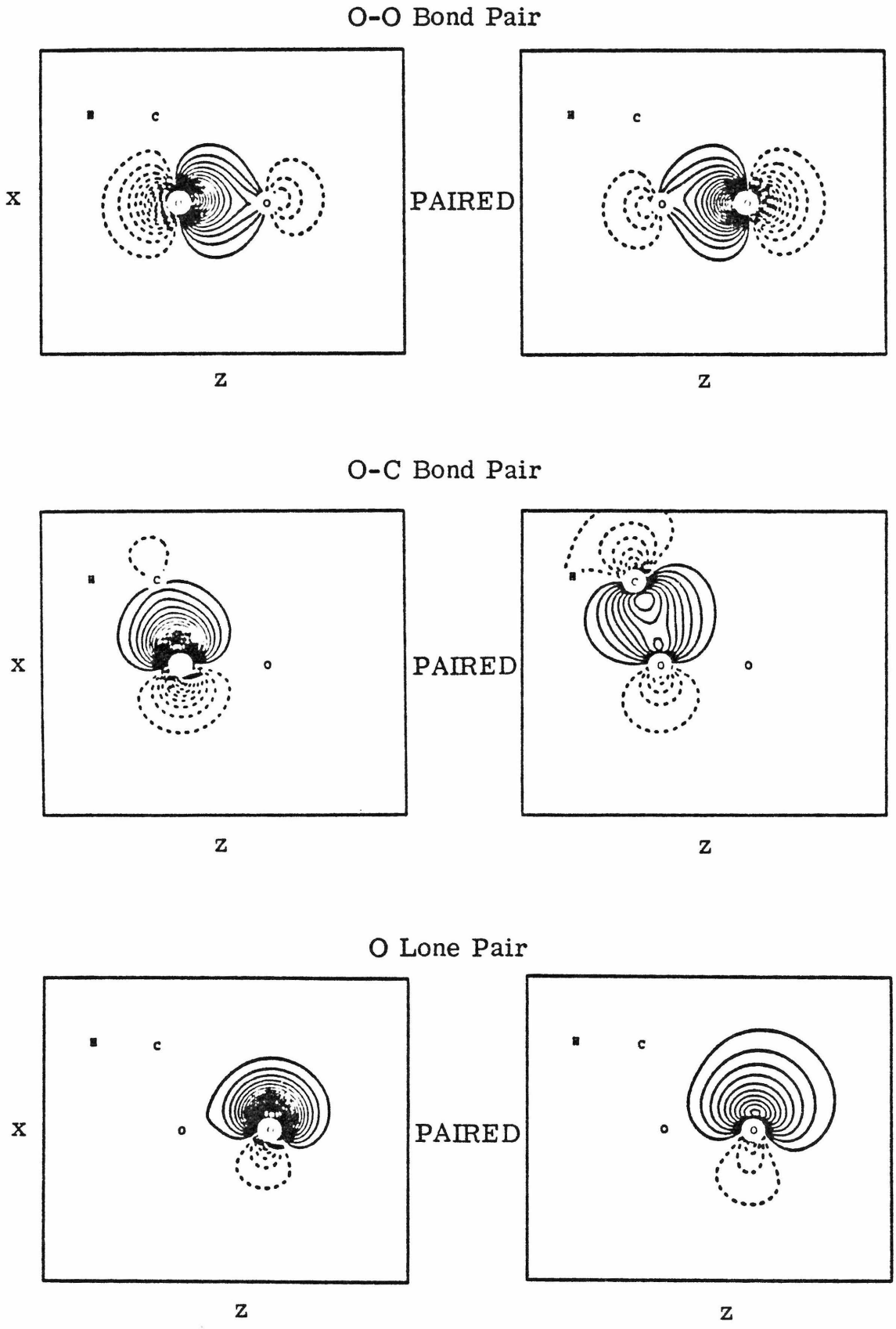

Figure 4b. GVB Orbitals of CH_3OOH.

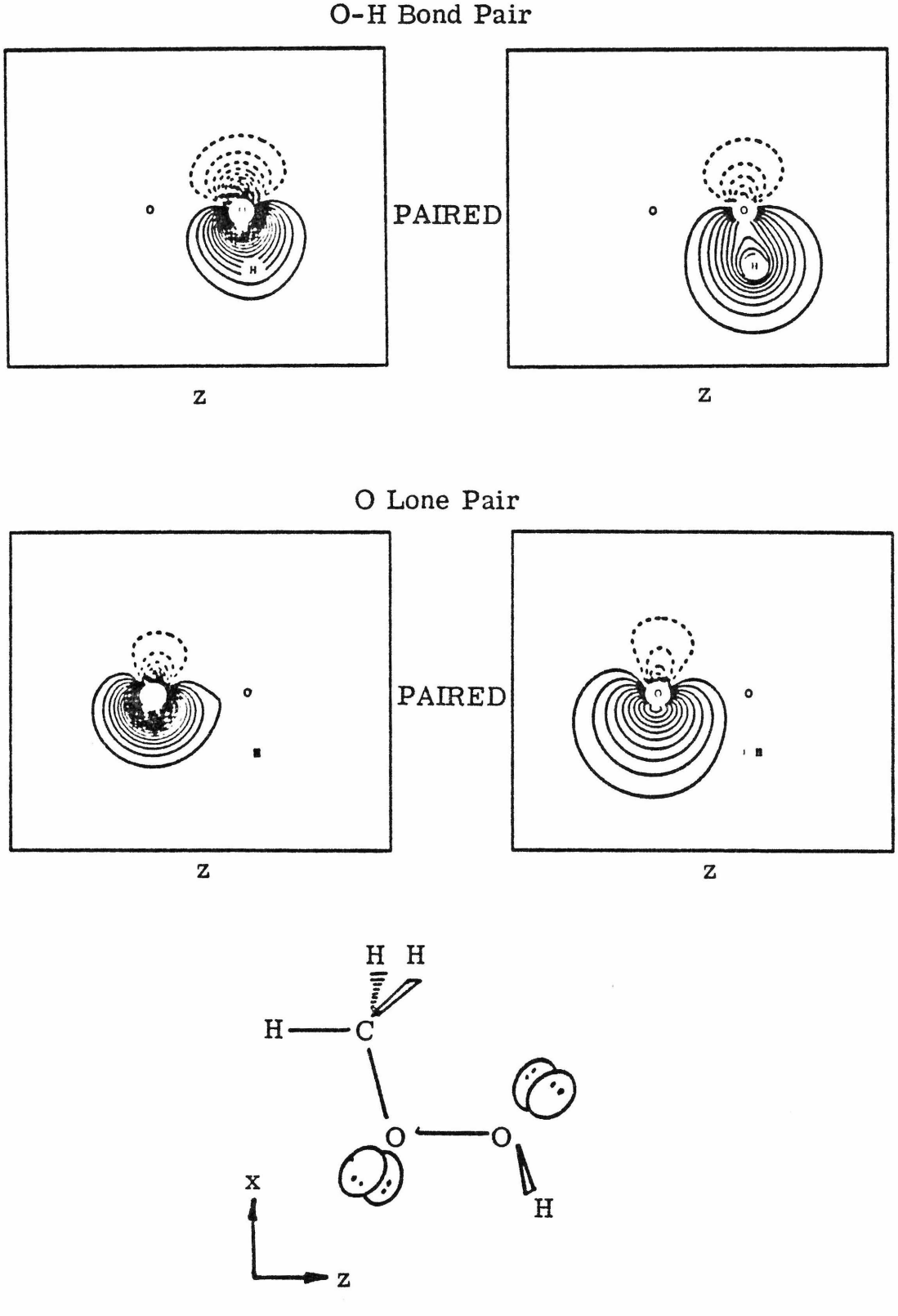

Figure 5a. GVB Orbitals of CH_3OOCH_3.

O-O Bond Pair

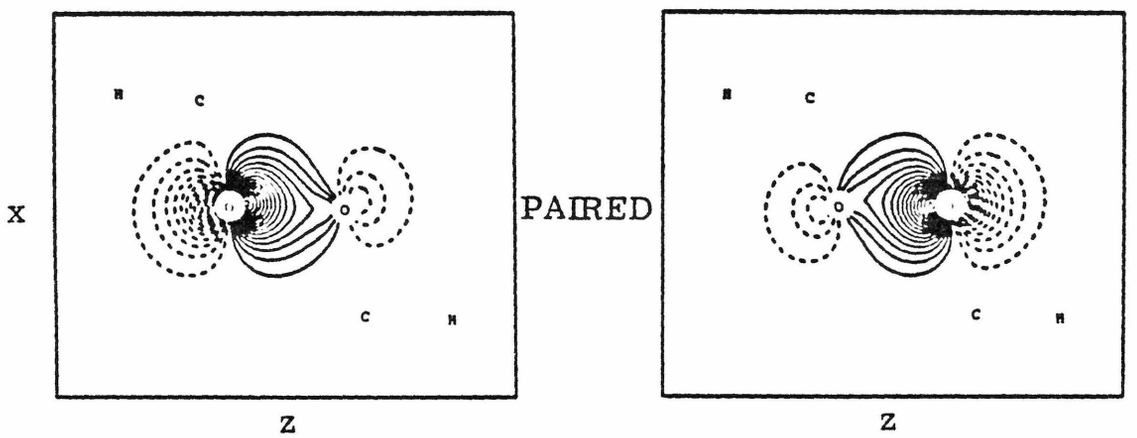

O-C Bond Pair

(One of two equivalent O-C bonds)

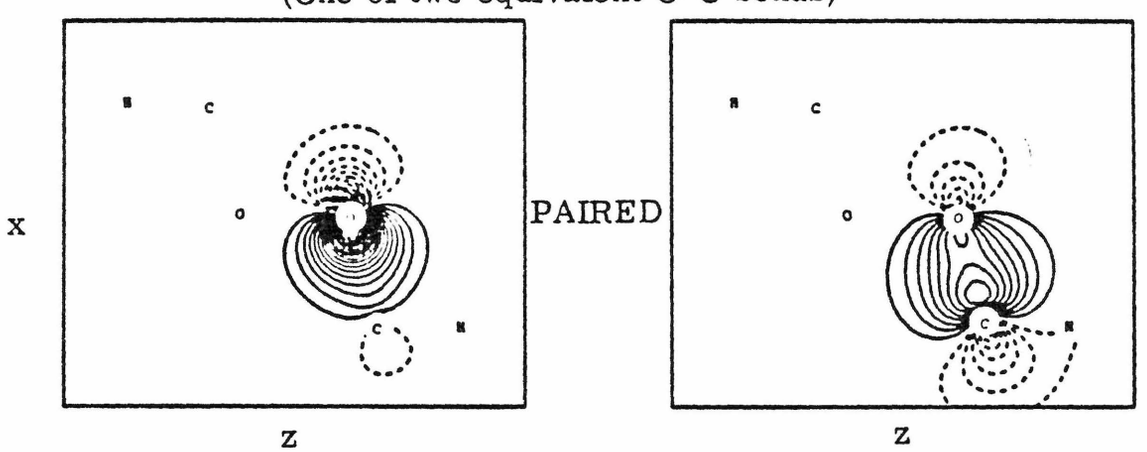

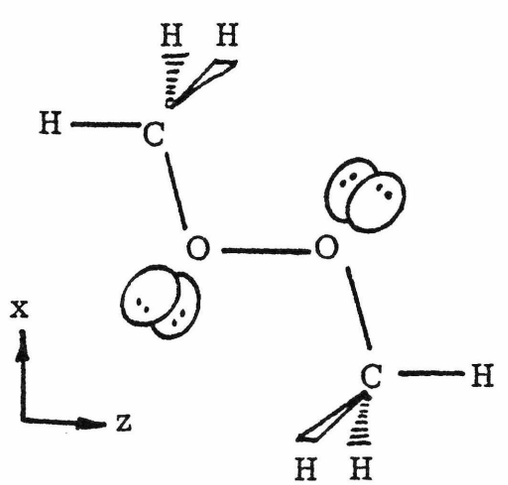

Figure 5b. GVB Orbitals of CH_3OOCH_3.

O Lone Pair

(One of four equivalent lone pairs)

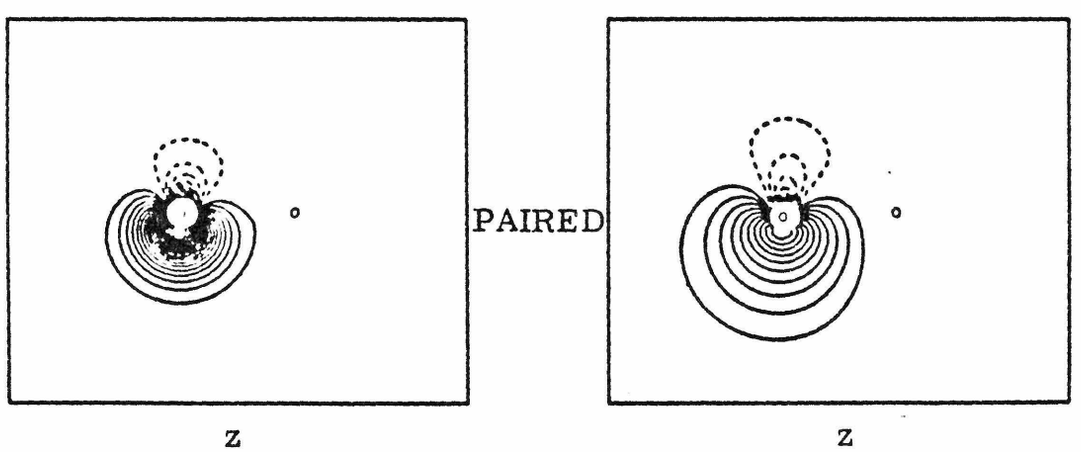

Figure 6a. GVB Orbitals of HO_2.

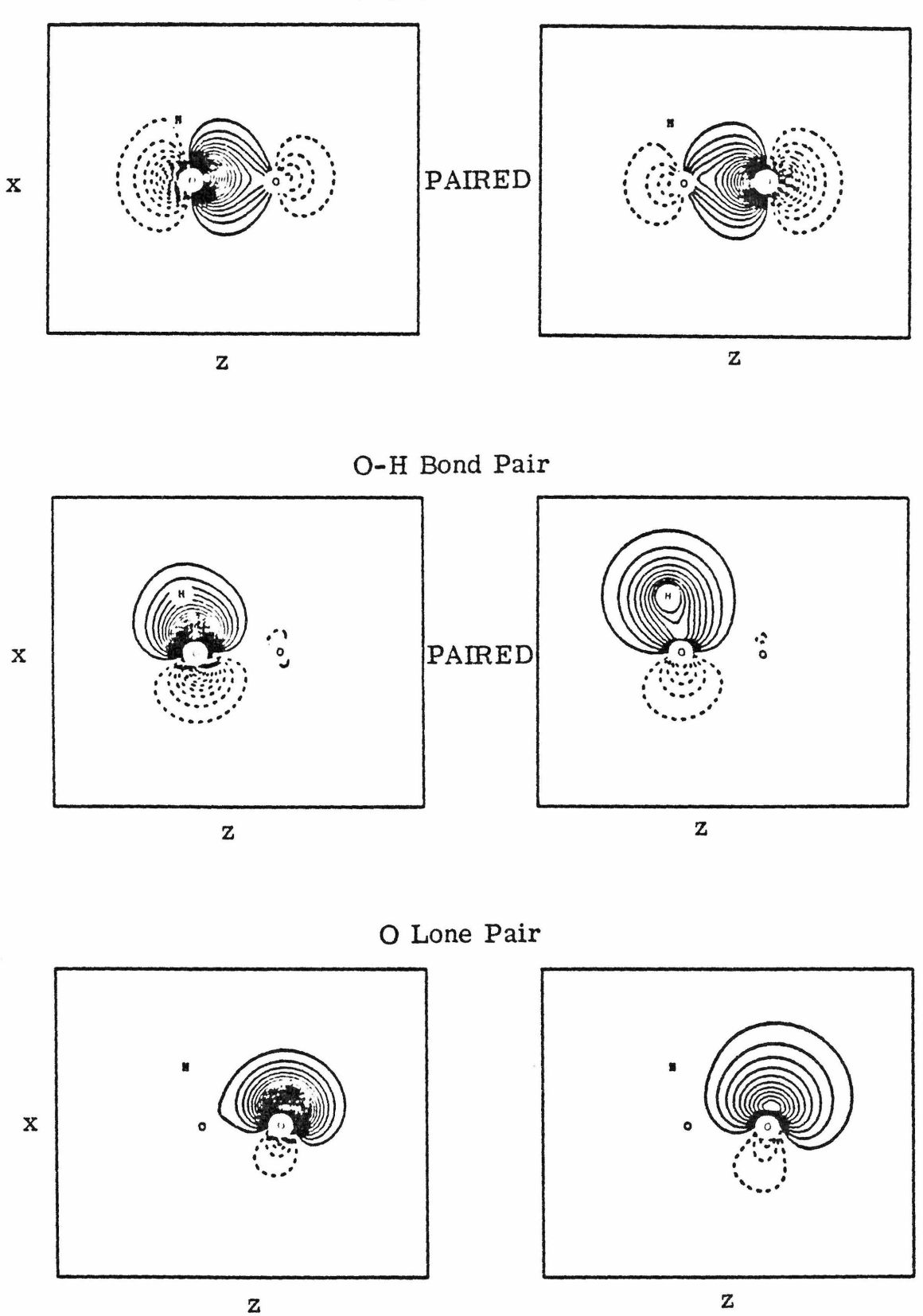

Figure 6b. GVB Orbitals of HO_2.

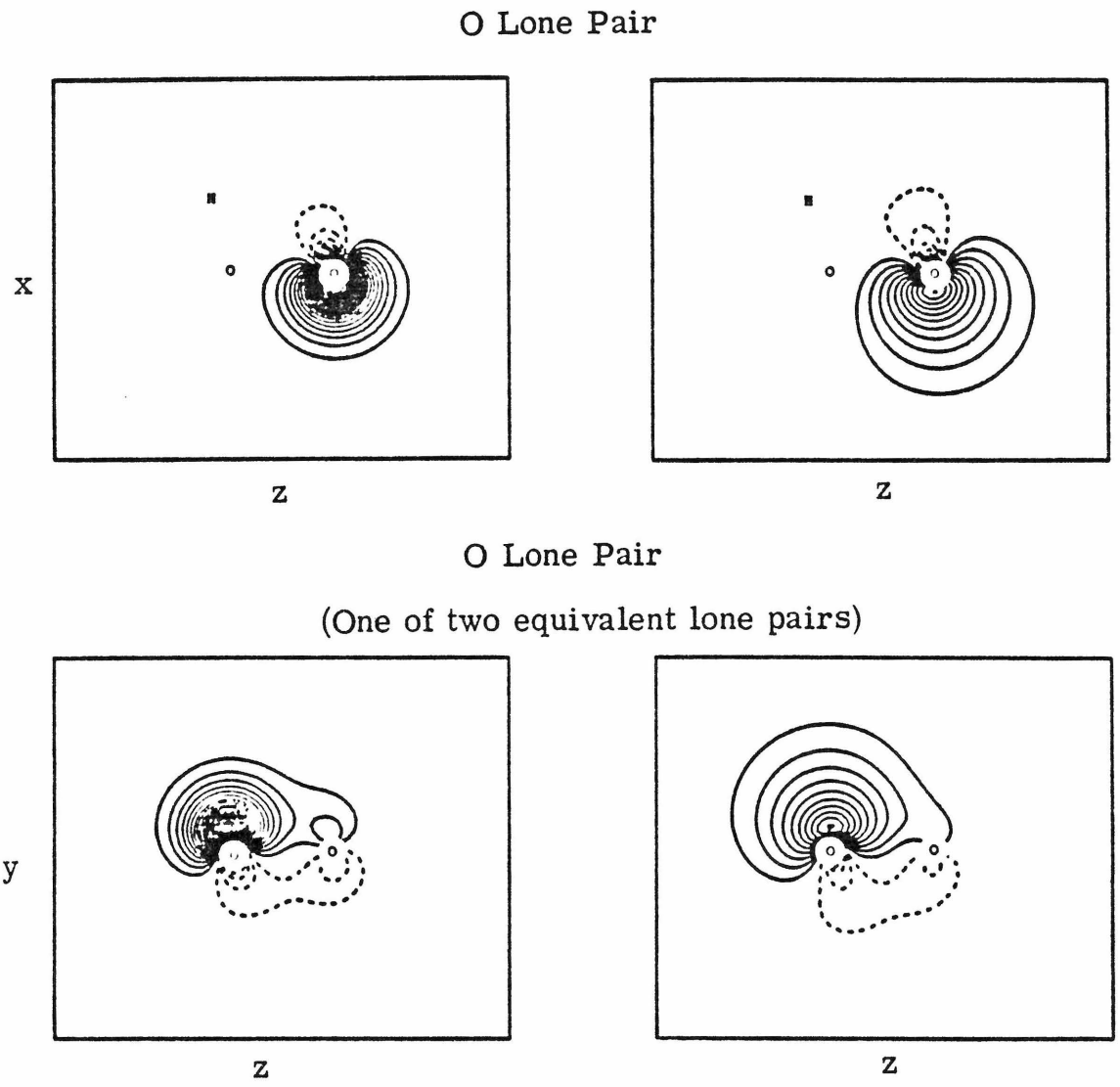

Figure 7a. GVB Orbitals of CH_3O_2.

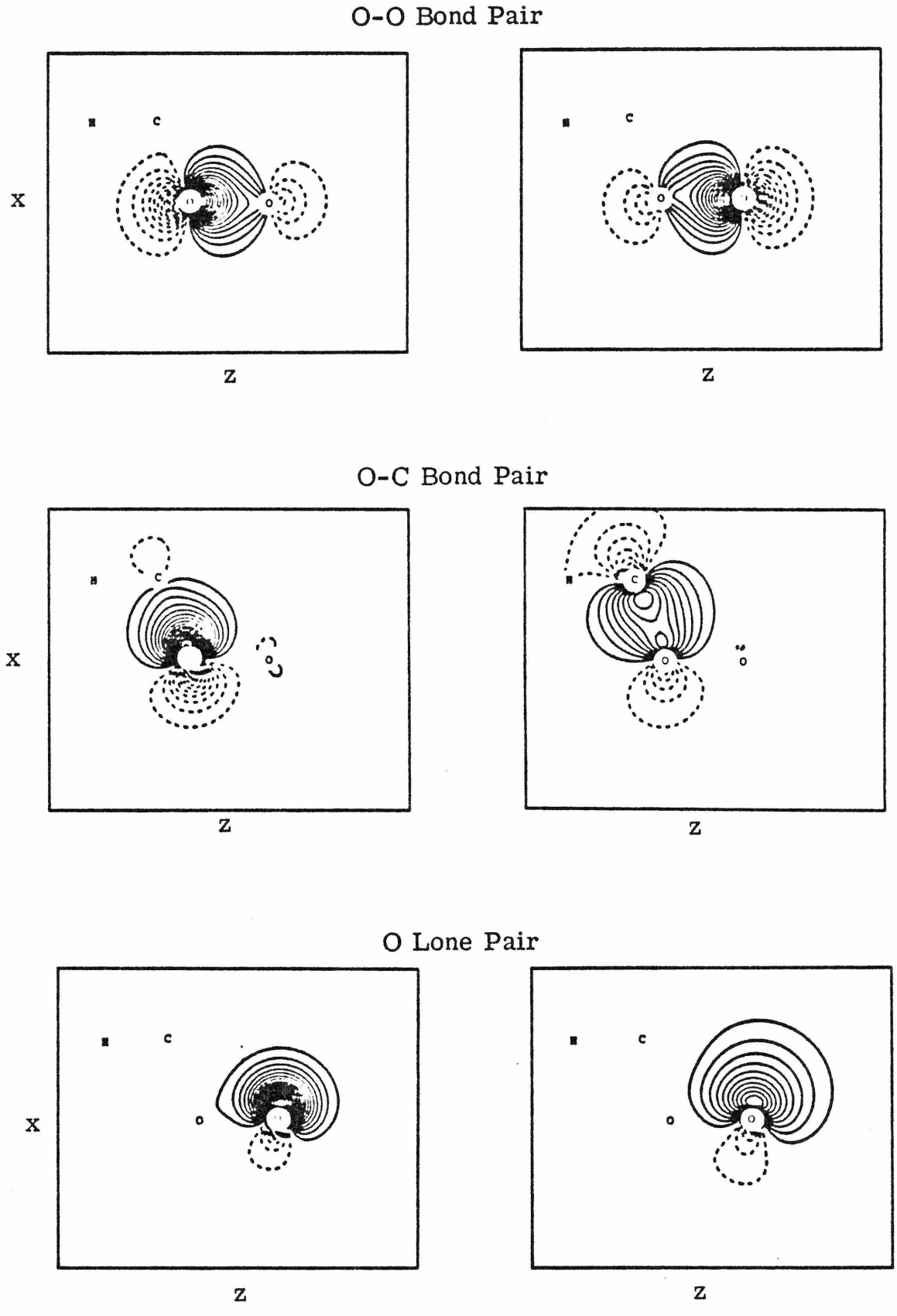

Figure 7b. GVB Orbitals of CH_3O_2.

O Lone Pair

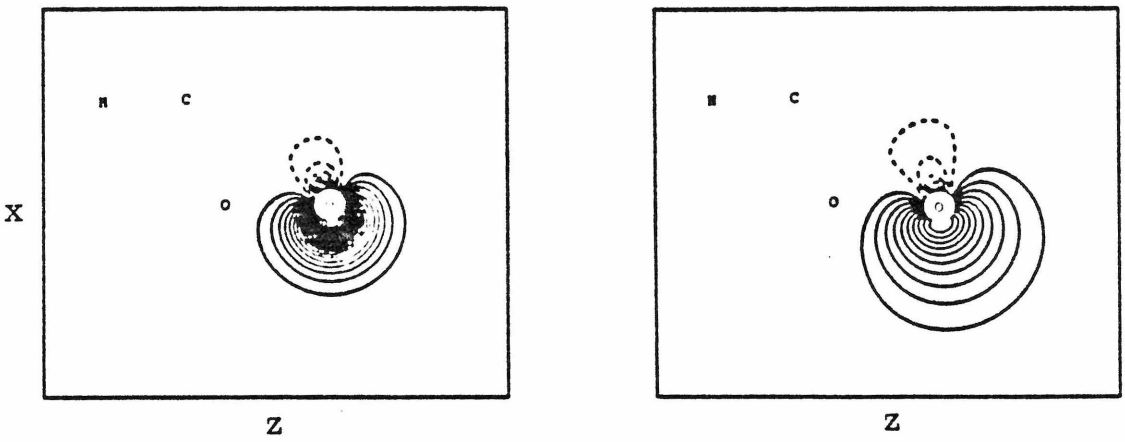

O Lone Pair

(One of two equivalent lone pairs)

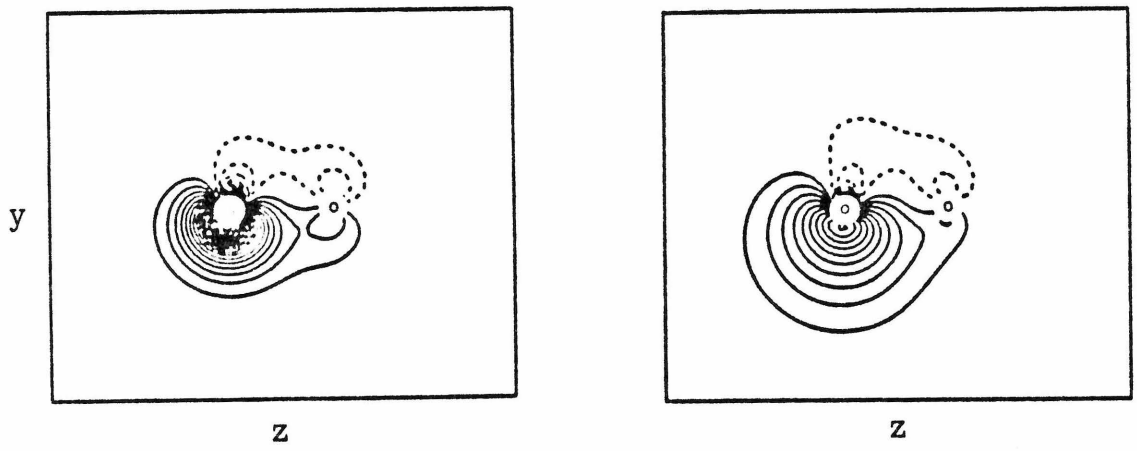

O Radical Orbital

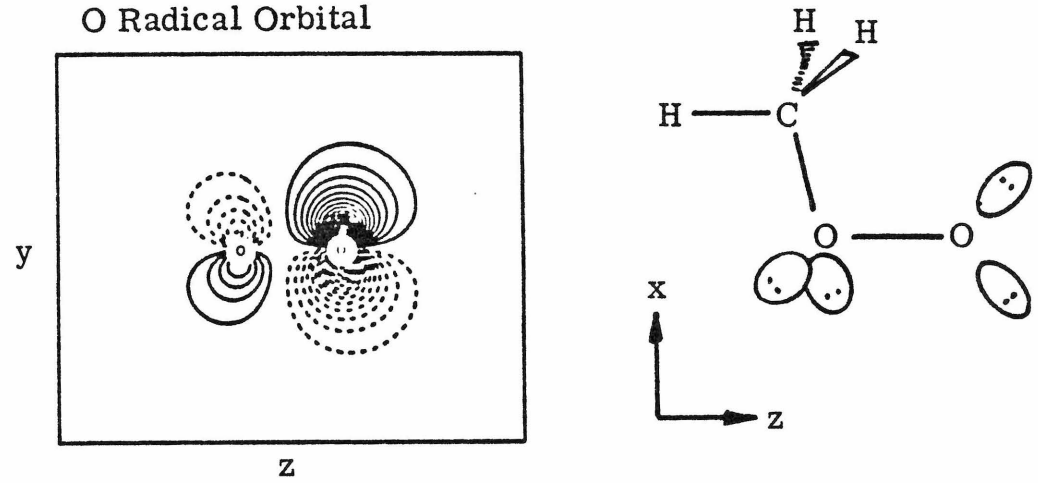

TABLE IV. Calculated Total Energies for GVB+CI Wavefunctions of Peroxides and Peroxy Radicals.

Molecule	Energy (hartree)	Molecule	Energy (hartree)
HOOH	-151.0216	HOO•	-150.3982
CH_3OOH	-190.0302	CH_3OO•	-189.4090
CH_3OOCH_3	-229.0391		

References and Notes

(1) S. Huzinaga, J. Chem. Phys., 42, 1293 (1965).

(2) T. H. Dunning, Jr., and P. J. Hay, In "Methods of Electronic Structure Theory", H. F. Schaefer III; Plenum Press: New York, 1977; p. 23.

(3) GVB2.5 was written R. A. Bair in 1977. This program is an extensively rearranged version of GVBTWO (written by F. W. Bobrowicz and W. R. Wadt in 1973) which avoids the extensive I/O requirements for cases with larger numbers of GVB pairs.

(4) R. L. Redington, W. B. Olson, and P. C. Cross, J. Chem. Phys., 36, 1311 (1962).

(5) D. Cremer and D. Christen, J. Mol. Spectrosc., 74, 480 (1979).

(6) D. Cremer, J. Chem. Phys., 69, 4440 (1978).

(7) K. Ohkubo, T. Fujita, and H. Sato, J. Mol. Struct., 36, 101 (1977).

(8) J. A. Pople and D. L. Beveridge, "Approximate Molecular Orbital Theory"; McGraw-Hill: New York, 1970; p. 85.

(9) K. Ohkubo and F. Kitagawa, Nippon Kagaku Kaishi, 2147 (1973); Bull. Chem. Soc. Jpn., 47, 739 (1974).

(10) K. Ohkubo and F. Kitagawa, Bull. Chem. Soc. Jpn., 48, 703 (1975).

(11) P. W. Allen and L. E. Sutton, Acta Crystallogr., 3, 46 (1950).

(12) U. Blukis, P. H. Kasai, and R. J. Meyers, J. Chem. Phys., 38, 2753 (1963).

(13) P. Rademacher and W. Elling, Leibigs Ann. Chem., 1473 (1979).

(14) Y. Beers and C. J. Howard, J. Chem. Phys., 64, 1541 (1976).

(15) A. Hinchliffe, J. Mol. Struct., 66, 235 (1980).

(16) T. H. Dunning, Jr., S. P. Walch, and M. M. Goodgame, J. Chem. Phys., in press.

(17) D. H. Liskow, H. F. Schaefer III, and C. F. Bender, J. Am. Chem. Soc., 93, 6734 (1971).

Conclusions

The purpose of the research in Part B of this thesis was to develop a method for calculating bond dissociation energies which is general enough to be applied to whole classes of molecules and accurate enough to calculate substituent effects. At the onset we felt that the calculations would have to be very consistent from molecule to molecule to produce the level of accuracy we desired (3 kcal or better). This led to the incorporation of GVB and CI methods for calculating dissociation-consistent wavefunctions. As the bond of interest is stretched, the molecular wavefunction becomes precisely two fragment wavefunctions. This way we do not correlate one species better than another, and avoid errors and inconsistencies in the bond energies. In addition, we focused the calculations on obtaining a good description of the molecule in the region of the centers whose bond would be broken. This makes good chemical sense, and is borne out by the success of group additivity concepts. Nevertheless, we found that for the radical fragments, substituents have important modes of correlation with the radical orbital. When these correlations were included consistently, the accuracy of the bond energies of the substituted molecules became comparable to the corresponding unsubstituted cases. We emphasized minimizing the size of the CI calculations, which required understanding of the important electronic correlations.

Overall, the benchmark calculations show that the method is successful in calculating good quality bond energies. The R-H bond energies are very consistent, whether the R-H bond is ionic or covalent. They are almost all 3 kcal too small, which should let us make some very accurate predictions for unknown species. For the R-R′ dissociation there is more

scatter in the calculated results; however, calculations on a series of like bonds (e.g., various C-O bonds) produce consistent errors. Thus we should also be able to make predictions about unknown or uncertain R-R bond strengths.

In the beginning, the focus was on organic species, with the intent of calculating the bond energies involved in proposed combustion mechanisms. Hence, calculations were performed on the bonds of organic peroxides. However, the success of this research gives us confidence that this method can be directly applied to many inorganic species as well. Calculation of the bond dissociation energies of the single bonds of saturated, closed-shell species should be simply a matter of following the prescription we have developed.

However, there are many interesting problems that still need to be addressed. First, we need to extend our method to bonds of molecules with radical orbitals (e.g., H-O$^{\cdot}$, H-OO$^{\cdot}$, HO-$\mathring{C}H_2$). This would broaden our ability to attack the thermochemistry of combustion intermediates. Unfortunately, the extra radical orbitals introduce many new modes of electron correlation, which must be included consistently. Also, it seems likely that dissociation-consistent ideas can be applied to the calculation of accurate transition state energies as well. This would provide useful chemical information for determining the relative rates of competing reaction pathways. Thus, as usual, success at solving one set of difficult problems leads us to consider even more difficult cases.